

1703 FILE COPY

(2)

RADC-TR-89-352  
Final Technical Report  
February 1990

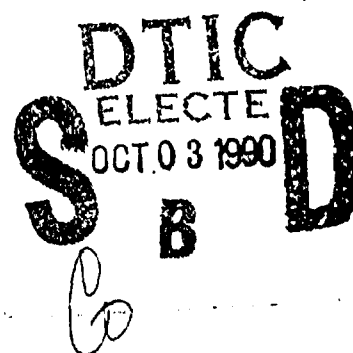
AD-A227 303



## QUANTUM WELL LASER

Plesscor Optronics Inc.

P. J. Williams, A.C. Marshall, D.J. Robbins



APPROVED FOR PUBLIC RELEASE; DISTRIBUTION UNLIMITED.

Rome Air Development Center  
Air Force Systems Command  
Griffiss Air Force Base, NY 13441-5700

90 10 02 036

This report has been reviewed by the RADC Public Affairs Division (PA) and is releasable to the National Technical Information Service (NTIS). At NTIS it will be releasable to the general public, including foreign nations.

RADC-TR-89-352 has been reviewed and is approved for publication.

APPROVED:



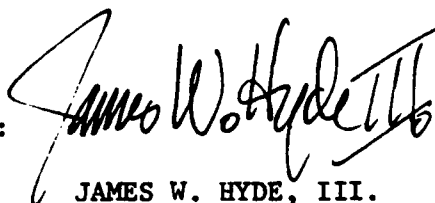
JOSEPH P. LORENZO  
Project Engineer

APPROVED:



HAROLD ROTH  
Director of Solid State Sciences

FOR THE COMMANDER:



JAMES W. HYDE, III.  
Directorate of Plans & Programs

If your address has changed or if you wish to be removed from the RADC mailing list, or if the addressee is no longer employed by your organization, please notify RADC (ESOC) Hanscom AFB MA 01731-5000. This will assist us in maintaining a current mailing list.

Do not return copies of this report unless contractual obligations or notices on a specific document require that it be returned.

UNCLASSIFIED

SECURITY CLASSIFICATION OF THIS PAGE

## REPORT DOCUMENTATION PAGE

Form Approved  
OMB No. 0704-0188

1a. REPORT SECURITY CLASSIFICATION UNCLASSIFIED			1b. RESTRICTIVE MARKINGS N/A		
2a. SECURITY CLASSIFICATION AUTHORITY N/A			3. DISTRIBUTION/AVAILABILITY OF REPORT  Approved for public release; distribution unlimited.		
2b. DECLASSIFICATION/DOWNGRADING SCHEDULE N/A					
4. PERFORMING ORGANIZATION REPORT NUMBER(S) N/A			5. MONITORING ORGANIZATION REPORT NUMBER(S) RADC-TR-89-352		
6a. NAME OF PERFORMING ORGANIZATION Plesscor Optronics Inc.		6b. OFFICE SYMBOL (if applicable)		7a. NAME OF MONITORING ORGANIZATION Rome Air Development Center (ESOC)	
6c. ADDRESS (City, State, and ZIP Code) 20200 Sumburst Street Chatsworth CA 91311-6289			7b. ADDRESS (City, State, and ZIP Code) Hanscom AFB MA 01731-5000		
8a. NAME OF FUNDING/SPONSORING ORGANIZATION Rome Air Development Center		8b. OFFICE SYMBOL (if applicable) ESOC		9. PROCUREMENT INSTRUMENT IDENTIFICATION NUMBER F19628-85-C-0172	
8c. ADDRESS (City, State, and ZIP Code) Hanscom AFB MA 01731-5000			10. SOURCE OF FUNDING NUMBERS		
			PROGRAM ELEMENT NO 61102F	PROJECT NO 2306	TASK NO J2
11. TITLE (Include Security Classification) QUANTUM WELL LASER					
12. PERSONAL AUTHOR(S) P. J. Williams, A. C. Marshall, D. J. Robbins					
13a. TYPE OF REPORT Final		13b. TIME COVERED FROM Sep 85 to Mar 88		14. DATE OF REPORT (Year, Month, Day) February 1990	
15. PAGE COUNT 132					
16. SUPPLEMENTARY NOTATION N/A					
17. COSATI CODES			18. SUBJECT TERMS (Continue on reverse if necessary and identify by block number)		
FIELD	GROUP	SUB-GROUP	Quantum Well, Indium Phosphide Heterostructures, <i>100</i>		
20	12				
19. ABSTRACT (Continue on reverse if necessary and identify by block number)					
<p>During the first year of the program, basic materials growth experiments were carried out in order to develop the necessary capability for the growth of quantum well lasers by Atmospheric Pressure MOVPE (AP-MOVPE). In the latter part of the program, this technology was transferred to a Low Pressure MOVPE (LP-MOVPE) reactor which demonstrated superior materials and interface qualities with respect to structures prepared by AP-MOVPE. By correlating SIMS data and Hall analysis, conditions were determined for the growth of high quality and abrupt p-doped and n-doped InP of known carrier concentration. In this way p-doped In<sup>+</sup> over the range mid <math>10^{17}</math> cm<sup>-3</sup> to <math>2 \cdot 10^{18}</math> cm<sup>-3</sup> could be grown, with carrier concentrations extended up to <math>10^{19}</math> cm<sup>-3</sup> for p++ InGaAs contact layers. Quantum well laser structures were grown and tested.</p>					
20. DISTRIBUTION/AVAILABILITY OF ABSTRACT <input checked="" type="checkbox"/> UNCLASSIFIED/UNLIMITED <input type="checkbox"/> SAME AS RPT <input type="checkbox"/> DTIC USERS			21. ABSTRACT SECURITY CLASSIFICATION UNCLASSIFIED		
22a. NAME OF RESPONSIBLE INDIVIDUAL Joseph P. Lorenzo			22b. TELEPHONE (Include Area Code) (617) 377-3598		22c. OFFICE SYMBOL RADC (ESOC)

DD Form 1473, JUN 86

Previous editions are obsolete.

SECURITY CLASSIFICATION OF THIS PAGE  
UNCLASSIFIED

# CONTENTS

	Page No.
1. Introduction	1
1.1 Outline Achievements	1
1.2 Key Achievements for the First Twelve Months of Program	2
1.3 Key Achievements for the Final Eighteen Months of Program	3
1.4 State of the Art Long Wavelength Quantum Well Lasers	4
2. Materials	6
2.1 Introduction	6
2.2 MOVPE Growth of P-N Junctions in InP	7
2.3 Preparation of InGaAs/InP Double Heterostructure and First Pass MQW Laser Source Material by AP-MOVPE	7
2.4 MQW Test and Device Structures Grown by AP-MOVPE	8
2.4.1 Device Growth and Assessment of Materials by TEM	8
2.4.2 Double Crystal X-Ray Diffraction Studies	9
2.4.3 Photoluminescence and Absorption Spectra	10
2.5 Growth of MQW Material by LP-MOVPE	11
2.6 Growth of Laser Structures by LP-MOVPE	12
2.7 Transverse Injection MQW Lasers	13
2.8 Growth and Characterisation of GaAlInAs	13
2.9 InGaAs/AlInAs MQW Structures	15
3. Preparation and Characterisation of DH and MQW Lasers	16
3.1 Preparation of MOVPE InGaAs/InP DH Lasers	16
3.2 Preparation and Characterisation of Advanced Index Guided DH InGaAs Lasers	17
3.3 Preparation and Characterisation of Broad Area InGaAs/InP MQW Lasers	17
3.3.1 Introduction	17
3.3.2 Characterisation of Broad Area "thick barrier" ( $>100\text{\AA}$ ) InGaAs/InP MQW Lasers under Electrical Injection	18
3.3.3 Investigation of MQW and DH Lasers by Optical Pumping	19
3.3.4 Additional Studies of Non Uniform Carrier Capture	21
3.3.5 Characterisation of Broad Area "thin barrier" ( $<100\text{\AA}$ ) InGaAs/InP MQW Lasers under Electrical and Optical Injection	22
3.4 Preparation of Transverse Injection MQW and DH Lasers	24
3.5 Preparation and Characterisation of CW Buried Ridge Waveguide InGaAs/InP MQW Lasers	25
3.6 InGaAs/InP MQW Laser High Frequency Response Characteristics	25
3.7 Characterisation of GaAlInAs Active DH Oxide Stripe Lasers	26
4 Design and Modelling Studies	27
4.1 Introduction	27
4.2 Quantum Well Laser Model	27
4.3 Device Design and Optimisation	28
4.4 Carrier Capture and Equilibration	31
4.5 Spontaneous Emission Spectra	33
5. Conclusions	35
References	37
Appendix 1	



PROGRAM OBJECTIVE

To conduct research and development into new technology for laser sources based on quantum well structures in the InP alloy system.

1. INTRODUCTION

1.1 Outline Achievements

The report given below represents the conclusion of the above named program of research and development into long wavelength quantum well laser sources carried out over the period. Since the previous twelve month interim report, further significant progress in all aspects of the program: materials growth, device preparation and theoretical modelling, has been achieved. As outlined below, all MOVPE room temperature, cw lasing, MQW InGaAs/InP Buried Ridge lasers have been prepared for the first time. Low threshold (60mA) devices have been characterised and broad area lasers,  $J_{th} = 2.9 \text{ kA.cm}^{-2}$  indicate some improvement in  $T_0$  over conventional long wavelength DH lasers. A comprehensive theoretical model has been developed during the program to include the detailed effects of Auger and Intervalence Band absorption. These studies also include the effect of reducing the barrier width on lasing characteristics. Experimental studies have been carried out which confirm the theoretical predictions. An additional separate report (Modelling and Design of Quantum Well Lasers in the InP Based Materials System) gives a more in depth account of these studies than presented here. Materials growth of InGaAs, InP and AlInAs has been extended to include a wide range of lattice matched GaAlInAs compounds suitable for use as active and guide layers in DH and MQW, M-MQW and GRIN-SCH lasers. On this program  $1.24 \mu\text{m}$  wavelength GaAlInAs active layer DH lasers have been prepared for the first time by low pressure MOVPE. Materials technology required to prepare M-MQW and GRIN-SCH MQW lasers, the next step towards achieving higher performance quantum well lasers, has therefore been proven.

## 1.2 Key Achievements for the First Twelve Months of Program

(As reported in the separate interim report - September 1985 to September 1986)

- (i) Growth and characterisation of lattice matched InGaAs and AlInAs on InP by Atmospheric Pressure (AP) and Low Pressure (LP) MOVPE
- (ii) Establishment of doping types and concentrations suitable for laser structures by AP and LP MOVPE
- (iii) Establishment of useful Quantum Well Laser models
- (iv) Preparation and Characterisation of Oxide Isolated InGaAs DH lasers.  $J_{th} \sim 3.5 \text{ kA.cm}^{-2}$
- (v) Preparation and Characterisation of Index Guided InGaAs DH lasers
  - (a) MOVPE source, LPE infill DCPBH structure: minimum room temperature lasing threshold current 60mA
  - (b) MOVPE source, VPE infill DCPBH structure: minimum room temperature lasing threshold current 30mA
- (vi) Preparation and Characterisation of first pass 8-well InGaAs/InP MQW lasers. Low temperature operation:  $J_{th} \sim 15 \text{ kA.cm}^{-2}$  at 240K. Emission wavelength  $1.59 \mu\text{m}$ .

### 1.3 Key Achievements for Final Eighteen Months of Program

- (i) Room temperature InGaAs/InP MQW laser operation achieved by optical pumping. Demonstrated lowest room temperature threshold yet reported for 1.55 $\mu$ m MQW laser operation under optical pumping:  $J_{th} \text{ opt.} \sim 700 \text{ A.cm}^{-2}$
- (ii) Importance of achieving uniform carrier injection across MQW lasers recognised
- (iii) Experiments with MQW lasers featuring thinner 55 and 25Å barriers carried out
- (iv) Preparation of room temperature lasing InGaAs/InP lasers with thinner 25Å barriers achieved under electrical injection and devices characterised:  $J_{th} \sim 2.9 \text{ kA.cm}^{-2}$ . Hence theoretical predictions confirmed.
- (v)  $T_0$  measured on broad area InGaAs/InP MQW lasers of 69K in temperature range -50 to +50°C represents an improvement over conventional GaInAsP active DH material
- (vi) All MOVPE Index Guided Buried Ridge InGaAs/InP MQW lasers prepared for the first time. Room temperature, CW operation achieved: Minimum lasing threshold currents 60mA, with front facet efficiency of 30%. Emission wavelength 1.53 $\mu$ m.
- (vii) Oxide isolated GaAlInAs active layer DH lasers aimed at 1.3 $\mu$ m operation prepared for the first time. Room temperature threshold current densities for broad area devices as low as 4.8kA.cm<sup>-2</sup>. Emission wavelength 1.24 $\mu$ m. Typical  $T_0 \sim 85\text{K}$ .

- (viii) Comprehensive theoretical model for long wavelength quantum well lasers established and verified. Separate report to be issued.
- (ix) Deliverable submounts and pigtailed module, 1.53 $\mu$ m InGaAs/InP MQW lasers fabricated, characterised and delivered to RADC, Hanscom
- (x) Long wavelength GaAlInAs oxide isolated DH lasers also delivered
- (xi) Papers covering
  - \*(a) The importance of thin barriers in long wavelength MQW lasers .....
  - +(b) Lasing action in GaAlInAs DH lasers....., submitted to Electronics Letters.

#### 1.4 State of the art Long Wavelength Quantum Well lasers

Quantum well lasers for 1.3 $\mu$ m-1.55 $\mu$ m have long been expected to exhibit performance advantages over their DH counterparts in the same way as GaAs-based devices have been shown to do. The apparent potential offered by these structures has encouraged continuing attempts to prepare GaInAsP/InP quantum well lasers by LPE [1,2] and more recently [3] LPE grown M-MQW lasers operating at 1.3 $\mu$ m have been demonstrated with pulsed threshold currents ~15-20mA, and  $T_0$  ~50K above 30°C. Growth of 1.3 $\mu$ m MQW laser structures by Hydride VPE has also been reported [4]. However, the growth of very thin layer structures by LPE and Hydride VPE has proved difficult, and reported devices which generally have well widths in the region of 200-400Å, lie in a regime where the effects of size quantisation are weak. It is, therefore, to the growth techniques of MOCVD, MBE and CBE that one must look for realisation of truly quantum well structures. Despite almost a decade of research into long wavelength QW lasers, from which has arisen several encouraging but isolated results spread over a wide range of

\* now published Williams et al Elec. Lett., 1988, 24 pp 859-860

+ now published Davies et al Elec. Lett., 1988, 24 pp 732-733



device types and growth techniques (Table 1), it is only very recently that a number of groups have reported device results with characteristics which compare favourably with DH- GaInAsP lasers. A notable exception has been an early report of InGaAs/AlInAs MQW lasers, grown by MBE, with threshold current densities of  $J_{th} \sim 2400 \text{ A.cm}^{-2}$  and  $T_0 \sim 70\text{--}83\text{K}$  [5] and room temperature CW operation has recently been achieved by a different group but in essentially the same structure with a threshold current of 530mA [6]. The most recent results including our own for InGaAs/InP MQW 1.55  $\mu\text{m}$  devices, which together represent the current world state-of-the art, are given in Table 2. From the data in Table 2 it is clear that QW device characteristics which offer a distinct margin of improvement over DH laser characteristics have now been achieved by several laboratories. Additionally, there is good reason to anticipate further improvements with the advent of more advanced structures such as the GRIN-SCH structure in the GaAlInAs/InP system.

Materials system	Growth technique	Device type
InGaAs/InP	Hydride-VPE LPE,MBE,MOCVD*	SQW,MQW,MMQW
(GaAl)InAs/InP	MBE,MOCVD*	MWQ,MMWQ
GaSb/(GaAl)Sb	MBE	MQW,MMQW

\*Plessey Caswell

TABLE 1 Summary of 1.3-1.55 $\mu\text{m}$  state-of-the-art QW Laser Research

Ref.	Growth Technique	Structure	$J_{th}$ (A.cm <sup>-2</sup> )	$I_{th}$ (mA)	$T_o$ (K)
[7]	CBE	MQW	1500-2100	-	65-80
[8]	MOVPE	MMQW-DCPBH	-	35(Pulsed)	120*
[9]	AP-MOVPE	MMQW-SIPBH	-	20(CW)	54
Plessey	LP-MOVPE	MQW /BR	2900	60(CW)	69 (Broad Area)

\*Cavity length 650  $\mu$ m.

TABLE 2 InGaAs/InP QW laser device results

## 2. MATERIALS

### 2.1. Introduction

During the first year of the program, basic materials growth experiments were carried out in order to develop the necessary capability for the growth of quantum well lasers by Atmospheric Pressure MOVPE (AP-MOVPE). In the latter part of the program, this technology was transferred to a Low Pressure MOVPE (LP-MOVPE) reactor which demonstrated superior materials and interface qualities with respect to structures prepared by AP-MOVPE. We report below on these experiments; the section headings can be broadly related to the milestones defined at the start of the program.

## 2.2. MOVPE Growth of P-N Junctions in InP

Initial work was aimed at establishing the capability for the growth of p- and n-type InP and InGaAs of calibrated carrier concentrations, together with the growth of well defined and accurately positioned p-n junctions.

Preliminary studies of p-type InP using dimethylzinc diluted in hydrogen as the p-type dopant source were carried out by AP-MOVPE. Observation of stained cross-section samples (using optical microscopy with Nomarski interference contrast) of p-doped InP epitaxial layers grown on Fe-doped semi-insulating substrates, showed a contrast change below the substrate/layer interface. This indicated that Zn diffusion into a lower undoped layer could be occurring which was confirmed by elemental Zinc profiles obtained from depth profiling SIMS analysis (Fig.1).

By correlating SIMS data and Hall analysis, conditions were determined for the growth of high quality and abrupt p-doped InP of known carrier concentration. In this way p-doped InP over the range mid  $10^{17} \text{ cm}^{-3}$  to  $2 \cdot 10^{18} \text{ cm}^{-3}$  could be grown, with carrier concentrations extended up to  $10^{19} \text{ cm}^{-3}$  for p++ InGaAs contact layers.

An equivalent exercise for the growth of n-type InP using both  $\text{H}_2\text{Se}$  and  $\text{H}_2\text{S}$  (diluted in hydrogen) as the dopant sources revealed that diffusion of these dopants was not a problem. Conditions were found for n-type InP at  $2 \cdot 10^{18} \text{ cm}^{-3}$ , suitable for the lower InP guide layer in a laser structure.

## 2.3. Preparation of InGaAs/InP Double Heterostructure and First Pass MQW Laser Source Material by AP-MOVPE

In order to assess the quality of MOVPE grown material for quantum well

lasers, a number of simple double heterostructure laser source wafers were grown with an  $\text{In}_{0.53}\text{Ga}_{0.47}\text{As}$  active layer (lattice matched to InP) of nominal thickness 1500Å. Earlier assessment of thick InGaAs single epitaxial layers had demonstrated highly crystalline material suitable for the active layer of a laser. Doping levels in the guide layers were determined by SIMS ( $\text{Zn}=8.10^{17}\text{cm}^{-3}$ ;  $\text{S}=2.10^{18}\text{cm}^{-3}$ ) and found to be abrupt as previously described.

Lasing action from these wafers, (described in section 3) was sufficiently encouraging to commence the growth of first pass MQW lasers.

Materials structures containing 8 InGaAs wells clad in InP were prepared. The thickness of wells and InP barriers were nominally 110Å and 100Å respectively, as calculated from growth rate data.

#### 2.4. MQW Test and Device Structures Grown By AP-MOVPE.

In addition to the first pass MQW laser source wafers described in the previous section, a series of 5, 8 and 30 period MQW structures were grown and characterised by transmission electron microscopy (TEM), double crystal X-ray diffraction (XRD) and photoluminescence (PL).

##### 2.4.1 Device Growth and Assessment of Materials by TEM

Detailed TEM examinations of the first pass MQW laser structure showed the wells to be of equal thickness. The interfaces appeared coherent, with no stacking faults or dislocation networks. Interfaces were seen to be abrupt, but whilst interfaces of InGaAs on InP were planar, those of InP on InGaAs were rippled. This effect occurred on all MQW wafers. Experiments to investigate methods of improving the planarity of this interface were designed and carried out.

The effect of pausing growth between the deposition of the InGaAs wells and the InP barrier layers was studied to examine the significance of the group-V switching operations. It was thought that inefficient exchange of group-V

precursors on the growing surface of the crystal when switching from  $\text{AsH}_3$  to  $\text{PH}_3$  could cause this 'rippling' effect, and that paused growth might produce an improved interface. However, a deterioration in the interface planarity was observed in MQW test and device structures employing this paused growth technique.

The influence of growth temperature (between  $600^\circ\text{C}$  and  $700^\circ\text{C}$ ) on the planarity of the wells was also investigated and a small improvement was noted at elevated temperatures ( $T_g = 700^\circ\text{C}$ ). However an intermediate growth temperature of  $650^\circ\text{C}$  was eventually decided upon, because of the lower background carrier concentrations and improved uniformity achieved in bulk layers of InGaAs and InP grown at this temperature compared with those grown at higher temperatures[10]. A cross-sectional TEM micrograph of a InGaAs/InP MQW structure prepared under these conditions is shown in Figure 2.

Both 8 and 5 well InGaAs/InP lasers were prepared featuring wider, nominally  $200\text{\AA}$  barriers aimed at improving well uniformity and interface planarity. Well/barrier thicknesses as found from cleaved corner edge TEM analysis [11] were  $125/180\text{\AA}$  and  $85/143\text{\AA}$  for the 8 and 5 well structures respectively. This result implied some non-uniformity in growth conditions for the two consecutive growths. Further analysis of wafer OB 684 (8 wells) indicated variable thickness active wells of  $130\text{--}170\text{\AA}$ . Evidence from the same sample also suggested that well/barrier interfaces were not improved by the introduction of thicker barriers.

Additional undoped InP spacer layers  $500\text{\AA}$  thick, adjacent to each side of the active region, were included in these device structures to investigate possible effects due to guide layer dopant diffusion (particularly Zinc)

#### 2.4.2 Double Crystal X-Ray Diffraction Studies

Fig.3 shows a fourth order X-ray rocking curve of a 30 period MQW test structure (OB 461). The angular separation of the substrate and epilayer diffraction maxima (zero order) provide the information about the composition of the ternary alloy in the wells. In this case the Indium content was 52.5%. This sample clearly exhibits satellite peaks, which are indicative of highly crystalline

material of regular period and sharp interfaces[12]. The period of the "well plus barrier" thickness is determined from the angular separation of the satellites[12] and was found to be  $309 \pm 10 \text{ \AA}$  for OB461.

In the case of the 8 well structures, neither the zero order maxima from the InGaAs layers nor the quantum well satellite peaks could be observed. It was concluded that because of the relatively small volume of material and the small number of periods, the diffraction signals were extremely weak, and that the technique could not provide the composition and periodicity information required. Prior to growing 8 well laser structures, it was therefore found necessary to grow a 30 period test structure in order to characterise growth rates (from the satellite peak separation) and material quality from the XRD rocking curves.

#### 2.4.3 Photoluminescence and Absorption Spectra

Room temperature PL was used to investigate the optical properties of 30 period MQW structures and the spectra for 2 such wafers are shown in figure 4. High resolution TEM on sample OB461 showed wells of thickness  $140 \pm 5 \text{ \AA}$ . The composition of material in the wells was calculated from XRD to be  $\text{In}_{0.525}\text{Ga}_{0.475}\text{As}$ . Bulk InGaAs of this composition is expected to exhibit a bandgap of 0.735 eV ( $\lambda=1.687 \mu\text{m}$ ) if it is unconfined [13]. However, the PL peak at  $1.58 \mu\text{m}$  in OB461 corresponds to a shift in energy of 50 meV due to quantum confinement.

In the case of OB440, bulk material of the same composition as that used in the wells ( $\text{In}_{0.586}\text{Ga}_{0.414}\text{As}$ ) had a bandgap of 0.705 eV ( $\lambda=1.759 \mu\text{m}$ ). The PL peak in OB440 occurs at  $1.66 \mu\text{m}$  i.e. a shift of 44 meV.

The second important feature of the PL spectra is the linewidth. In fig.4 values of 75 nm and 112 nm were observed, which are considerably lower than those observed for LPE GaInAsP layers emitting at the same wavelength (typically 130-150 nm for  $1.5 \mu\text{m}$  GaInAsP)

Low temperature PL ( $T=5K$ ) of 30 period structures have yielded exciton linewidths as low as 5.5 meV. This narrow linewidth implies that the composition of the InGaAs within each well and from well to well is very homogeneous. This also confirms the evidence from satellite peaks observed in double crystal XRD that the periodicity of the structure is extremely regular with abrupt interfaces.

### 2.5. Growth of MQW Material by LP-MOVPE

During the course of the program, a second MOVPE apparatus was commissioned for the growth of InP based materials at reduced pressure (nominally 200 mbar). Work on other programs had developed similar capabilities on this reactor to those achieved by AP-MOVPE. InP doping calibrations for n- and p-type guide layer carrier concentrations of  $n=1.10^{18} \text{ cm}^{-3}$  and  $p=7.10^{17} \text{ cm}^{-3}$  were employed, using  $\text{H}_2\text{S}$  and dimethylzinc respectively as the dopant sources. Growth conditions which had been established for lattice matched InGaAs epitaxial layers with double crystal XRD FWHM as low as 19 arc secs were also used. (The crystallinity of this alloy prepared by LP-MOVPE is superior to that achieved by using the AP-MOVPE reactor which regularly produces material of FWHM ca.40 arc secs.)

In order to characterise quantum well structures grown in the low pressure reactor, a 30 period MQW test structure with nominally 100Å InGaAs wells and 350Å InP barriers was grown (OE 61). Conventional cross-sectional TEM investigation of this structure gave well and barrier thicknesses of 95Å and 350Å respectively which were uniform throughout the structure. In particular, the planarity of the InGaAs/InP interfaces was equal to that of the InP/InGaAs interfaces, which was not the case for material prepared by AP-MOVPE.

The fourth order rocking curve for this structure is shown in Fig.5. Very intense, sharp satellite peaks are observed to the third order, indicating the highly periodic nature of the structure with abrupt interfaces. The 'well plus barrier' period is calculated to be 425Å from the angular separation of the higher order diffraction peaks (c.f. 445Å by TEM-see section 2.6).

Low temperature PL investigation of OE 61 produced linewidths as low as 5.0 meV. Initial characterisation suggested a more well defined 2-D structure in the absorption spectra for material grown at atmospheric pressure compared

to equivalent material grown at low pressure (Figs.6 and 7). However, subsequent spectra from OE61 (30 MQW structure) resolved the  $n=1$  light hole (Fig.8), which had not previously been resolved in similar material grown at atmospheric pressure.

It was concluded from these characterisation techniques that the crystallinity, periodicity and interface planarity of MQW structures prepared by LP-MOVPE were superior to those of similar structures grown by AP-MOVPE. The reproducibility of material from the low pressure reactor was also considered to be an improvement over AP-MOVPE, once the material uniformity had been studied (section 2.6).

## 2.6. Growth of Laser Structures by LP-MOVPE

Subsequent to wafer OE 61, a DH (InGaAs active layer) and a MQW laser structure were prepared. These wafers were mismatched by +0.16% and +0.2% respectively with respect to the InP substrate. This mismatch was considerably worse than that measured for OE 61 (0.015%) and was attributed to an instability of source temperature control. Repeat growths produced material within mismatch specification at +0.031% for the MQW laser and -0.031% for the DH laser. Room temperature DH lasing threshold current densities of  $\sim 3.5 \text{ kA.cm}^{-2}$  indicated the suitability of the material for MQW lasers.

8 well MQW InGaAs/InP laser wafers with thinner barriers were grown. Prior to preparing these wafers, a 30 period MQW test structure was grown with nominally 100Å thick wells and 400Å thick barriers. The thickness uniformity in the reactor cell was assessed by double crystal XRD, and the 'well plus barrier' period calculated. As shown in Fig.9, the period varied between 480Å and 550Å, with the thicker material being 'upstream' of the gas flow in the reactor. This result was consistent with bulk growth rate trials which indicated thickness variations of  $\pm 5\%$  for InGaAs and  $\pm 10\%$  for InP over the same 2" length of the reactor ( $T_g=650^\circ\text{C}$ ).

Two laser structures were grown with nominal InP barrier thicknesses 50Å (OE 240) and 30Å (OE 241). Well thicknesses were nominally 110Å for both wafers. Cleaved corner edge TEM near the centre of each wafer gave measured well/barrier



thicknesses as 115/54Å and 100/26Å respectively. Thicknesses in other areas of the wafer can be deduced from the uniformity study. Double crystal XRD of the InGaAs cap layer indicated the mismatch to be less than 0.01% for both wafers.

## 2.7. Transverse Injection MQW Lasers

Transverse injection laser source wafers were grown to investigate possible improvements in carrier uniformity across multi-well structures. 8 well InGaAs/InP wafers were prepared by LP-MOVPE. In addition, a single DH transverse injection source wafer and a MQW laser of nominal well/barrier thicknesses 110/150Å, were grown by AP-MOVPE. Cleaved corner edge TEM measurements gave thicknesses of 75/150Å with some variability in evidence for the barriers.

Wafers grown by LP-MOVPE featured nominally 110Å thick wells. The first wafer (OE 242) contained nominally 125Å thick barriers. In the second wafer the barriers consisted of: 50Å undoped InP; 50Å p-InP ( $p=7.10^{17} \text{ cm}^{-3}$ ); 50Å undoped InP. Both structures were shown to be lattice matched to within  $\pm 0.05\%$ , with measured well/barrier thicknesses near the centre of each wafer of 103/119Å and 109/183Å respectively.

## 2.8. Growth and Characterisation of GaAlInAs

The use of a combination of InP and/or AlInAs outer guide layers with different GaAlInAs quaternary alloys for active, barrier and inner guide layers represents the favoured approach to achieving M-MQW and GRIN-SCH MQW lasers.

Preliminary studies of GaAlInAs lattice matched to InP were attempted by AP-MOVPE. However the ability to grow highly crystalline AlInAs (double crystal XRD FWHM of ca. 20 arc secs) lattice matched to InP by LP-MOVPE resulted in the majority of quaternary work being investigated by growth at low pressure. This study has been supported by materials research carried out on other parallel programs.

Aluminium containing compounds have a higher lattice energy than those

containing Gallium and Indium. As a consequence, a higher growth temperature ( $T_g=680^{\circ}\text{C}$  to  $710^{\circ}\text{C}$ ) is required for GaAlInAs than for InGaAs ( $T_g=650^{\circ}\text{C}$ ) to achieve good crystallinity and surface morphology. In order to prepare device structures at a constant temperature and avoid the need to pause growth whilst the substrate temperature is changed, a growth temperature of  $680^{\circ}\text{C}$  was determined to be compatible for the successful deposition of layers both with and without Aluminium.

Lattice matching of GaAlInAs to InP was regularly achieved to less than 0.1% as characterised by double crystal XRD e.g. fig.10 ( $\Delta a/a = -0.086\%$  and  $+0.03\%$ ). The material was highly crystalline with XRD FWHM as low as 22 arc secs.

Fourier Transform Infra-Red Spectroscopy (FTIR) studies of GaAlInAs revealed abrupt band-edge cut-off (Fig. 11); low temperature PL linewidths as low as 5.2meV were attained. These results are comparable with the best reported by any growth technique.

A wide range of quaternary compositions lattice matched to InP are required for preparing M-MQW and GRIN-SCH laser structures. Fig. 12 illustrates the range achieved to date. Bandgap energy (determined by FTIR cut-off) is plotted as a function of Aluminium content (determined by electron probe microanalysis). Our results [14] broadly follow the trends reported by other laboratories for MBE material [15, 16], as indicated in the graph.

In order to assess the quality of our GaAlInAs and its suitability for inclusion in the active region of a MQW laser, a simple DH laser source wafer with a quaternary active layer was prepared (OE 280). The wafer consisted of p- and n-type InP guide layers (as previously described), a nominally undoped 1500Å thick active layer, and a 1500Å thick p-InGaAs contact layer ( $p=10^{19}\text{ cm}^{-3}$ ). The active layer composition was determined from a thick single epitaxial layer grown immediately before the laser wafer. An abrupt FTIR band-gap cut-off of  $\lambda=1280\text{ nm}$  was measured. XRD of the laser structure showed a mismatch of -0.07%.

## 2.9. InGaAs/AlInAs MQW Structures

The use of  $\text{Al}_{0.48}\text{In}_{0.52}\text{As}$  (lattice matched to InP) was investigated as an alternative to InP for both guide and barrier layers. The advantages of AlInAs (which has a larger band-gap than InP) include improved current confinement at the active-guide hetero-interface, and the relaxation of the required well width for a given device emission wavelength (due to the increased energy shift).

An initial study of AlInAs was made by AP-MOVPE. A structure with variable InGaAs well widths (5 wells between 50Å and 200Å thick), with 2000Å thick AlInAs barriers was compared with a similar structure utilising InP barriers. PL spectra plotted at 5K showed that improvements in linewidth and intensity had been obtained by using AlInAs. TEM investigations showed that AlInAs/InGaAs and InGaAs/AlInAs interfaces were of equal planarity, whereas the use of InP produced 'rippled' interfaces by AP-MOVPE as previously described. This improvement had been achieved by eliminating the requirement for switching the different group V elements, As and P, at the well/barrier interfaces. 8 well MQW lasers containing AlInAs barriers (08385 and 08387) and a DH laser with AlInAs guide layers grown by AP-MOVPE, demonstrated higher than expected turn-on voltages ( $>6\text{V}$ ) and residual resistive characteristics (30-50 $\Omega$ ). This is possibly the result of residual oxygen contamination within the AlInAs layers in the atmospheric pressure system.

Development of AlInAs was subsequently continued by LP-MOVPE, which had demonstrated substantially superior material to that produced by AP-MOVPE (as indicated by XRD FWHM of single epitaxial layers). Doping levels were calibrated using  $\text{H}_2\text{S}$  and DMZ as the n- and p-type dopant sources respectively. A DH laser wafer (OE360) with a nominally 1500Å thick InGaAs active layer was grown. 1 $\mu\text{m}$  thick n-type ( $\text{ca. } 10^{18} \text{ cm}^{-3}$ ) and 1.5 $\mu\text{m}$  thick p-type ( $\text{ca. } 2 \cdot 10^{18} \text{ cm}^{-3}$ ) AlInAs guides were used. A lattice mismatch of 0.01% was determined from XRD assessment of the wafer.

### 3. PREPARATION AND CHARACTERISATION OF DH AND MQW LASERS

Detailed results for lasers prepared and characterised during the first twelve months of the program were previously given in the interim report covering the period September 1985 to September 1986. For completeness, some of those results are also reproduced below.

#### 3.1 Preparation of MOVPE InGaAs/InP DH Lasers

In order to test the electrical and optical properties of the MOVPE source material, first pass laser diodes were prepared with simple oxide isolated structures as shown in Figure 13. Oxide isolated laser chips, 250 $\mu$ m long and 300 $\mu$ m wide were prepared. Devices featured either 10 $\mu$ m or 100 $\mu$ m wide electrically active regions which were arranged by photoengraving and etching windows in the oxide isolation layer deposited prior to depositing the TiZnAu p-metallisation on top of the p-InGaAs cap. Wafers were thinned to 65 $\mu$ m and then an n-metal contact of InGeAu was evaporated and defined with a bare 100 $\mu$ m wide window positioned directly over the active pumped stripe. This allows for the assessment of material uniformity by observing the spontaneous emission emitted from the active stripe during electrical excitation. Also, the window allows access for assessing the DH and MQW lasers under optical excitation.

After preliminary assessment for current/voltage and light/current characteristics, selected devices were bonded p-side down onto gold plated submounts to enable more detailed characterisation to be carried out. Such lasers, featuring bulk InGaAs active layers were successfully prepared: initially from material grown by AP and then subsequently LP MOVPE. Minimum threshold current densities for material grown by AP MOVPE were 3.6kA.cm<sup>-2</sup> at room temperature for broad area 100 $\mu$ m wide, 250 $\mu$ m long devices. Typical lasing characteristics are given in Figure 14. Observed  $T_0$  values were in the region of 50-60 K over the temperature range 200-300°C. Minimum room temperature threshold current densities achieved for device material grown by LP MOVPE were similar at 3.5kA.cm<sup>-2</sup>.

### 3.2 Preparation and Characterisation of Advanced Index Guided DH InGaAs Lasers

Two types of index guided DH lasers featuring additional current and optical confinement layers were fabricated during the period. Both types were of a double channel planar buried heterostructure (DCPBH) design, the first implemented using LPE infill, and the second by high purity VPE. Threshold currents achieved for particular slices were 70mA and 30mA respectively with efficiencies up to 30% per facet which is indicative of good quality source material. Structures and light current characteristics are given in Figures 15 and 16. The VPE infill structure offers a simpler fabrication process and an increase in frequency response due to its inherently lower capacitance.

Wavelengths for both gain and index guided InGaAs lasers were measured. Results showed wavelengths ranging from 1.58-1.65 $\mu$ m, which was due to slight lattice mismatch in some slices. However, these structures demonstrated that the MOVPE growth capability had advanced sufficiently to enable first pass quantum well devices, designed within the existing laser modelling program to be prepared.

### 3.3 Preparation and Characterisation of Broad Area InGaAs/InP MQW Lasers

#### 3.3.1 Introduction

During the term of the quantum well laser research program, a wide range of alternative designs and structures for achieving low threshold, room temperature long wavelength MQW lasing action were investigated. Source wafers were grown initially by AP and then by LP MOVPE which as described in section 2 proved to produce superior quality quantum well layers. Different broad area devices prepared included oxide isolated lasers with both conventionally doped InP guides (Figure 17) and those with the outer guide layers close to each side of the active region (~500Å) left intentionally undoped in order to test for reduced IVBA loss, by reducing potential dopant diffusion from the guides into the active region.

As our theoretical model matured and further device characteristics, both by electrical and optical pumping, were obtained, it became clear that the main cause for first pass devices not achieving low threshold, room temperature operation in multi-well lasers was that of non uniform carrier pumping across the wells. Hence oxide isolated and buried ridge (BR) InGaAs/InP MQW lasers with reduced barrier thicknesses, and novel Transverse Injection BR lasers, both aimed at achieving more uniform carrier pumping across the wells were investigated. At this stage, due to its inherently better uniformity, source material was grown exclusively by LP MOVPE. However, AP MOVPE was used for the ridge overgrowth where relevant (sections 3.4 and 3.5)

### 3.3.2 Characterisation of Broad Area "thick barrier"(>100Å) InGaAs/InP MQW Lasers under Electrical Injection

Lasing action was achieved for first pass oxide isolated AP MOVPE 8-well MQW devices under pulsed current drive conditions at reduced temperatures. Nominal well and barrier widths were 110 and 100Å respectively. Generally, pulse lengths of 50-150ns were employed with duty cycles ranging from 0.01 to 1%. Maximum operating temperatures were found to be ~240K at which the pulsed threshold current density was  $\sim 15\text{kA.cm}^{-2}$  reducing to  $4\text{kA.cm}^{-2}$  at 80K (Figure 18).  $T_0$  values were found to be between 65 and 90K for temperatures <220K reducing to 35K for temperatures >220K (figure 19). Corresponding emission wavelengths as measured in the range of 169-210K were  $1.59\mu\text{m}$ . The lasing spectrum of MQW device OB296#11 (AP MOVPE) taken at 159K under pulsed drive (1.2A, 10%duty cycle) is given in figure 20. This wavelength was somewhat longer than expected and was attributed to slight lattice mismatch together with some variation in the quantum well width across the slice.

Subsequently, similar 8-well oxide isolated lasers were prepared by LP MOVPE. The light/current characteristics for second pass lattice matched LP MOVPE MQW lasers are shown in figure 21. Lasing action was achieved at temperatures up to 230K at which the threshold current density for the  $100\mu\text{m}$  wide,  $375\mu\text{m}$  long device shown was  $3.2\text{kA.cm}^{-2}$  thus confirming the improved quality of LP MOVPE MQW source

layers compared to those grown by AP MOVPE. Plots of the threshold current versus temperature for a range of MQW and DH devices grown by LP MOVPE are shown in figure 22. A broad range of  $T_0$  values were obtained over the temperature range 150-250K being 43 and 59K for the two MQW laser characteristics and 63 and 106K for the DH devices.

### 3.3.3 Investigation of MQW and DH Lasers by Optical Pumping

To test the hypothesis that non-uniform carrier pumping across the wells was a major contributor to the high threshold currents observed (section 4), and in order to pump the wells more uniformly, typical MQW (and DH) lasers were investigated under optical pumping at room temperature. As shown in figure 23, light from a Q-switched 1.06 $\mu$ m Nd-YAG laser was focussed through the n-contact window of the semiconductor laser under test. Optically pumped, the light emitted from the laser facet was collected through a microscope objective and directed into a grating spectrometer/detector. Conventional 1.55 $\mu$ m wavelength GaInAsP active DH and InGaAs/InP MQW lasers with 5 to 30 wells were investigated in this manner. The general form of the input and output laser characteristics are shown in figure 24. Typical light output versus input optical pump intensity plots for 8-well AP and LP MOVPE InGaAs/InP MQW devices and a conventional 1.55 $\mu$ m GaInAsP DH laser are shown in figures 25-27. Similarly, a plot showing the room temperature optically pumped lasing spectrum of a 5-well (85Å wide wells) device, showing a peak emission at 1.471 $\mu$ m is presented in figure 28. Details of first pass quantitative results for DH and InGaAs/InP MQW lasers with 5 to 30 wells are given in table 3. As discussed previously [19] by assuming an absorption coefficient of  $3.5 \cdot 10^4 \text{ cm}^{-1}$ ,  $I_{th}$  optical may be inferred from  $J_{th \text{ opt.}} = P \cdot \exp(-\alpha d) / E$ .

Here  $P$  is the incident optical power density,  $d$  the total active layer thickness and  $E$  the incident photon energy.

Device No.	No. of Wells	Total active thickness	Fraction of laser pulse absorbed	Optical lasing threshold power density	Inferred threshold current density
OB482B#38	30	Nominally 3300Å	73%	3.0kW.cm <sup>-2</sup>	1.3kA.cm <sup>-2</sup>
OB296#19	8	Nominally 880Å	30%	16.0kW.cm <sup>-2</sup>	2.9kA.cm <sup>-2</sup>
OB685#30	5	440Å(TEM)	17%	31.7kW.cm <sup>-2</sup>	3.2kA.cm <sup>-2</sup>
OE132#49	8	1024Å(TEM)	35%	4.0kW.cm <sup>-2</sup>	840A.cm <sup>-2</sup>
G110#9	1.55µm DH grown by LPE	Nominally 1500Å	46%	4.0kW.cm <sup>-2</sup>	1.kA.cm <sup>-2</sup>
Absorption coefficient $\alpha = 3.5 \times 10^4 \text{cm}^{-1}$					

TABLE 3: Threshold current densities under optical injection for a range of MQW and DH lasers

As shown, room temperature lasing action was achieved for devices under optical excitation over the whole range investigated with minimum inferred threshold current densities for the more optimised 8-well structures of 840A.cm<sup>-2</sup>. This contrasts strongly with the results obtained for MQW lasers under electrical injection as given in section 3.3.2 (best threshold current densities for 8-well MQW lasers of 3.2kA.cm<sup>-2</sup> at 240K and no lasing action observed for 30 well structures up to 10kA.cm<sup>-2</sup>). Hence these experimental investigations gave strong confirmation of our modelling studies regarding the potential effects of non-uniform carrier pumping. A series of source growths was therefore initiated for 8-well InGaAs/InP MQW lasers featuring the same, nominally 110Å wells for 1.55µm operation but with thinner, nominally 50 and 30Å barriers (compared to previous standard 100Å InP barriers).



### 3.3.4 Additional Studies of Non Uniform Carrier Capture

Parallel studies of carrier equilibration across MQW structures have also been carried out at Oxford University in conjunction with Plessey Research Caswell on material provided on other programs. At Oxford, optical time of flight techniques with picosecond resolution have been used to study time resolved photoluminescence. In these experiments, a frequency-doubled mode-locked Nd:YAG laser is used to synchronously pump an R6G dye laser at 607nm. Part of the laser beam is used to excite luminescence from the sample, and part taken via a variable time delay line and focussed colinearity with the luminescence into a  $\text{LiIO}_3$  crystal. The sum frequency of the laser and PL is, therefore, only generated when the delayed laser pulse arrives at the crystal. Hence, by varying the delay time, the intensity of luminescence as a function of time can be recorded [17]. It has been found that carrier capture efficiencies for quantum wells increase from ~20% at 4K to ~80% at 200K largely as a result of the reduction in mean carrier velocity. A capture time ~4ps is observed over a wide temperature range which suggests that in a MQW structure the majority of the carriers may be captured within the first few wells at normal operating temperatures and hence would not uniformly pump a multi-well structure.

One difference in the above experiment as compared to a laser operation is that optically excited carriers, created at the surface of the material under test due to the high energy laser pulse, reach the wells by ambipolar diffusion. This is in contrast to the laser situation where electrons and holes are injected from opposite sides of the active wells. Broadly speaking the experiment measures the capture efficiency of the slower species, i.e. the holes. Furthermore, the capture efficiency will be well width dependent in a non-trivial way as a result of resonances in the LO-phonon emission rate as a function of well width [18,19].

From the above experiments and our own observations, very efficient capture is indicated such that preferential hole capture must occur. A theoretical model has been developed to describe these effects and this is discussed in section 4.4 below.

### 3.3.5 Characterisation of Broad Area "thin barrier" (<100Å) InGaAs/InP MQW Lasers under Electrical and Optical Injection

Following the confirmation of our modelling studies concerning non uniform carrier pumping across multi-well systems, additional two source wafers were prepared featuring nominally 110Å InGaAs wells but different thickness, nominally 55 and 30Å, InP barriers. Results obtained for nominally 100, 55 and 30Å barrier oxide isolated MQW lasers under electrical and optical pumping are summarised in table 4, which includes barrier thicknesses for each wafer as found by subsequent TEM studies.

BARRIER THICKNESS (Å)	OPTICAL PUMP INTENSITY	THRESHOLD CURRENT DENSITY (Amps.cm <sup>-2</sup> )	
(Cleaved corner Edge TEM)	(kW.cm <sup>-2</sup> )	INFERRED OPTICAL J <sub>th</sub> (Opt) at 20°C	ELECTRICAL J <sub>th</sub> (Elec)
100	4	1100	3500 at -40°C
54	3	820	8000 at -12°C
26	3.3	700	3200 at +20°C

TABLE 4 Threshold current densities under optical and electrical injection for 8-well InGaAs/InP MQW lasers: nominally 110Å wells, variable thickness barriers

As can be seen, a clear trend towards reduced lasing thresholds and higher temperature operation under electrical injection is evident for devices featuring thinner barriers. In contrast, no significant difference, within experimental error was found for the inferred optically pumped threshold current densities. However, it may be noted that the  $700\text{A.cm}^{-2}$  threshold current density inferred for the  $25\text{\AA}$  barrier device represents a demonstration of the lowest threshold yet reported for  $1.55\mu\text{m}$  MQW laser operation under optical excitation.

As shown in table 4 and figure 29, electrically pumped room and elevated temperature lasing of devices with  $25\text{\AA}$  barriers was achieved. Electrically pumped lasing characteristics for one such device, measured over the temperature range of  $-50$  to  $+50^\circ\text{C}$  are shown in the figure. The room temperature lasing threshold corresponds to a threshold current density  $J_{th}$  of  $3.2\text{kA.cm}^{-2}$ . The above values are lower than the best threshold current density,  $3.5\text{kA.cm}^{-2}$ , observed for InGaAs DH devices previously prepared on this program and grown on the same LP MOVPE apparatus.

A plot of the electrically pumped threshold currents of the same MQW device versus temperature, shown in figure 30, gives  $T_0$  to be  $69\text{K}$  across the whole temperature range which is higher than  $T_0$  values observed for more conventional long wavelength DH devices. The peak emission wavelength was found to be  $1.544\mu\text{m}$  as shown in figure 31 which is consistent with our theoretical modelling studies, hence confirming the 2-D nature of the Quantum Well system.

Investigations into the performance of nominally  $50\text{\AA}$  thick InP barrier devices showed no lasing action for drive currents up to  $10\text{kA.cm}^{-2}$ . However, devices did exhibit lasing action at reduced temperatures of  $\sim -10^\circ\text{C}$  (higher than that for  $100\text{\AA}$  barrier devices) at which the threshold current densities were  $\sim 8\text{kA.cm}^{-2}$ . The above results therefore represent confirmation of our previous experimental and theoretical studies which suggested preferential hole capture to be partly responsible for the excessive threshold currents observed for previous devices

with thicker, 100Å barriers. As a reminder, previous best devices with 100Å barriers showed highest operating temperatures of  $\sim -40^{\circ}\text{C}$  with lasing threshold current densities of  $3.5\text{kA.cm}^{-2}$  at this temperature. Above this temperature lasing efficiency decreased rapidly, such that a threshold could not be observed.

### 3.4 Preparation of Transverse Injection MQW and DH Lasers.

As given in section 2.7, source slices suitable for preparing transverse MQW (and DH control) devices, aimed at providing an alternative means to employing thinner barriers for improving the injected carrier uniformity across multi well structures, were also grown by AP- and LP-MOVPE. Although good 2-D lasing characteristics were obtained by employing thinner barriers, as discussed above, due to the nature of the structure, employing progressively thinner barriers will ultimately degrade the Quantum Well laser performance. Hence the transverse injection laser design, employing thicker  $>100\text{\AA}$  barriers, offers the potential of achieving lasing action in MQW devices without in any way compromising the 2-D nature of the structure. To investigate potential device benefits offered, a slice each of MQW and DH laser source material grown by AP-MOVPE, were processed into transverse stripe injection devices as illustrated in fig.32.

Current/voltage characteristics for both DH and MQW transverse injection lasers showed some variability with diode switch-on voltages of  $\sim 0.4$  to  $0.9\text{V}$ . Preliminary investigations on bonded devices showed a low yield of room temperature, CW lasing InGaAs DH lasers with minimum thresholds of  $30\text{mA}$  at  $20^{\circ}\text{C}$ . The peak wavelengths for two devices tested were  $\sim 1.64$  and  $1.65\mu\text{m}$  respectively. No lasing action was observed for the MQW devices at room temperature. Lasers from both wafers tended to show evidence of additional InP emission along the active stripe, as viewed through the n-contact window, suggesting excessive current leakage through the parallel InP blocking layers due to insufficient conductivity through the DH active layer and MQW barriers and wells. Improved second pass MQW designs featuring spiked doped barrier layers aimed at improving the transverse injection were planned though due to the timescale and success of the thinner barrier structures, no further devices were processed.

### 3.5 Preparation and Characterisation of CW Buried Ridge Waveguide InGaAs/InP

#### MQW Lasers

Following the successful preparation of room temperature lasing 'thinner barrier' InGaAs/InP MQW oxide stripe lasers, index guided Buried Ridge structures were prepared using the same 8-well active layer with 100Å wells and 25Å barriers. A schematic of the structure is shown in figure 33. Active mesa ridges, 1.5-2µm wide were defined and etched using standard photographic resist and wet etch techniques and the wafer subsequently overgrown by Atmospheric Pressure MOVPE. Variable length lasers were then processed and cleaved and scribed to size. Room temperature cw lasing was achieved with threshold currents as low as 60mA and efficiencies as high as 30% per facet implying high internal efficiency and low cavity loss. Typical light current characteristics are shown in figure 34. To our knowledge, no report prior to this has yet been given in the literature regarding room temperature cw operation of InGaAs/InP MQW lasers. The peak emission wavelength as shown in figures 35, and 36 was 1.53µm, consistent with that expected for 100Å InGaAs wells.

Figure 37 shows the buried ridge MQW lasers to have in general good far field emission characteristics in the plane of the active region with FWHM of ~20°. Some devices showed evidence of multimoded far fields which was attributed to too wide an active region, later confirmed by SEM studies, an artifact of too thick a p-InP guide layer on these first pass devices.

Selected lasers of the above design were bonded onto submounts and into a full module for final deliverables. The characteristics for these devices, delivered to DOD, RAOC, Hanscom, March 1988, are given in Appendix 1. The coupling efficiency for an MQW buried ridge laser into 50µm core fibre is shown in figure 38.

#### 3.6 InGaAs/InP MQW Laser High Frequency Response Characteristics.

In addition to lower lasing thresholds, increased  $T_0$  and material independent wavelength tuning, a further predicted advantage of 2-D Quantum Well Lasers is that of higher frequency response over conventional DH lasers due to an increased gain slope. Hence, the resonant frequency of a number of 8-well cw InGaAs/InP MQW devices were investigated over a range of cw drive currents. A typical series of small signal (Modulated Power Output)<sup>2</sup> vs Frequency plots is shown in figure 39. The same data is replotted as (Resonance Frequency)<sup>2</sup> vs

Drive Current in figure 40. Resonance frequencies in excess of 4GHz were observed for the 500 $\mu$ m long devices. As shown, some roll-off of the resonance frequency is observed for frequencies in excess of 4GHz which is due to the effect of chip parasitics in this structure. Initial comparison of these results with those of our 1.55 $\mu$ m DH DFB lasers suggests an increase in gain slope by a factor of between 1.5 to 2 in favour of the MQW devices. The effect is somewhat masked in current devices due to the limiting operating range above threshold and the relatively large parasitic capacitance of the BR device. The variable factor observed may in part be due to the variability in gain slope found for DFB lasers which depends on the matching of the grating wavelength with the spontaneous emission spectrum of each device. Hence further comparative work with DH devices of the same type is required to fully assess any improvements gained.

A plot of the large signal high frequency response for a second device showing a good high data rate performance at 2Gbit/s is shown on figure 41.

### 3.7 Characterisation of GaAlInAs Active DH Oxide Stripe Lasers

As described in section 2.8, a single source wafer suitable for preparing oxide isolated GaAlInAs active layer DH lasers aimed at 1.3 $\mu$ m wavelength operation was grown during the program. Oxide stripe lasers with 10 and 100  $\mu$ m wide active stripes were then successfully prepared (for the first time using GaAlInAs grown by MOVPE) and devices characterised. Room temperature pulsed lasing action has been achieved for these devices with minimum threshold currents of 340mA for a 10 x 250 $\mu$ m<sup>2</sup> stripe device. The lowest threshold current density  $J_{th}$ , observed for a 100 x 250 $\mu$ m<sup>2</sup> device was 4.8kA.cm<sup>-2</sup>. Typically,  $J_{th}$  values were 6.4kA.cm<sup>-2</sup>. Light current characteristics as a function of temperature for a 10 $\mu$ m wide stripe device are presented in figure 42. Here, the total output power is an over-estimate of the front facet emission by ~ 25% due to reflections directed from the rear of the package, coupled with the use of a large area detector. As shown in figure 43 a  $T_0$  value of 85-96K is inferred which may be compared with approximately 65K expected for 1.3 $\mu$ m wavelength lasers with GaInAsP active layers. The lasing spectrum shown in figure 44 shows the peak emission to be ~ 1.24 $\mu$ m which is in close agreement with the photoluminescence and FTIR characteristics reported in the 8th quarterly report for first pass lattice matched single layer materials. Further device results for additional delivered devices are presented in Appendix 1.

## 4. DESIGN AND MODELLING STUDIES

### 4.1 Introduction

Here an overview of the contributions made by the modelling and design work during the course of this program is given. This falls into three main areas of activity which have already been discussed at some length in the quarterly reports as indicated below :

- (1) Device design and optimisation [20,21,22]
- (2) Modelling of carrier collection effects in MQW structures [21,23]
- (3) Analysis of spontaneous emission spectra [23]

A detailed technical discussion of the first two items above is to be found separately in the final Modelling and Design report, so that here the main results of the work are reviewed without discussing details of the models involved. The development of the computer models for QW lasers described below has been carried out as part of other supporting programs of work. Particular to this program has been the utilisation of this background both to support device design and optimisation studies, and in the interpretation of the experimental results.

### 4.2 Quantum Well Laser Model

For completeness a flow diagram of the computer program structure is given in Figure 45. This necessarily presents a simplified view but it indicates main input data : the layer structure adopted, temperature  $T$ , broadening energy  $\Delta E$  and loss rates ( $\alpha_L$ ), and the device parameters simulated : Threshold current ( $J_{th}$ ),  $T_0$  parameter, linewidth enhancement factor ( $\alpha$ ) and gainslope ( $dg/dn$ ). A separate solution of the scalar wave equation yields the optical overlap ( $\Gamma$ ) with the electrically active quantum wells for a given layer structure. The present calculation of the spontaneous and stimulated emission rates adopts a lifetime broadened k-selection model. In addition, optical matrix elements which take into account the different selection rules for transitions involving light or heavy holes for TE or TM modes in a 2D system are also included [24]. In these

respects the model is similar to that of Asada et al [25]. Unless special steps are taken to select the TM mode, a quantum well laser, as a 3D double heterostructure laser, will naturally adopt the TE mode since this mode has the highest net gain, and the calculations described below are restricted to the TE case. The temperature sensitivity  $T_0$  of a laser for 1.3-1.55 $\mu\text{m}$  operation is largely determined by the Intervalence Band Absorption (IVBA) and Auger recombination processes, and this point is discussed in detail below. The exact balance of emphasis between the two processes remains a matter of some debate in the literature, as it did at the outset of this program. The most recent publications in this field [26,27] suggest that these processes have only a weak well width dependence over the range of interest here and that the rate constants are close to the values found in the bulk. Here the transition rate constants are assumed independent of well width and treated as additional parameters within the device simulation. The predicted device performance has then been investigated as a function of these parameters.

#### 4.3 Device Design and Optimisation

Predicted threshold currents and temperature sensitivity parameter  $T_0$  at 300K for a 1.55  $\mu\text{m}$  InGaAs/InP MQW laser are given in figures 46,47 and 48 as a function of the number of wells ( $N_w$ ) in the system for broadening energies in the range 0-15meV. It is expected both from consideration of the different mechanisms contributing to the broadening and from studies of the spontaneous emission spectra of our devices that  $\Delta E \sim 10$  meV. Parameter values for these calculations are given in Table 5.

T	300K
B Auger	$10^{-28} \text{ cm}^6 \text{ sec}^{-1}$
$\alpha$ IVBA	$40 \text{ cm}^{-1}$ at $p = 1.0 \cdot 10^{18} \text{ cm}^{-3}$
$\alpha$ mirror	$45 \text{ cm}^{-1}$ Mirror loss for cleaved facets and a cavity length of 250 $\mu\text{m}$ )
L z	110A

TABLE 5 Parameters for device simulations of Figures 46 - 48



These curves clearly show the important effect broadening has in reducing the peak gain available and so increasing the threshold current density. In Figure 46 the total threshold current is plotted as a function of the number of wells for an InGaAs/InP MQW structure. In Figure 47 just that part of the total current which is due to spontaneous emission is given. The dominant role played by Auger recombination in determining the total threshold current is evident from a comparison of the two. It is also the Auger recombination which dominates the temperature dependence of  $J_{th}$  (figure 48). These lasers will always be operating in a regime where Auger recombination is the larger contribution to the current because of the non-zero band edge density-of-states in a quantum well and the cubic dependence of the Auger current on carrier density. The additional effect of IVBA, which depends linearly on the hole concentration, is found to be smaller in these simulations. In obtaining Figure 48 both the Auger coefficients and the IVBA loss were assumed to be temperature independent. This is a fair approximation for the former [28], but more open to question for the latter [29], so that the values for  $T_0$  in Figure 48 remain slightly optimistic but indicate that improvements over the bulk DH laser are to be expected. It is apparent from Figure 48 that  $T_0$  optimises for large numbers of wells whereas  $J_{th}$  is optimal for ~8-wells. This difference arises from the larger gainslope available at the lower threshold gain required for large  $N_w$ , which means that the relative change in carrier concentration with temperature is smaller. Less obviously, large broadening energies also lead to slightly larger predicted  $T_0$  values, but the total range of the curves in Figure 48 is only ~10K. The sensitivity of the predicted  $T_0$  to the assumed IVBA loss and Auger coefficients is considered in the limit of  $\Delta E=0$  in Figure 49. It is clear that in these MQW lasers it is the Auger recombination which dominates the temperature sensitivity, at least for values in the expected range which is,  $5 \cdot 10^{-29} \text{ cm}^6 \text{ s}^{-1}$  to  $1 \cdot 10^{-28} \text{ cm}^6 \text{ s}^{-1}$  [27,30].

The theoretically predicted  $J_{th}$  for the parameters of Table 5, is compared with those inferred from optical pumping experiments (section 3.3.3) in Figure 50. The pairs of curves in Figure 50 span the expected range for Auger recombination

and are given for  $\Delta E = 0$  meV and  $\Delta E = 10$  meV, and show a satisfactory agreement between theory and experiment. More work is required to fully compare results and fix materials parameters, but the indications from Figure 50 are that both the broadening and the Auger recombination lie towards the lower end of the expected range.

Various possibilities exist for altering  $J_{th}$  and  $T_0$  by altering the cavity length, facet reflectivity and (assuming a suitable outer confining layer structure can be grown) the optical confinement factor. By reducing the mirror loss, the threshold current density can be substantially reduced. This feature has recently been exploited in the GaAs/GaAlAs system to produce threshold currents of less than 1mA [31]. However, it appears that at long wavelength, although  $J_{th}$  is improved, there is no improvement in the associated  $T_0$  values. The reason for this is that the Auger recombination current remains dominant for carrier concentrations down to  $\sim 5 \cdot 10^{17} \text{ cm}^{-3}$  while the minimum carrier density at which (positive) gain can be obtained is determined by the band edge density of states and is  $\sim 10^{18} \text{ cm}^{-3}$  for well widths  $\sim 100 \text{ \AA}$ , so the Auger current always dominates and, as has already been discussed, this severely limits  $T_0$ . Sample results for  $\Delta E = 0$  meV, a reflectivity of 0.8, and a total loss  $\alpha_L = 20 \text{ cm}^{-1}$  are given in Figures 51 and 52 where a value of the optical confinement factor typical of a GaAs/GaAlAs GRIN-SCH structure has been used ( $\Gamma = 4 \cdot 10^{-4} \text{ \AA}^{-1}$ ) in anticipation of like structures for the InP based system. Under such favourable conditions threshold current densities similar to those for GaAs QW lasers (with cleaved facets) are predicted with single well operation. A design specification for a  $1.55 \mu\text{m}$  InP:InGaAs MQW-GRIN-SCH structure has been generated (Figure 53). The undoped graded cladding regions, width  $1500 \text{ \AA}$ , are to be composed of an InP:InGaAs effective alloy with period  $60 \text{ \AA}$ . The barriers within the active region are also composed of an effective alloy with 50% InP:50% InGaAs composition. This GRIN-SCH structure allows good optical confinement (about half of that leading to Figures 51 and 52) for a small number of periods in the active region, and initially a 3-well structure is proposed. In the longer term investigation of structures with 2-5 wells would be of interest.

Consideration has also been given to the design of 1.3 $\mu$ m QW lasers in the (Al<sub>x</sub>Ga<sub>1-x</sub>)<sub>0.48</sub>In<sub>0.52</sub>As system. Figure 54 gives a relationship between the well width and Al -content of the active region required to achieve lasing at a given wavelength on the basis of a simple model. Where a full device simulation is to be performed these curves would undoubtedly be modified but they indicate the range of options available in the (AlGa)InAs system. Simulations of InGaAs/InP multiple quantum well lasers ( $y=0$ ) for 1.3 $\mu$ m operation have been performed in the limit  $\Delta E=0$  (k-selection). As expected, these show higher threshold currents than their 1.55 $\mu$ m counterparts as a result of the larger 2D density-of-states which is proportional to the inverse well width. A carrier concentration of  $\sim 3 \cdot 10^{18}$  cm<sup>-3</sup> is required to satisfy the inversion condition so that the Auger recombination current is always large. The threshold currents (Figure 55) optimise for 10-15 30Å wells in the active region which may lead to additional problems with carrier redistribution. For these reasons it is anticipated that a 1.3 $\mu$ m QW laser in this material system would use an Aluminium content in the active region of  $y=5-10\%$  and well widths in the region of 50-100Å.

#### 4.4 Carrier Capture and Equilibration

The device results plotted in Figure 50 for the inferred threshold current density under optical excitation for 8-well and 30-well quantum well laser structures are comparable in magnitude. Under electrical injection, however, the 8-well structures display far lower thresholds compared with the 30-well structures than would be expected after other factors have been taken into account. The most obvious remaining difference between the two measurements is that optical pumping leads to the generation of electron-hole pairs directly within the wells but under electrical injection, electrons and holes are injected from opposite sides of the active region. Under electrical injection the distribution of carriers across a multiple well system may not be uniform, and will certainly depend upon the efficiency of carrier capture in the wells for the different carrier types. It was proposed therefore, that the preferential capture of holes within the first few wells of the structure could lead to an increase in the observed threshold currents as a result of a polarisation of the electron and hole populations, and a suppression of the optical transition rates. This problem is potentially far more severe in an InGaAs/InP MQW system than for example in GaAs/GaAlAs, because of the large effective mass of the holes and the

large valence band discontinuity ( $\sim 350\text{meV}$ ) which combine to yield very short decay lengths for the wavefunctions and very low rates for interwell transfer. A rate equation model has been developed to describe the effects of preferential capture which has been extensively discussed in [21,23]. A number of simplifying assumptions had to be made in order to make the problem tractable. However, useful quantitative results have emerged which have both confirmed the high penalty paid in terms of threshold current for structures with large numbers of wells, and guided our active region specification in such a way as to minimise the effect, culminating in the successful demonstration of room temperature CW laser operation in an MQW InGaAs/InP structure (section 3.5).

In order to promote carrier equilibration between a group of quantum wells the simplest route is to make the barriers between those wells thinner in order to enhance tunnelling currents. In the limit of course the structure will become three-dimensional so there will exist some optimal thickness of the barriers for which carrier tunnelling is sufficiently strong and yet the advantages of two-dimensional confinement are not lost. Measurements of the capture efficiency into a  $50\text{\AA}$  well have been performed by our collaborators at Oxford University [17]. The nature of these experiments has already been described in section 3.3.4. The observed time-dependence of the photoluminescence leads to an observed capture time of  $\sim 4\text{ps}$  into a  $50\text{\AA}$  well which is largely independent of temperature. For a quantum well laser a capture time  $\sim 4\text{ps}$  implies an inverse capture length ( $\alpha_p$ ) in the region of  $2.5 \cdot 10^6 \text{ cm}^{-1}$ , for an injected hole current in the region of  $3000 \text{ Amps.cm}^{-2}$ . The calculated relationship between threshold current and inverse capture length is plotted in Figure 56 for an 8-well system with an inverse tunnelling time between the wells of  $T \cdot 10^{-8} \text{ s}^{-1}$ . If  $\alpha_p \sim 2.5 \cdot 10^6 \text{ cm}^{-1}$ , then Figure 56 shows that room temperature lasing will be achieved only if  $T > 20$ , i.e. a tunnelling time of  $< 0.5 \text{ ns}$ . As can be seen from Figure 57 which relates the calculated tunnelling time to the InP barrier width, barrier thicknesses in the region of  $25\text{-}30\text{\AA}$  will be required to promote the necessary heavy hole transfer. At the same time this will lead to an additional penalty in the form of an  $\sim 5 \text{ meV}$  broadening due to the interaction of the electron state between the wells, which will lead to some degradation of the lasing characteristics via the broadening of the spectral gain.

Reducing the temperature increases the carrier lifetime, allowing an increase in the tunnelling time or, equivalently, an increase in the maximum barrier thickness allowable to achieve efficient carrier redistribution thus reducing the value of  $T$  for which lasing will be achieved. This trend is evident in our device results with  $100\text{\AA}$ ,  $54\text{\AA}$  and  $26\text{\AA}$  barrier devices showing progressively higher temperatures for lasing as shown in Table 4 of 3.3.5. The theoretical curves qualitatively confirm this trend, but detailed calculations of the temperature dependence have not been carried out. Within the context of material grown on this program, theory and experiment agree that thin barriers are a prerequisite to low threshold lasing in these structures a view which is corroborated by the published results of Temkin et.al. for AlInAs/InGaAs [5]. However, this cannot be a complete explanation since although threshold currents reported in the literature for 'thick barrier' devices have often been very high [32-34], in one case values comparable with DH InGaAs lasers have also been reported [7]. The value of barrier thickness obtained theoretically here is a lower bound since a number of potential feedback mechanisms have not been explicitly included. The assumption of electrical neutrality provides for strong redistribution of the electrons in the system, but the hole population will additionally be susceptible to the effects of optical feedback due to reabsorption of the optical mode in the under pumped wells, and the tunnelling of light holes will further promote carrier transfer. It is our view that a number of mechanisms combine to produce the observed device characteristics and it is clear that differential pumping will degrade device performance if the active layer is not designed to eliminate this effect.

#### 4.5 Spontaneous Emission Spectra

Measurements of the spontaneous emission spectrum can provide new information about the active region of a laser under forward bias conditions. In addition to the usual structural information, which determines the subband energies and the density of states, the spontaneous emission depends upon the carrier density induced in the active region and on the broadening mechanisms introduced by material fluctuations and many body interactions. Direct estimates of the Fermi-level separation i.e. the carrier concentrations, and the broadening

energy may be extracted by fitting the measured spectra, information which cannot easily be inferred from measurements of the lasing characteristics alone. The computer model includes broadening by a Lorentz function. It should be noted that, strictly, only the lifetime broadening should be introduced in this way. If fluctuations in the structural parameters such as the well width are described by averaging over a Lorentzian distribution then, additionally, weak factors depending on the well widths and the photon energy arise. In the first instance it is reasonable to assume that all of the contributions to the broadening may be lumped into a single effective energy broadening parameter. Lastly, in order to compare directly with experiment, it is necessary to include an estimate for the band gap narrowing as a function of carrier concentration. This has recently been measured for GaAs/GaAlAs QW lasers [35], and here a simple power law fit is used. The specific case of the layer number OE132 was analysed in some detail in [23]. The n-window electroluminescence spectra ([22] Figure 10) is reproduced here in Figure 58. In order to obtain a fit to this data the allowed domains for  $n$  and  $\Delta E$  were determined to be :  $n < 10^{18} \text{ cm}^{-3}$  and  $10 \text{ meV} < \Delta E < 15 \text{ meV}$ . A fit is given in Figure 58 for the case  $n = 5 \cdot 10^{17} \text{ cm}^{-3}$  and  $\Delta E = 15 \text{ meV}$ . It may be noted that the threshold carrier concentration for lasing in this structure is considerably higher than that apparently achieved, being  $\sim 2 \cdot 10^{18} \text{ cm}^{-3}$ . In Figure 58 the peak emission intensity has been normalised to the experimental curve. It is clear that, although the latter provides a reasonable fit, the measured emission spectrum is somewhat wider, and a substantially improved fit within the bounds of the two parameters discussed was not found. It was estimated that the contribution of self absorption and re-emission effects within the ternary capping layer contribute to no more than a few percent of the total emission. It has also been shown recently [36], that excitonic contributions to the spontaneous emission spectrum are important in GaAs/GaAlAs MQWs at carrier concentrations up to  $\sim 10^{18} \text{ cm}^{-3}$  where previously it had been believed that free carrier screening would have prevented exciton formation. Both of these effects would lead to a small enhancement of the long wavelength emission in the observed spectrum. The suggestion here is that the observed spectrum is in fact a composite of spectra for a series of quantum wells each having different carrier concentrations, just as would be found if preferential hole capture were present.

It is difficult to extract precise information concerning such an additional broadening. In [23] the effect on the simulated spectra was simply illustrated by consideration of a specific example with a series of wells with different carrier concentrations,  $n=1.25, 1.0, 0.75, 0.5$  and  $0.25 \times 10^{18} \text{ cm}^{-3}$  and  $\Delta E = 10 \text{ meV}$ . It was demonstrated that the resulting theoretical spectrum matched the shape of the experimental curve somewhat better than if a single carrier concentration was assumed.

In conclusion, a study of the spontaneous emission spectrum for OE132 has found an energy broadening of  $\sim 10\text{-}15 \text{ meV}$  for this material. Since lifetime effects can be assumed to contribute to about half of this total and alloy broadening in the InGaAs a further  $2\text{-}3 \text{ meV}$  [37] it appears that the contribution due to material fluctuations alone is relatively small, indicative of a high degree of structural uniformity within the layers.

## 5. CONCLUSIONS

During the course of the program a full range of materials, InP, InGaAs, AlInAs and GaAlInAs, necessary for the preparation of advanced M-MQW and GRIN-SCH lasers have been developed. Key results of the program, representing state-of-the-art technology, include:

- (i) The preparation of room temperature lasing, broad area InGaAs/InP MQW lasers.
- (ii) The preparation of low threshold, CW room and elevated temperature operation, all MOVPE InGaAs/InP Buried Ridge MQW lasers for the first time.
- (iii) The development of a comprehensive laser model predicting the behaviour of long wavelength quantum well lasers and generating optimum designs.
- (iv) The preparation, for the first time, of MOVPE grown GaAlInAs DH lasers for  $1.3 \mu\text{m}$  operation.

- (v) CW operation, 1.53 $\mu$ m wavelength InGaAs/InP MQW pigtailed module (1) and submounts (3) prepared, characterised and supplied to RADC, Hanscom. (Appendix 1).
- (vi) Additional GaAlInAs 1.24 $\mu$ m wavelength DH laser submounts (3) supplied (Appendix 1).

The above results demonstrate that the technology necessary for preparing optimised design M-MQW and GRIN-SCH lasers for 1.3 and 1.55 $\mu$ m operation has now been demonstrated. This will enable the investigation not only of optimised GRIN-SCH quantum well lasers for reduced threshold, high speed and high  $T_0$  operation but also the possibility of other low dimensionality structures including optical bistable devices based on the effects of preferential hole capture across multi well systems predicted by our theoretical studies. Future possibilities for advanced lasers based on quantum structures we are now able to address include:

- (i) The design and fabrication of GRIN-SCH structures for 1300nm wavelength operation. Target  $J_{th}$  500A.cm<sup>-2</sup>,  $T_0$  100K, with quantum well enhanced gainslope for enhanced high speed operation.
- (ii) The design and fabrication of 1300-1550nm wavelength laser structures using strained layer active regions to suppress IVBA and Auger carrier loss mechanisms. Target  $J_{th}$  150A.cm<sup>-2</sup>,  $T_0$  120K, together with enhanced speed as in (i) above.
- (iii) The investigation of laser structures with further reduced dimensionality using novel growth techniques aimed at achieving additional threshold current reductions.
- (iv) Research into bistable and all-optical switching devices based on quantum well structures. Target: to demonstrate electrically and optically induced bistability in quantum well laser structures.



## REFERENCES

- [1] Rezek E.A, Holonyak Jr. N, and Fuller B.K. 'Temperature dependence of threshold current for coupled multiple quantum-well  $\text{In}_{1-x}\text{Ga}_x\text{P}_{1-z}\text{As}_z$  heterostructure laser diodes ' (1980) J. Appl. Phys. 51 2402-2405
- [2] Dutta N.K, Napholtz S.G, Yen R, Brown R.L, Shen T.M, Olsson N.A, and Craft D.C, '1.3 $\mu\text{m}$  GaInAsP Multiquantum-well lasers' (1984) Electron. Lett. 20 727-728
- [3] Sasai Y, Hase N, Ogura M, and Kajiwara T, 'Fabrication and lasing characteristics of 1.3 $\mu\text{m}$  GaInAsP multiquantum-well lasers ' (1986) J. Appl. Phys. 59 28-31
- [4] Yanasi T, Kato Y, Mito I, Yamaguchi M, Nishi K, Kobayashi K, and Lang R '1.3 $\mu\text{m}$  GaInAsP/InP multiquantum-well lasers grown by vapour-phase epitaxy ' (1983) E1. Lett. 19 700-701
- [5] Temkin H, Alavi K, Wagner W.R, Pearsall T.P, and Cho A.Y, '1.5-1.6- $\mu\text{m}$  InGaAs/AlInAs multiquantum well lasers grown by molecular beam epitaxy ' (1983) Appl. Phys. Lett. 42 845-847
- [6] Matsushima Y, Utaka K, Sakai K, and Tateuchi O, ' Room-temperature CW operation of MBE-grown InGaAs/AlInAs MQW lasers in 1.5  $\mu\text{m}$  range ', (1987) E1. Lett. 23 1271-1273
- [7] Tsang W.T, 'Chemical beam epitaxial growth of very low threshold  $\text{Ga}_{0.47}\text{In}_{0.53}\text{As}$  /InP double-heterostructure and multiquantum well lasers' (1986) Appl. Phys. Lett. 49 1010-1012, and  $\text{Ga}_{0.47}\text{In}_{0.53}\text{As}$  /InP double-heterostructure and multiquantum well lasers grown by Chemical beam epitaxy', IEEE QE-22 (1987) 936-942.
- [8] Thijs P.J.A, Kuindersma P.I, Dijksterhuis W, v. Dongen T, Tiemeyer L, Binsma J.J.M, v.d. Hofstad G.L, and Nijman W, ' DCPBH-laser diodes with an MOVPE grown separate confinement (SC)-multiple quantum well (MQW) active region, emitting at  $\lambda = 1.5 \mu\text{m}$  ' (1987) ECOC Conference paper
- [9] Koren U, Miller B.I, Su Y.K, Koch T.L, and Bowers J.E, ' Low internal loss separate confinement InGaAs/GaInAsP quantum well laser ' (1987) Appl. Phys. Lett. 51 1744-1746
- [10] Bass S.J, Barnett S.J., Brown G.T., Chew N.G., Collis A.G., Pitt A.D., Skolnick M.S., 'Effect of growth temperature on the optical, electrical and crystallographic properties of epitaxial Indium Gallium Arsenide grown by MOCVD in an atmospheric reactor' (1986) J. Crystal Growth, 79 378-385

- [11] Kakibayashi H., Nagata F., 'Composition dependence of equal thickness fringes in an electron microscope image of GaAs/Al(x)Ga(1-x)As multilayer structures' (1985) J.J.A.P. 24, L905-L907
- [12] Vandenberg J.M., Hamm R.A., Macrander A.T., Panish M.B., Temkin H., 'Structural characterisation of GaInAs(P)/InP quantum well structures grown by gas source molecular beam epitaxy' (1986) Appl. Phys. Lett. 49 1302-1304
- [13] Nakajima K., Yamaguchi A., Akita K., Kotani T., 'Composition dependence of the band-gaps of  $\text{In}_{1-x}\text{Ga}_x\text{As}_{1-y}\text{P}_y$  quaternary solids lattice matched on InP substrates' (1978) J.A.P. 49 5944-5950
- [14] Davies J.I., Marshall A.C., Scott M.D., Griffiths R.J.M.G., 'Structural and optical properties of GaAlInAs lattice matched to InP grown by LP-MOVPE (to be published)
- [15] Masu K., Mishima T., Horoi S., Konagai M., Takahasi K., 'Preparation of  $\text{Al}_x\text{Ga}_{1-x}\text{In}_y\text{As}_{1-y}$  ( $0 < x < 0.5$ ,  $y = 0.47$ ) lattice matched to InP' (1982) J.A.P. 53 7558-7560
- [16] Olego D., Chang T.Y., Silberg E., Caridi E.A., Pinczuk A., 'Compositional dependence of band-gap energy and conduction-band effective mass of  $\text{In}_{1-x-y}\text{Ga}_x\text{Al}_y\text{As}$  lattice matched to InP' (1982) Appl. Phys. Lett. 41 476-478
- [17] Westland D.J., Mihailovic D., Ryan J.F., and Scott M.D., 'Optical time of flight measurement of carrier diffusion and trapping in an InGaAs/InP heterostructure' (1987) Appl. Phys. Lett. 51 590-592
- [18] Babiker M. and Ridley B.K. 'Effective mass eigenfunctions in superlattices and their role in well-capture' (1986) Superlattices and Microstructures 2 279
- [19] Brum J.A. and Bastard G. 'Resonant carrier capture by Semiconductor quantum wells'. (1986) Phys. Rev. B.33 1420-1423
- [20] Fourth Quarterly report May 1986 - August 1986.
- [21] Sixth Quarterly report November 1986 - February 1987.
- [22] Seventh Quarterly report February 1987 - June 1987.

- [23] Eighth Quarterly report July 1987 - October 1987.
- [24] Yamanishi M, and Suemune I, ' Comment on Polarisation dependent Momentum matrix elements in Quantum Well Lasers ', (1984) Jap.J.Appl.Phys. 23 L35-L36.
- [25] Asada M,Kameyama A.and Suematsu Y, ' Gain and Intervalence Band absorption in Quantum-well Lasers ',(1984) IEEE QE-20 745-753
- [26] Smith C, Abram R.A, and Burt M.G,  
 ' Auger recombination in a quantum well heterostructure '  
 (1983) J. Phys. C. 16 L171-L175  
 ' Auger recombination in long wavelength quantum well lasers '(1984) Electron. Letts. 20 893-894  
 'Theory of Auger recombination in a quantum well heterostructure'  
 (1985) Super. and Micro. 1 119-123  
 Taylor R.I, Abram R.A, Burt M.G, and Smith C, IEE (1986) Proc 132J 364.
- [27] Sermage B. Chemla D.S. Sivco D. and Cho A. Y. ' Comparision of Auger recombination in InGaAs-AlInAs Multiple quantum wells and in bulk InGaAs ', (1986) IEEE QE-22 774-780
- [28] Asada M and Suematsu Y, 'The effects of loss and nonradiative recombination on the temperature dependence of threshold current in 1.5-1.5  $\mu$ m GaInAsP/InP lasers ', (1983) IEEE QE-19 917-923
- [29] Childs G.N, Brand S, and Abram R.A. ' Intervalence band absorption in semiconductor laser materials ', (1986) Semicond. Sci. Technol. 1 116-120
- [30] Henry C.H, Logan R.A, Merritt F.R, and Bethea C.G, ' Radiative and nonradiative lifetimes in n-type and p-type 1.6 $\mu$ m InGaAs ', (1984) Electronics letts. 20 358-359  
 Prize M.E,Taghizadeh M.R,Smith S.D,and Wherrett B.S, Appl.Phys.Lett. (1984) 45 652-654

- [31] Chen H.Z. Ghaffari A. Morkoc H and Yariv A. 'Very low threshold current densities (Under 100A/cm<sup>2</sup>) in AlGaAs/GaAs single quantum well GRINSCH lasers grown by molecular beam epitaxy ', (1987) Elect. Lett. 23 334-335
- Derry P.L. Yariv A. Lau K.Y. Bar-Chaim N. Lee K and Rosenberg J. 'Ultralow-threshold graded-index separate-confinement single quantum well buried heterostructure (Al,Ga)As lasers with high reflectivity coatings' (1987) Appl. Phys. Lett. 50 1773-1775
- Lau K.Y. Derry P.L. and Yariv A. 'Ultimate limit in low threshold quantum well GaAlAs semiconductor lasers' (1988) Appl. Phys. Lett. 52 88-90
- [32] Kawamura Y, Asahi H, and Wakita K (1984) 'InGaAs/InGaAlAs/InAlAs/InP SCH-MQW Laser diodes grown by Molecular-Beam Epitaxy ' (1984) Electronics Letts. 20 459-460
- [33] Kodama K, Komeno J, and Ozeki M, 'Photoexcited InGaAs/InP Quantum-well lasers with high characteristic temperatures', (1984) Electronics Letts. 20 43-44
- [34] Nelson A.W, Moss R.H, Regnault J.C, Spurdens P.C, and Wong S, 'Double heterostructure and multiquantum-well lasers at 1.5-1.7  $\mu$ m grown by atmospheric pressure MOVPE ', (1985) Electronics Letts. 21 329-331
- [35] Tomita A. and Suzuki A ' Carrier-induced lasing wavelength shift for quantum well laser diodes' (1987) IEEE QE-23 1155-1159
- [36] Bottcher E.H., Ketterer K., Bimberg D., Weimann G. and Schlapp W. 'Excitonic and electron-hole contributions to the spontaneous recombination rate of injected charge carriers in GaAs-GaAlAs Multiple quantum well lasers at room temperature' (1987) Appl. Phys Lett 50 1074-1076
- [37] Charreaux C., Guillot G., and Nouailhat A. ' Alloy broadening in photoluminescence spectra of In<sub>0.53</sub>Ga<sub>0.47</sub>As ', (1986) J. Appl. Phys. 60 768-772

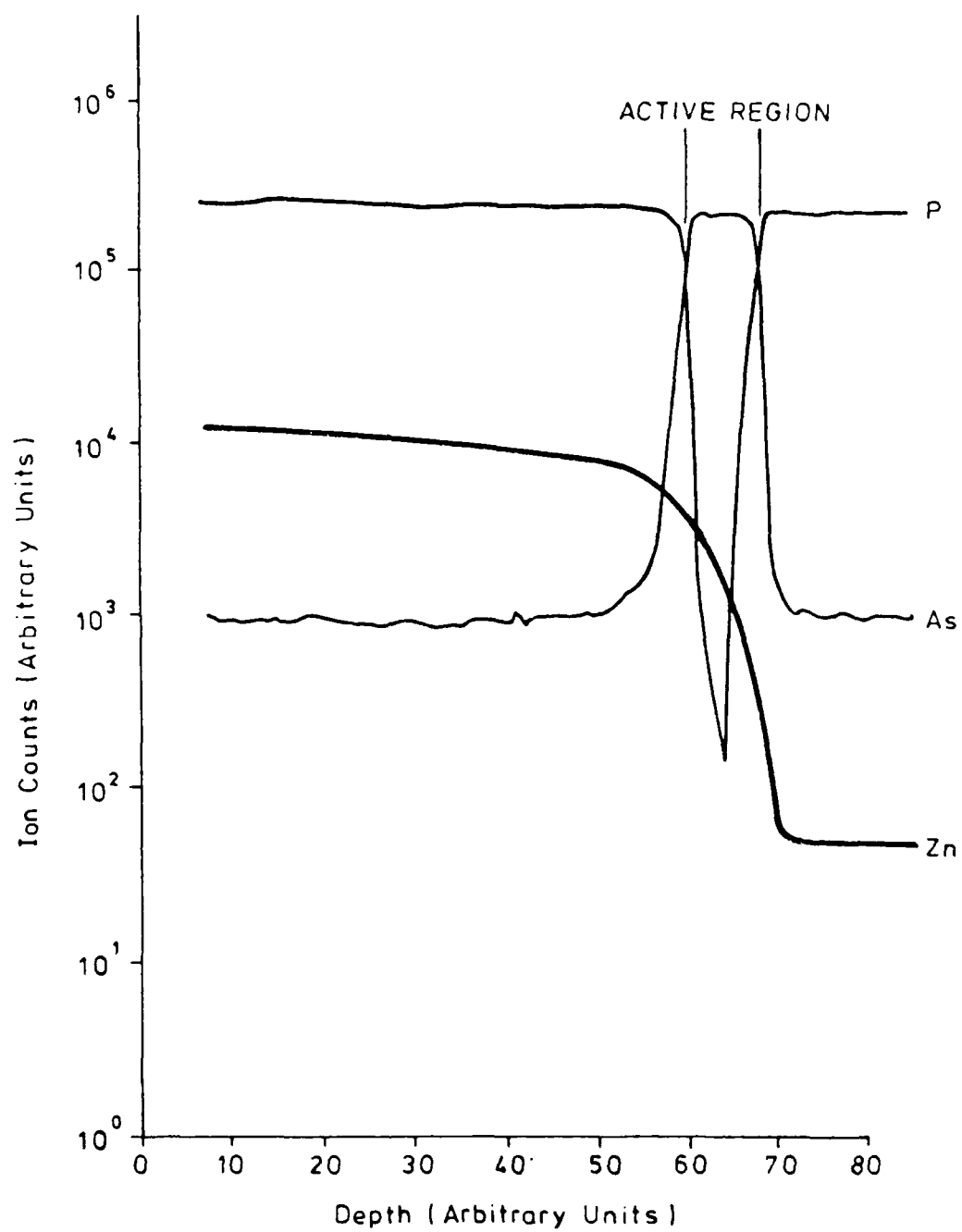


FIG.1 SIMS RAW DATA

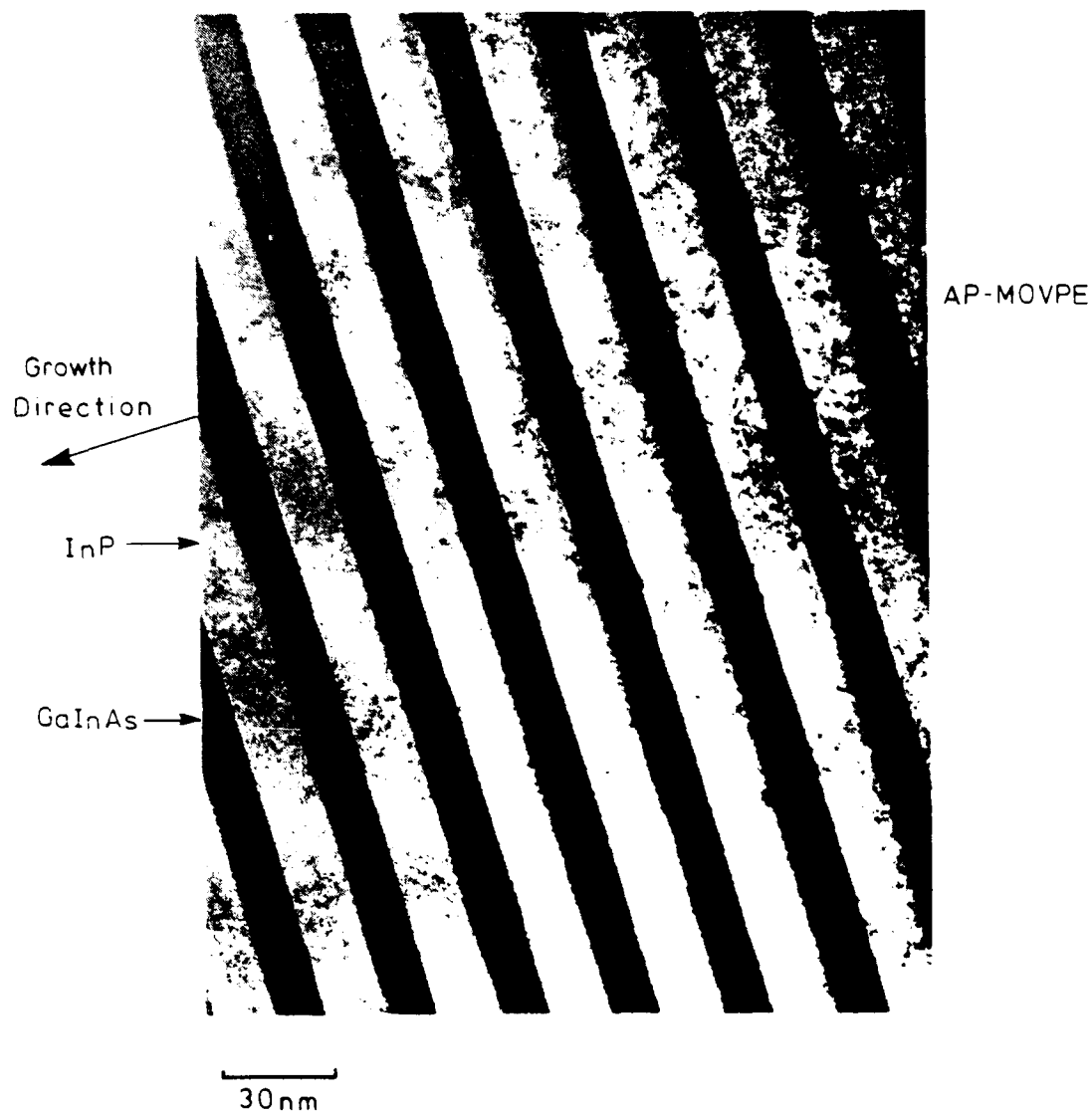


FIG 2 TEM MICROGRAPH OF A GaInAs/InP MQW STRUCTURE.

Sample : OB461(A)  
 Material : Ga In As / InP (30 Wells)  
 $T_g = 650^\circ\text{C}$   
 On Orientation (100)

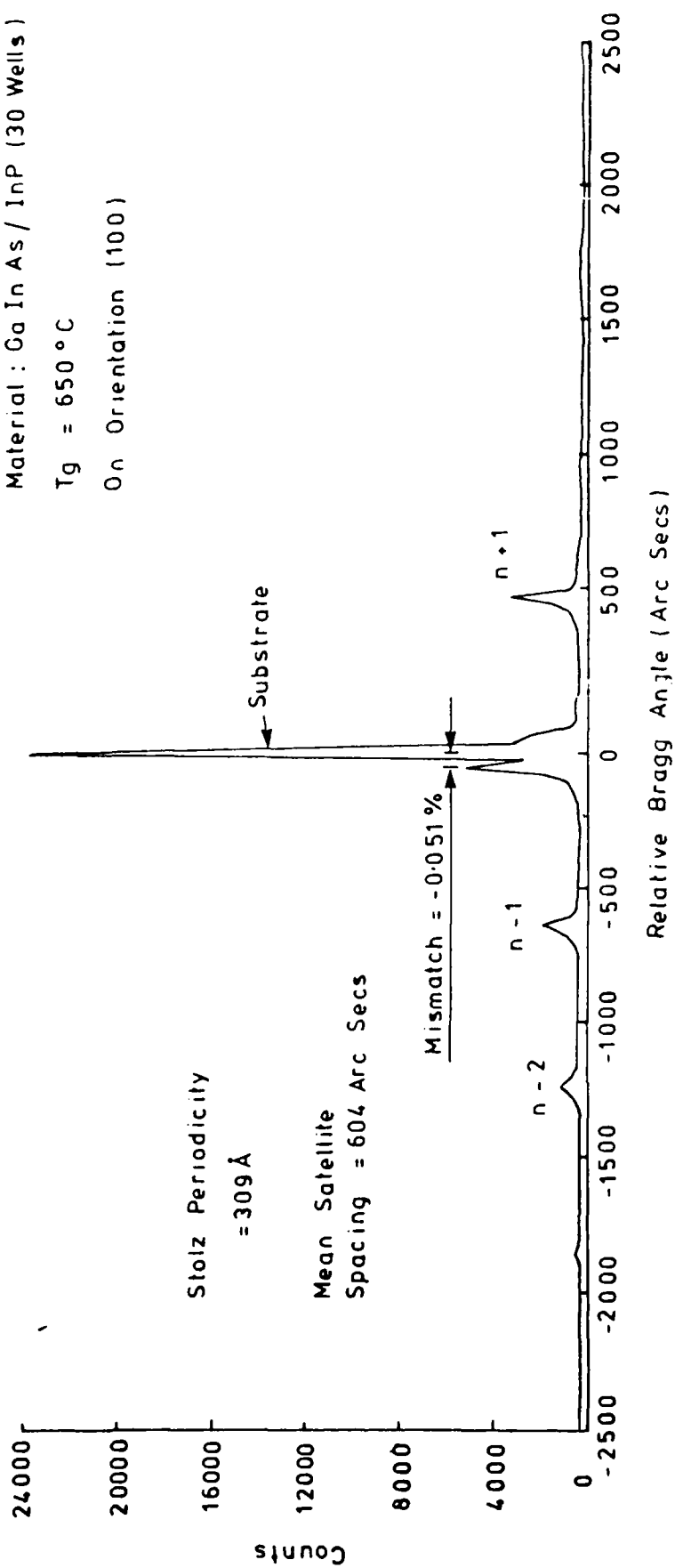


FIG. 3 EXPERIMENTAL ROCKING CURVE

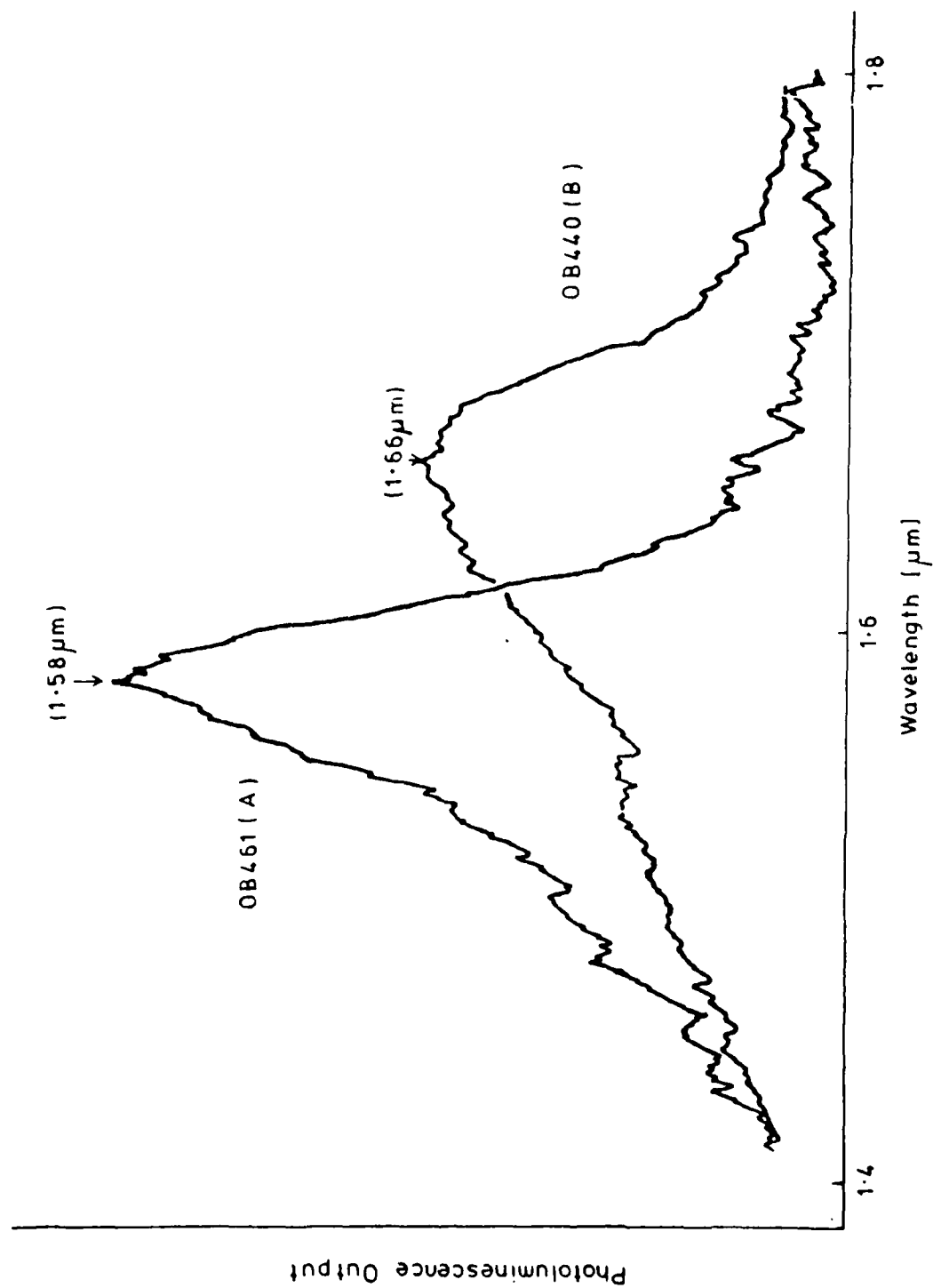


FIG. 4 ROOM TEMPERATURE PHOTOLUMINESCENCE.



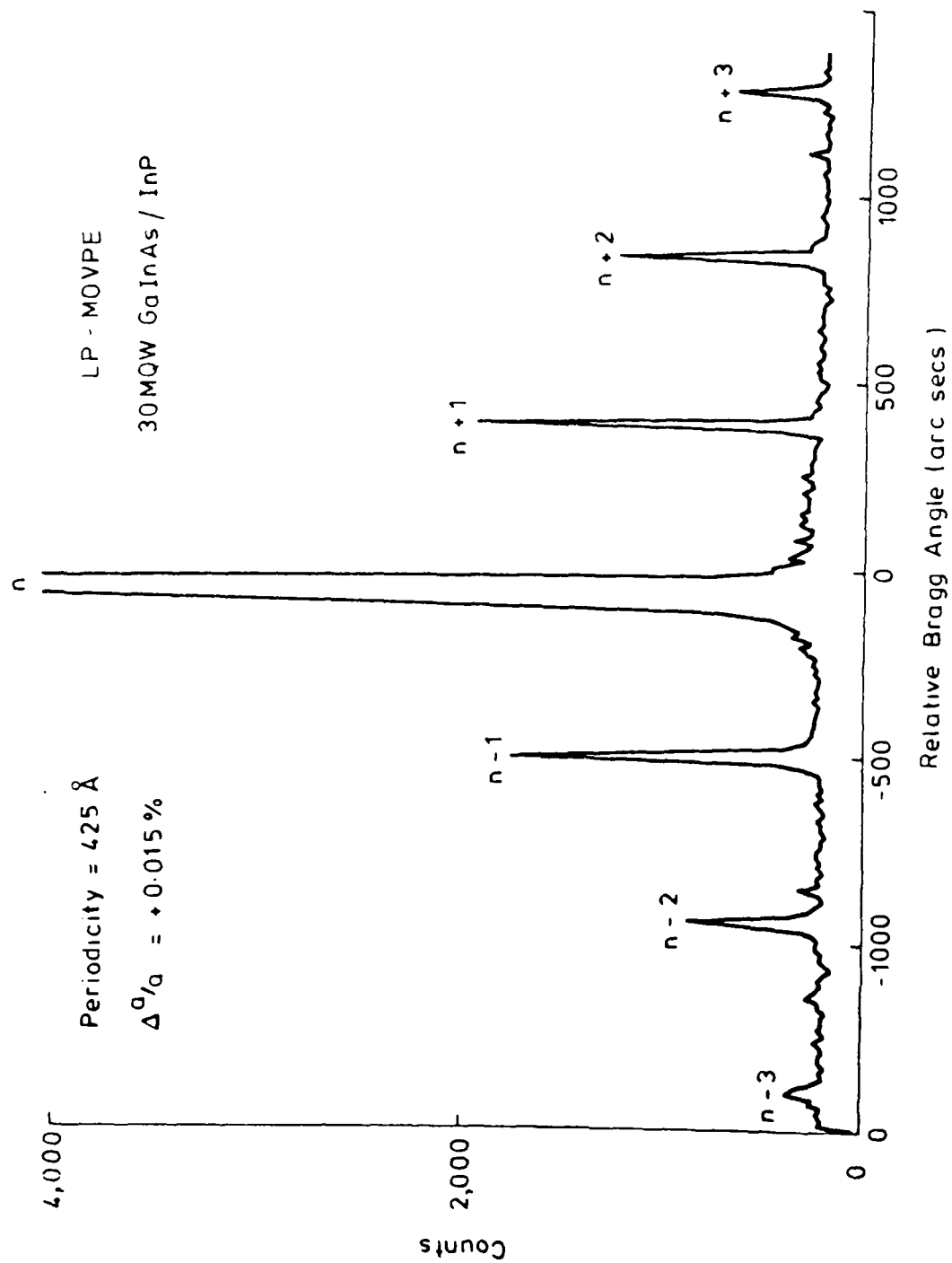


FIG. 5 EXPERIMENTAL ROCKING CURVE

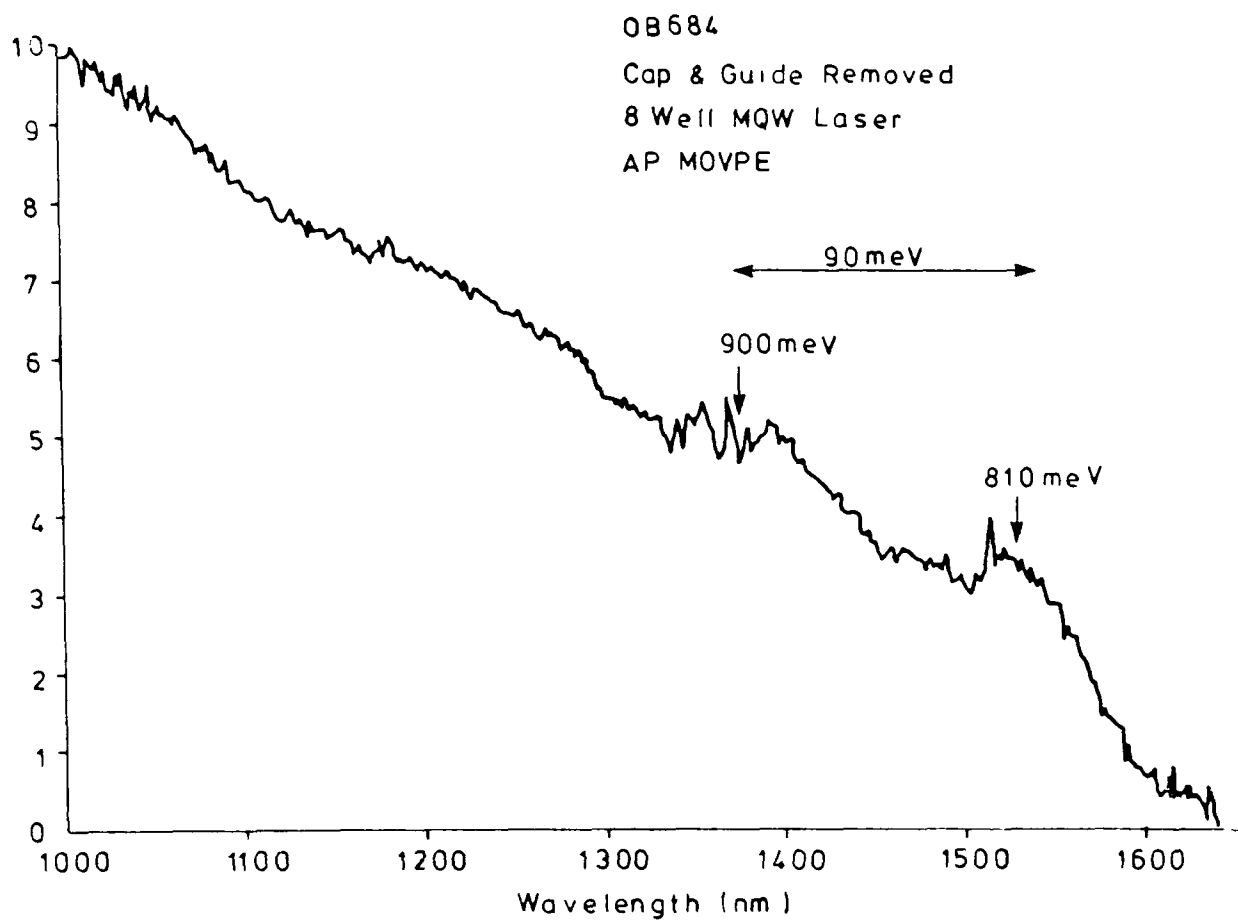


FIG.6 ABSORPTION SPECTRUM.

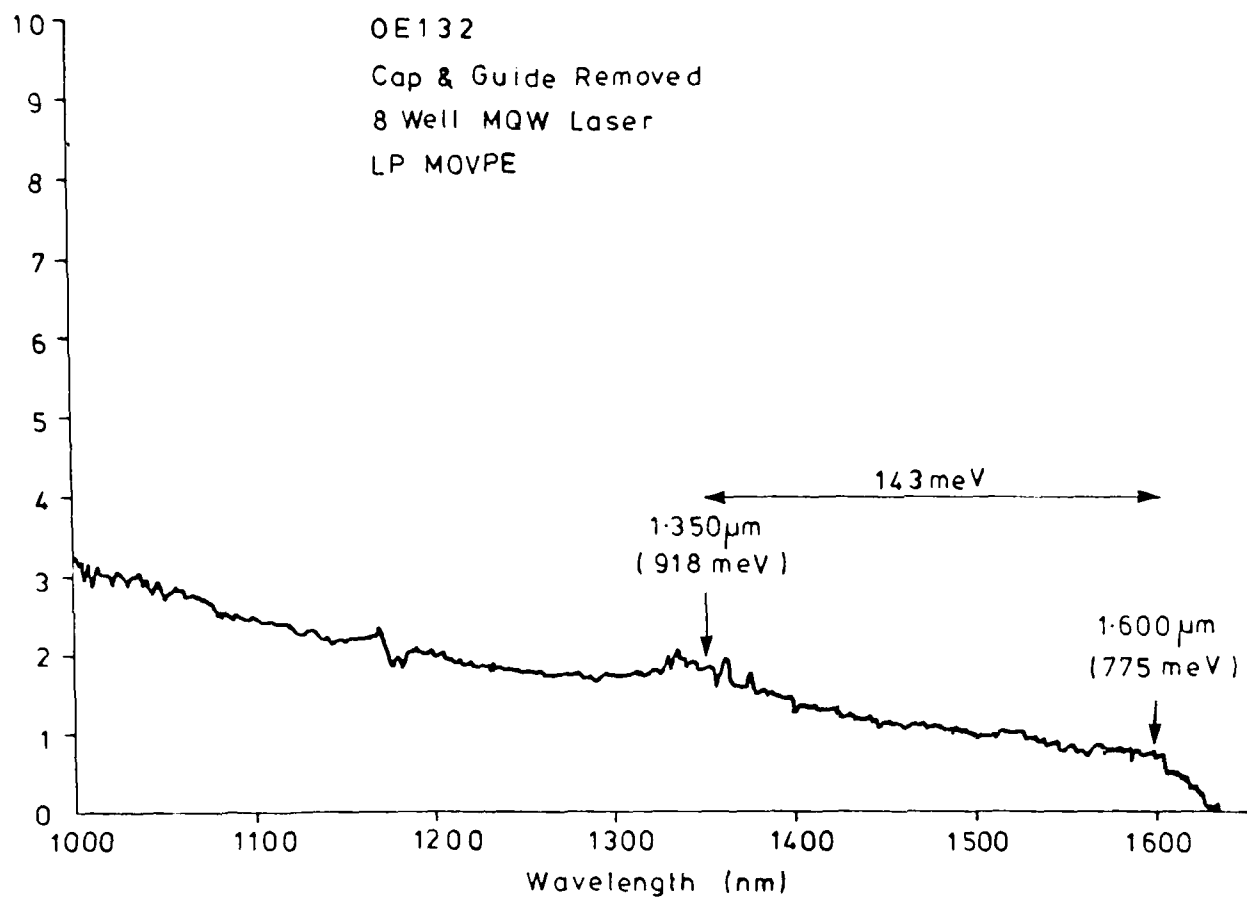


FIG. 7 ABSORPTION SPECTRUM.

OE 61

30 Well MQW Structure

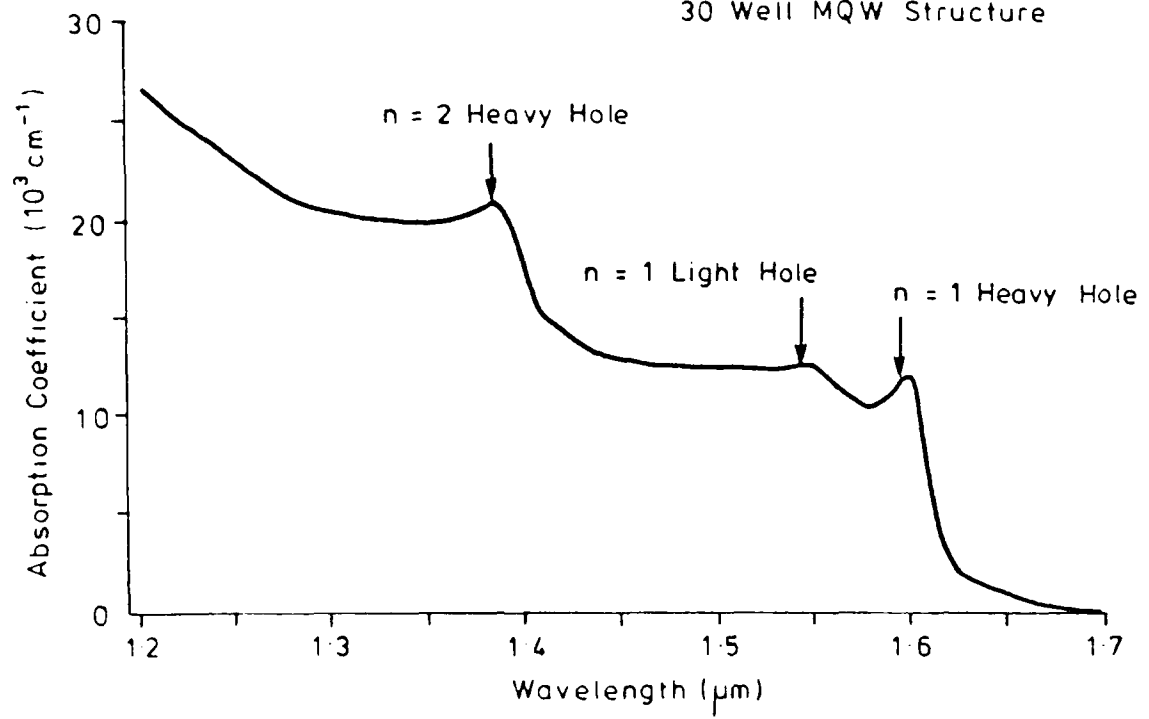


FIG 3 ABSORPTION SPECTRUM

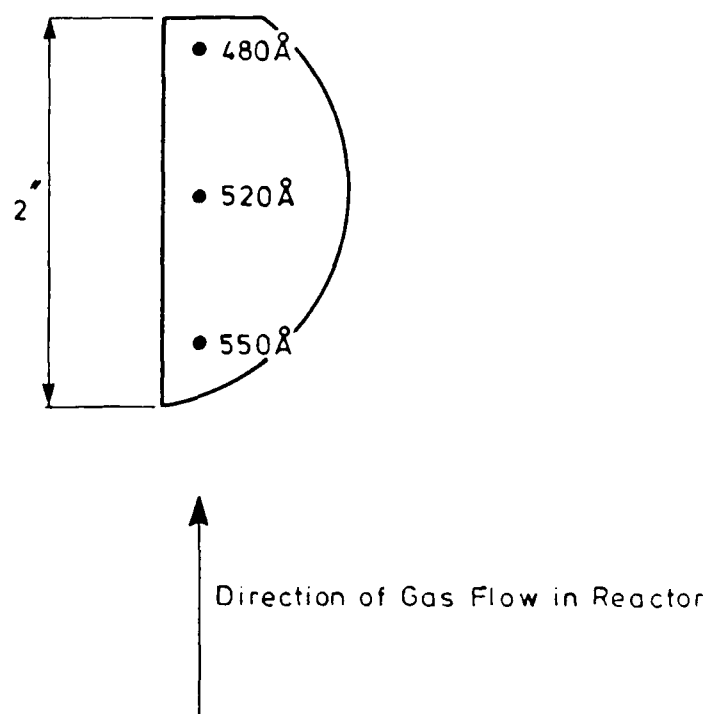


FIG. 9 VARIATION OF WELL PLUS BARRIER PERIOD ALONG  
A 2" LENGTH OF THE SUSCEPTOR ON OE 234.

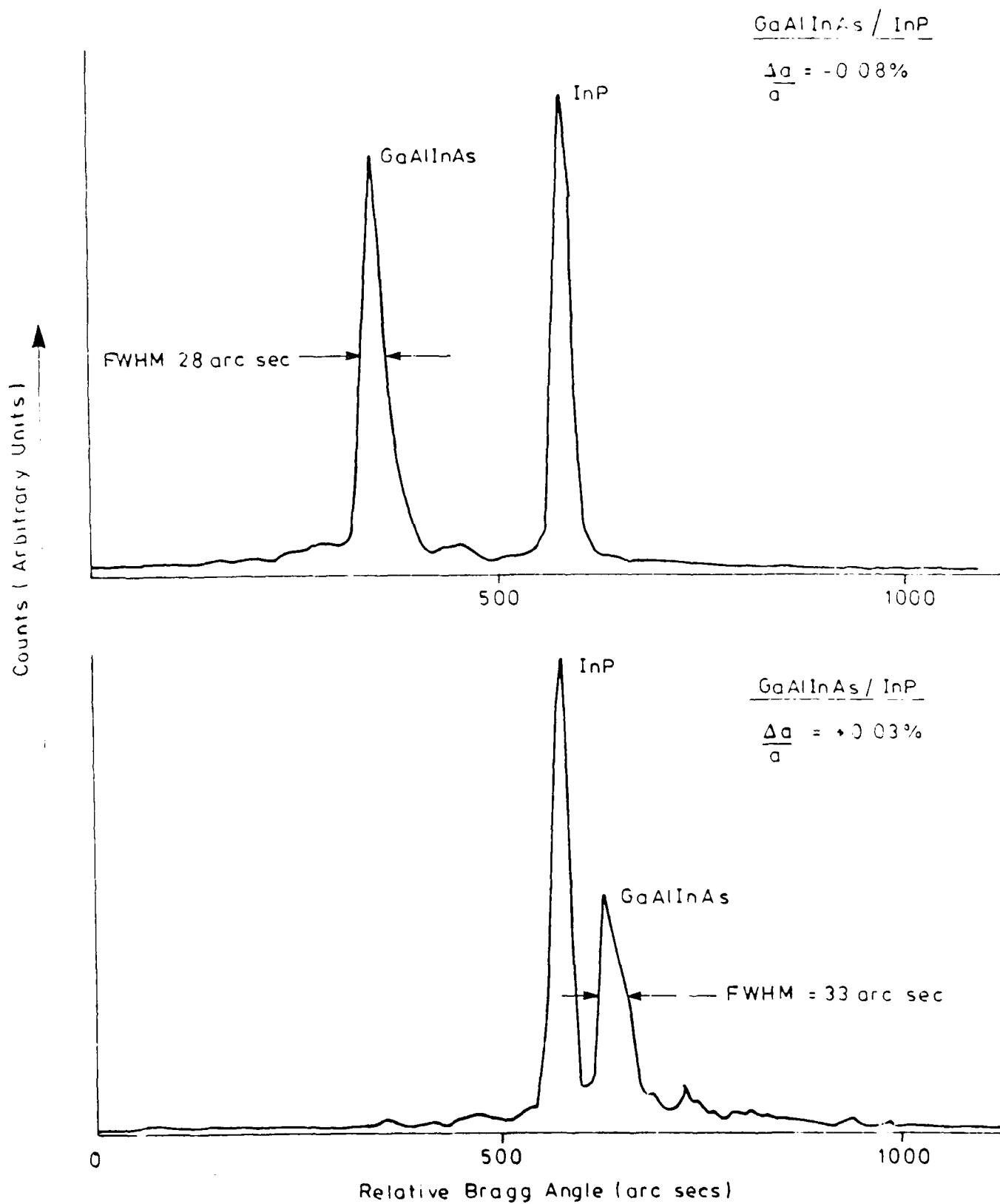


FIG. 10 DOUBLE CRYSTAL X-RAY ROCKING CURVES FOR GaAlInAs LAYERS ON InP

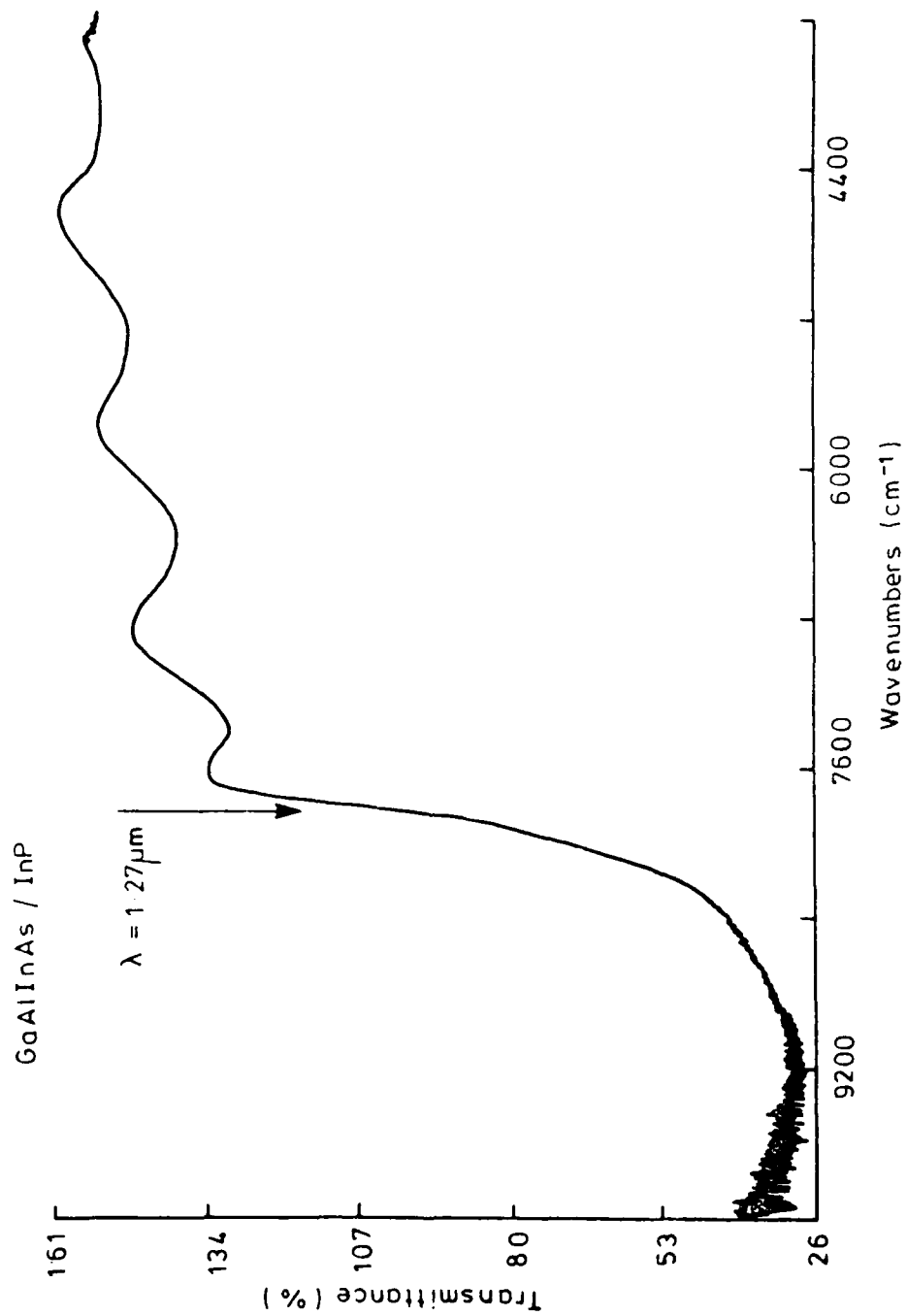


FIG. 11 ROOM TEMPERATURE FTIR ABSORPTION SPECTRUM.

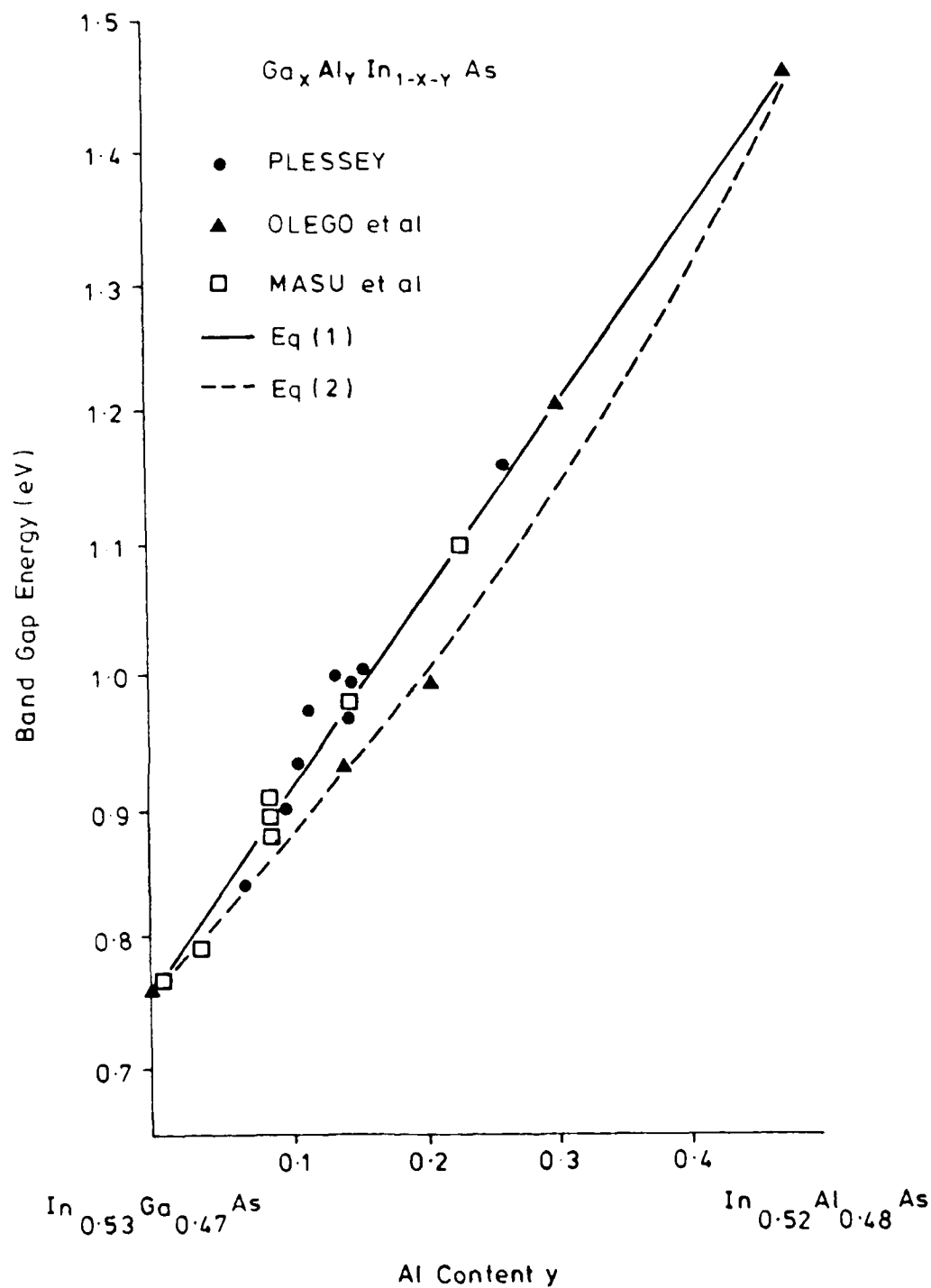


FIG.12 VARIATION OF BAND GAP ENERGY WITH COMPOSITION FOR  
 $\text{Ga}_x\text{Al}_y\text{In}_{1-x-y}\text{As}$  LATTICE MATCHED TO InP.



1500 Å	$\text{Ga}_{0.47}\text{In}_{0.53}\text{As}$	$\text{Zn,p} > 10^{18} \text{ cm}^{-3}$
2.5 μm	p - InP	$\text{Zn,p} = 8 \cdot 10^{17} \text{ cm}^{-3}$
1500 Å	$\text{Ga}_{0.47}\text{In}_{0.53}\text{As}$	Undoped
1.5 μm	n - InP	$\text{Sn,n} = 2 \cdot 10^{18} \text{ cm}^{-3}$
	$n^+$ InP Substrate	

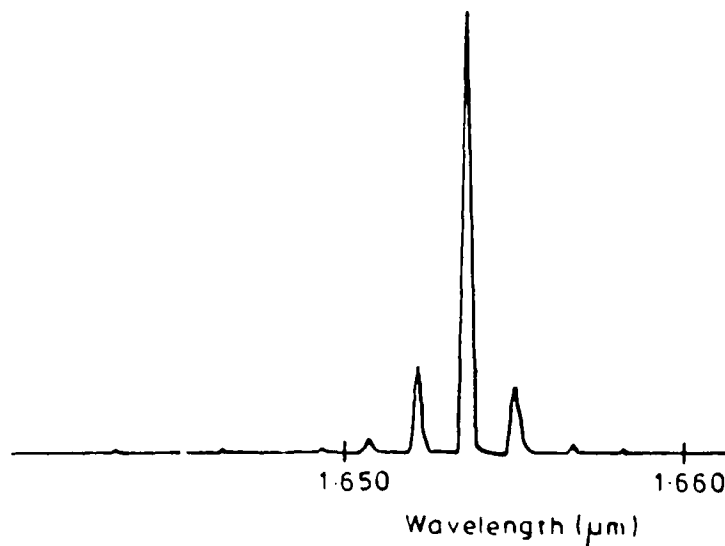
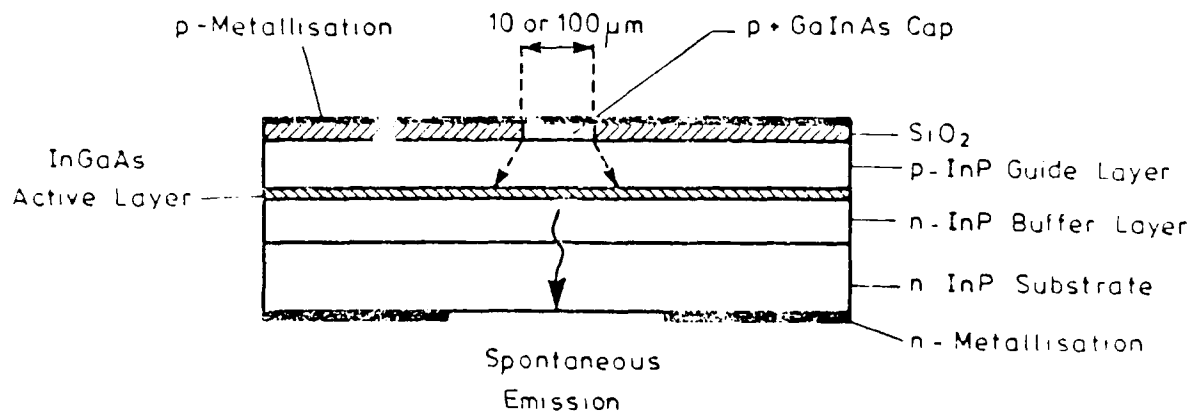


FIG. 13 STRUCTURE AND TYPICAL LASING CHARACTERISTICS FOR OXIDE ISOLATED MOVPE InGaAs DH LASER.

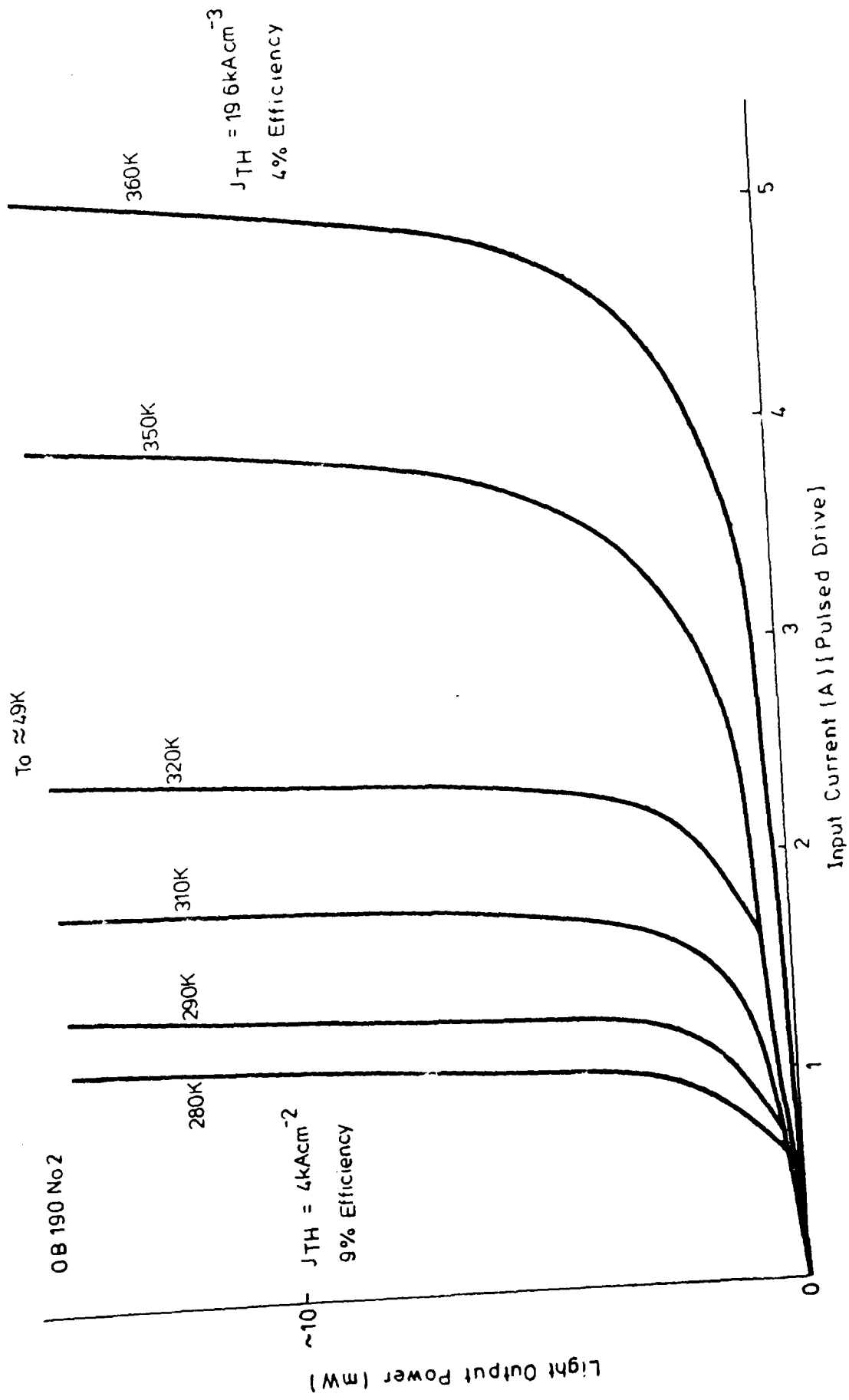


FIG. 14 BROAD AREA (100  $\mu\text{m}$  STRIPE WIDTH, 250  $\mu\text{m}$  LONG) OXIDE STRIPE InGaAs DH LASER.

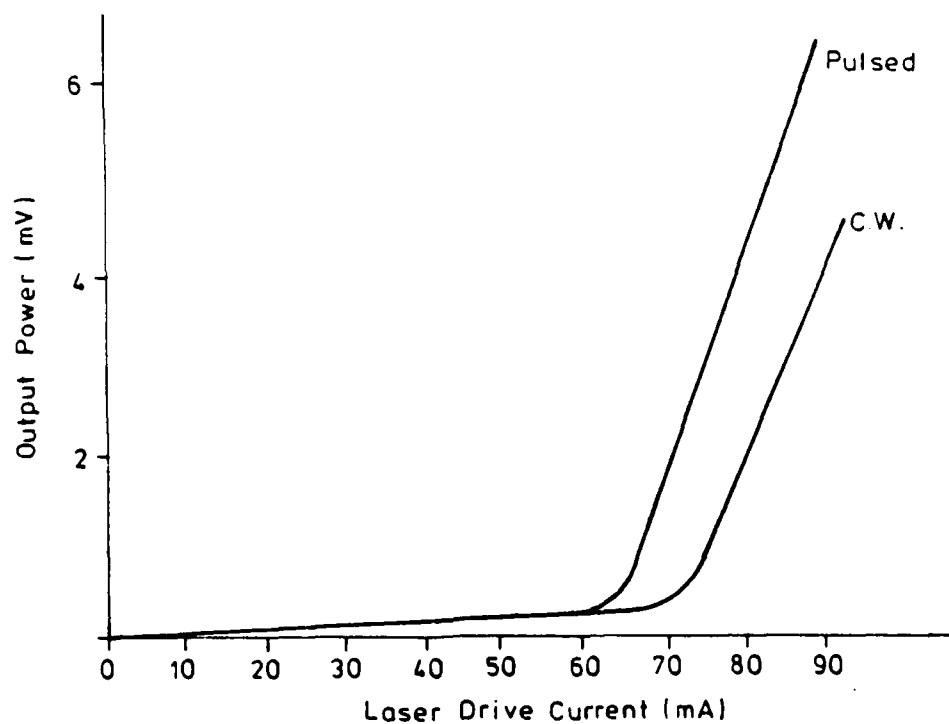
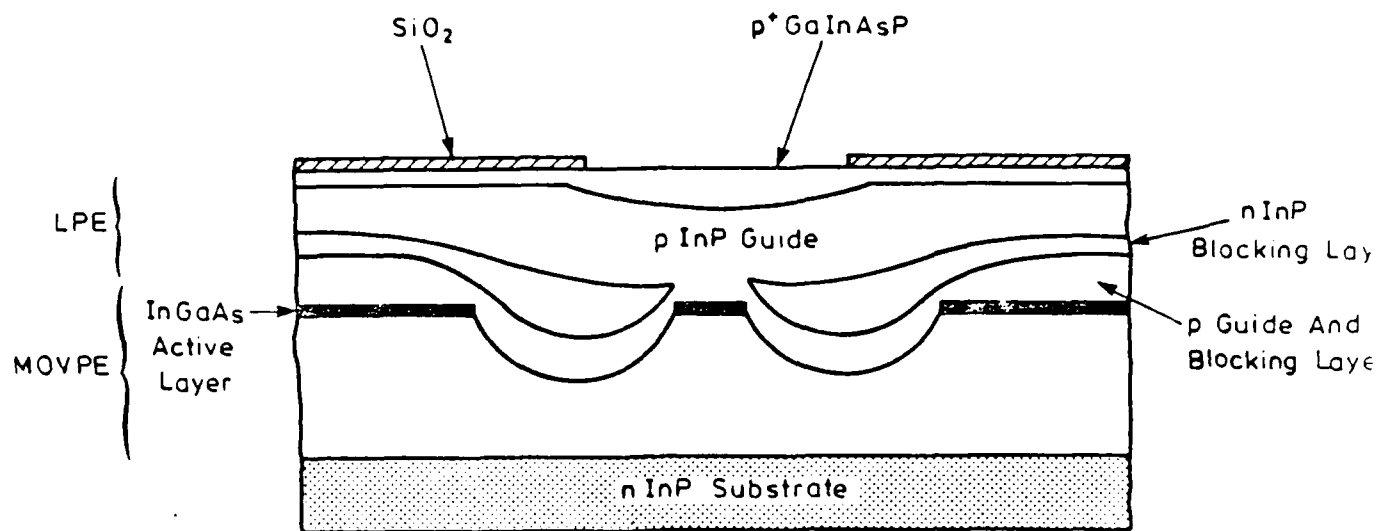


FIG.15 STRUCTURE AND LIGHT CURRENT CHARACTERISTICS FOR A DOUBLE CHANNEL PLANAR BURIED HETEROSTRUCTURE DCPBH InGaAs DH LASER.

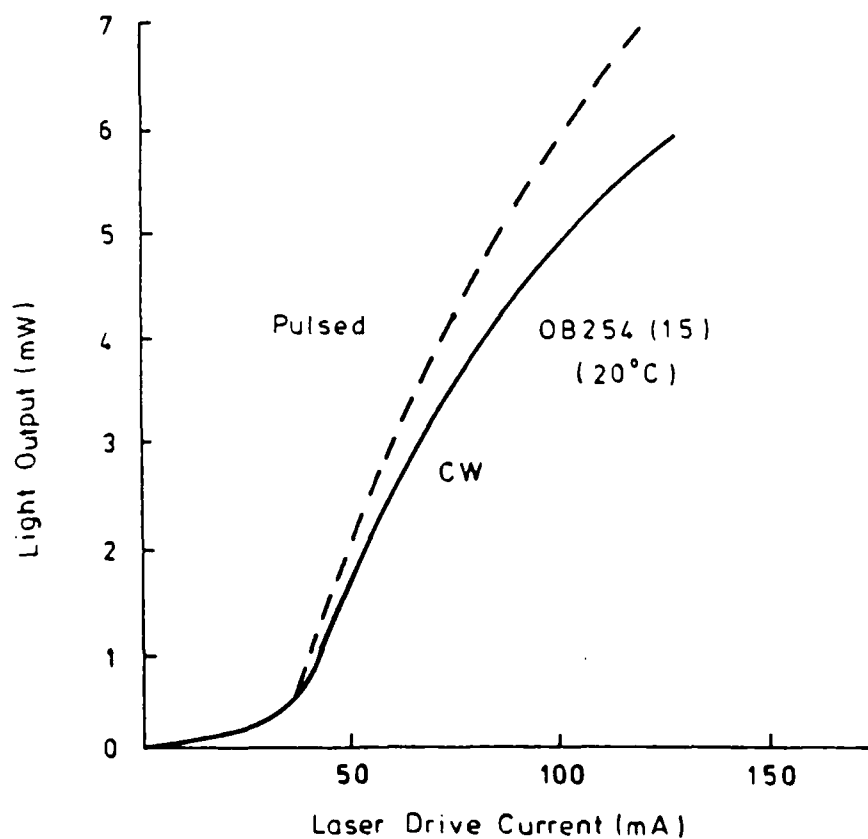
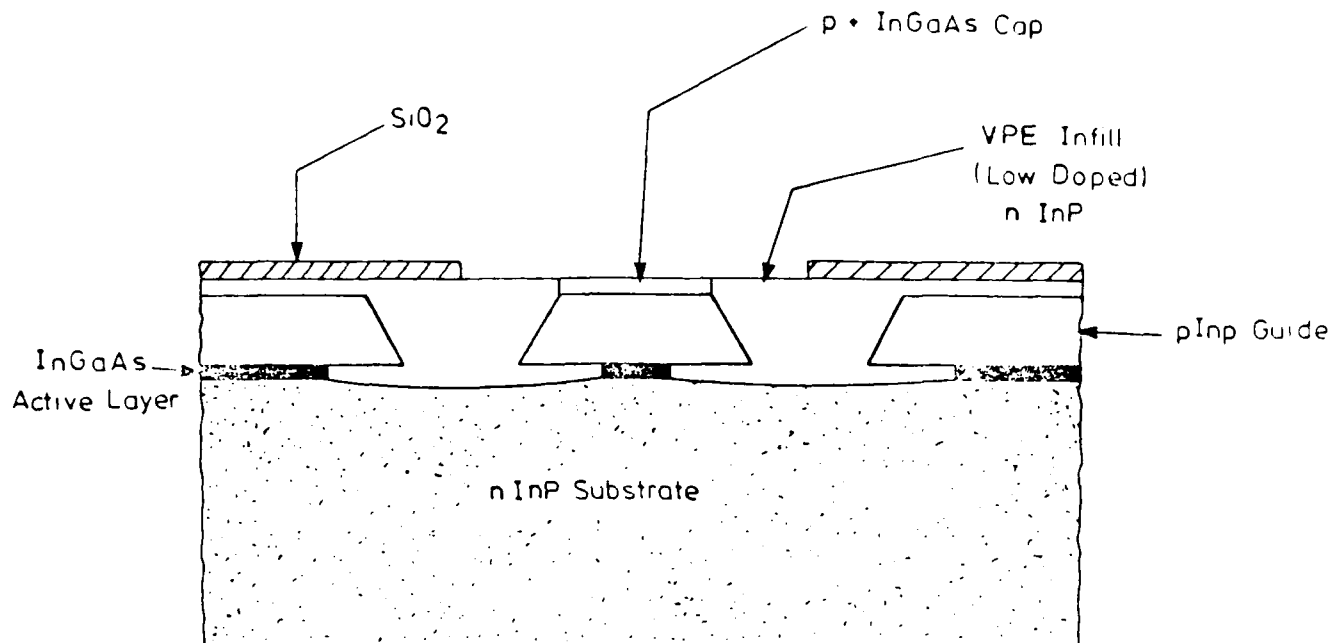


FIG. 16 STRUCTURE AND LIGHT/CURRENT CHARACTERISTIC FOR AN ALL VAPOUR PHASE MOVPE SOURCE, VPE INFILL InGaAs DH LASER.

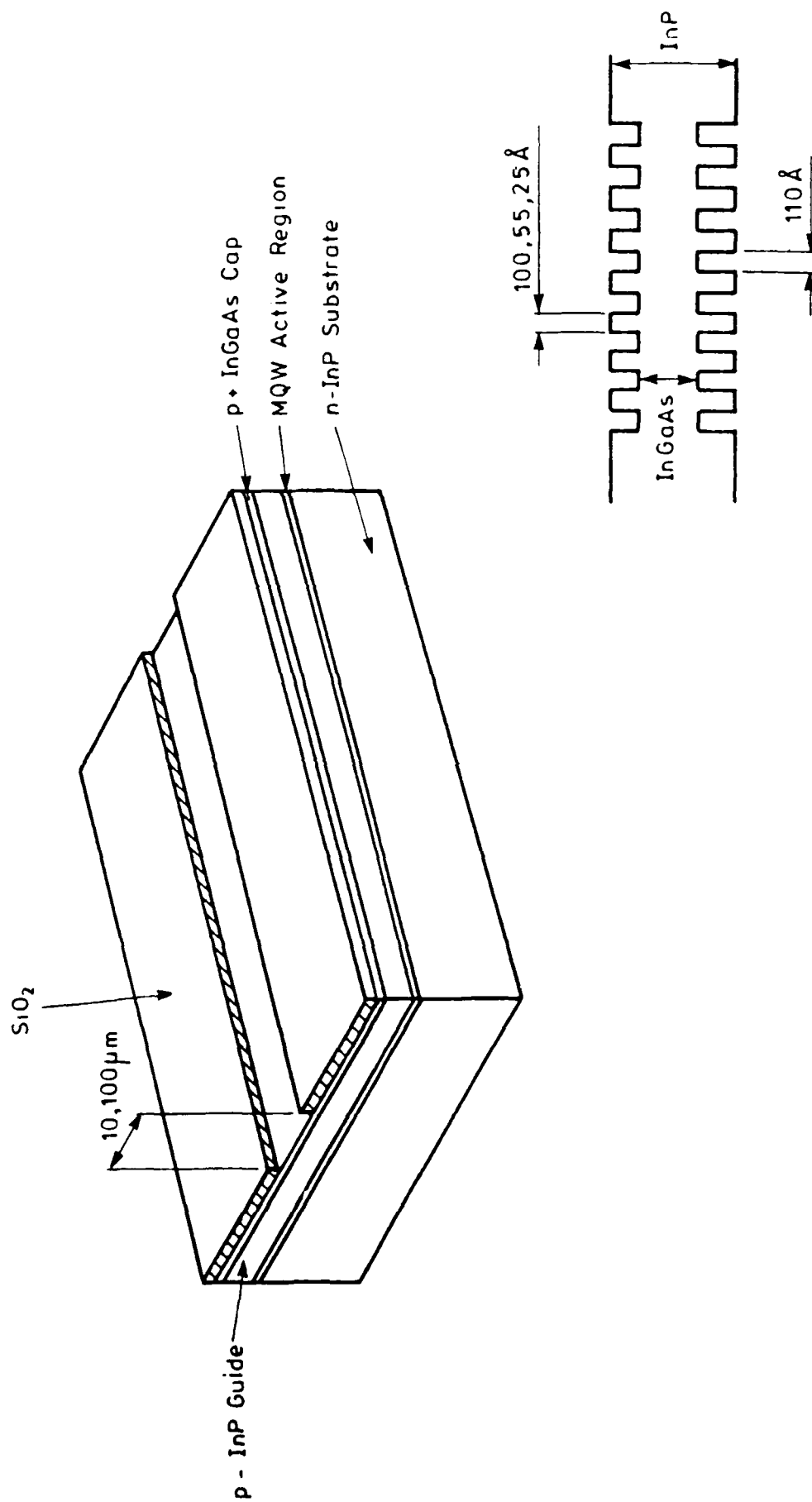


FIG. 17 OXIDE ISOLATED InGaAs / InP MQW LASER

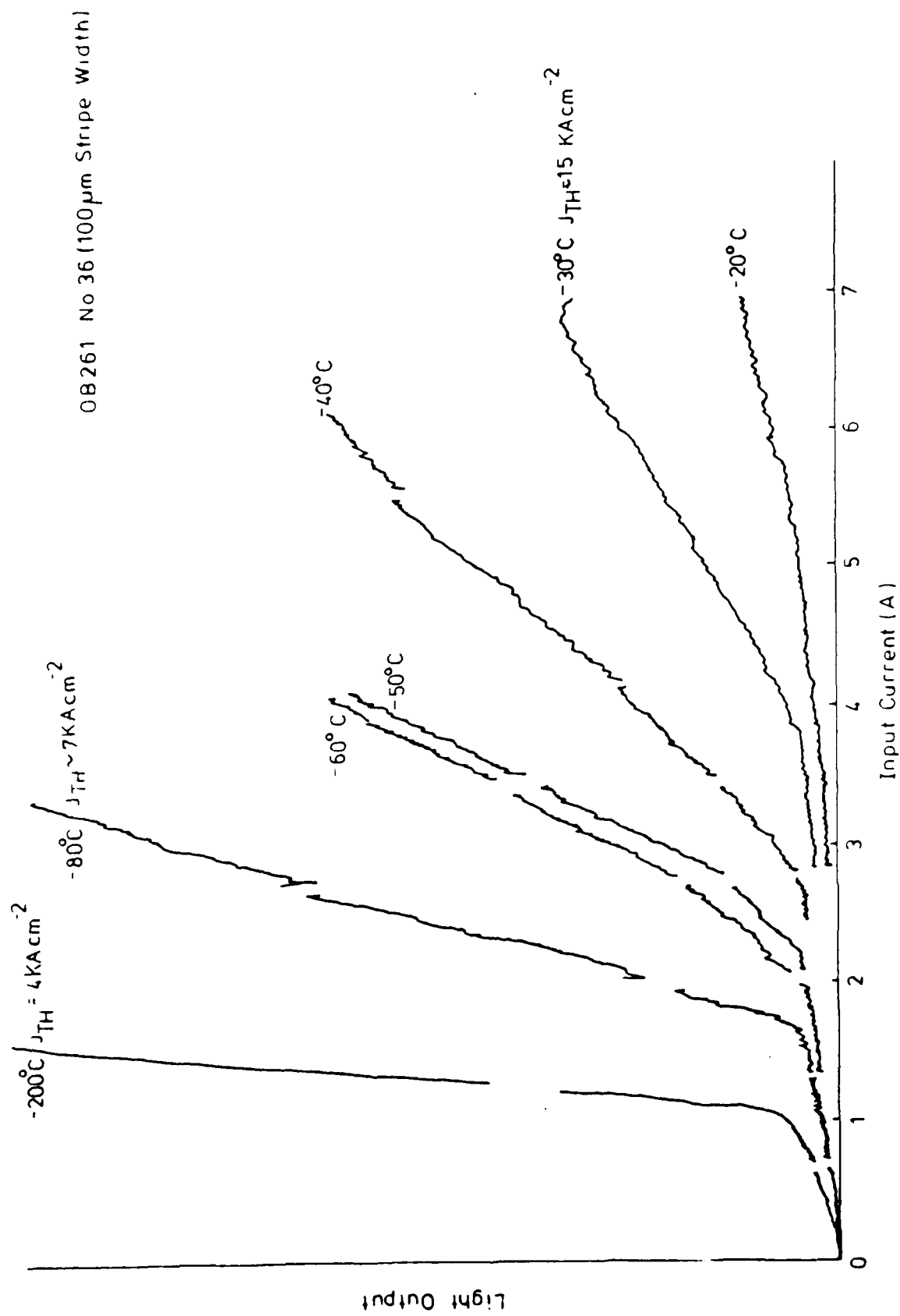


FIG. 18 8-WELL MULTI QUANTUM WELL InGaAs/InP (110 Å WELL, 100 Å BARRIER) OXIDE STRIPE LASER

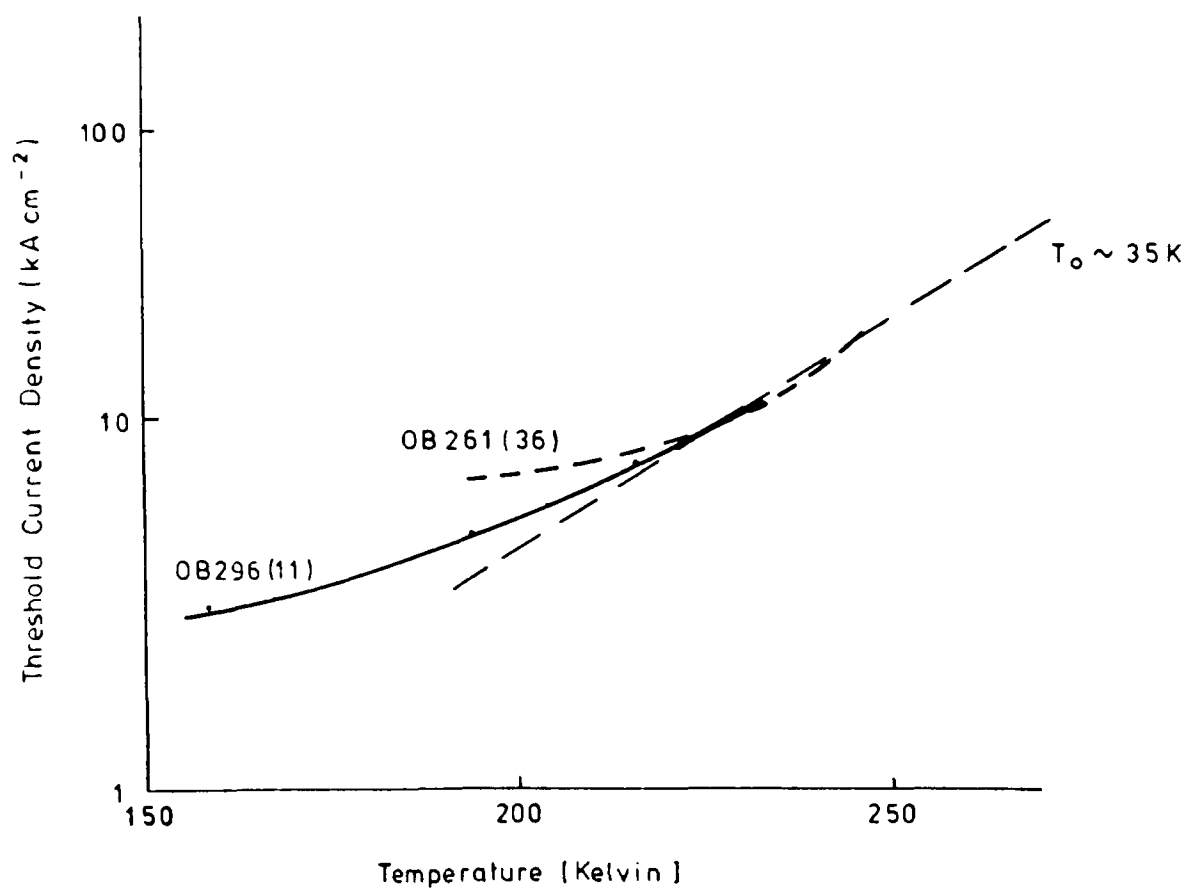


FIG. 19 THRESHOLD CURRENT DENSITY VERSUS TEMPERATURE FOR AN  
8-WELL InGaAs/InP MQW LASER WITH NOMINALLY 110 Å WELLS,  
100 Å BARRIERS.

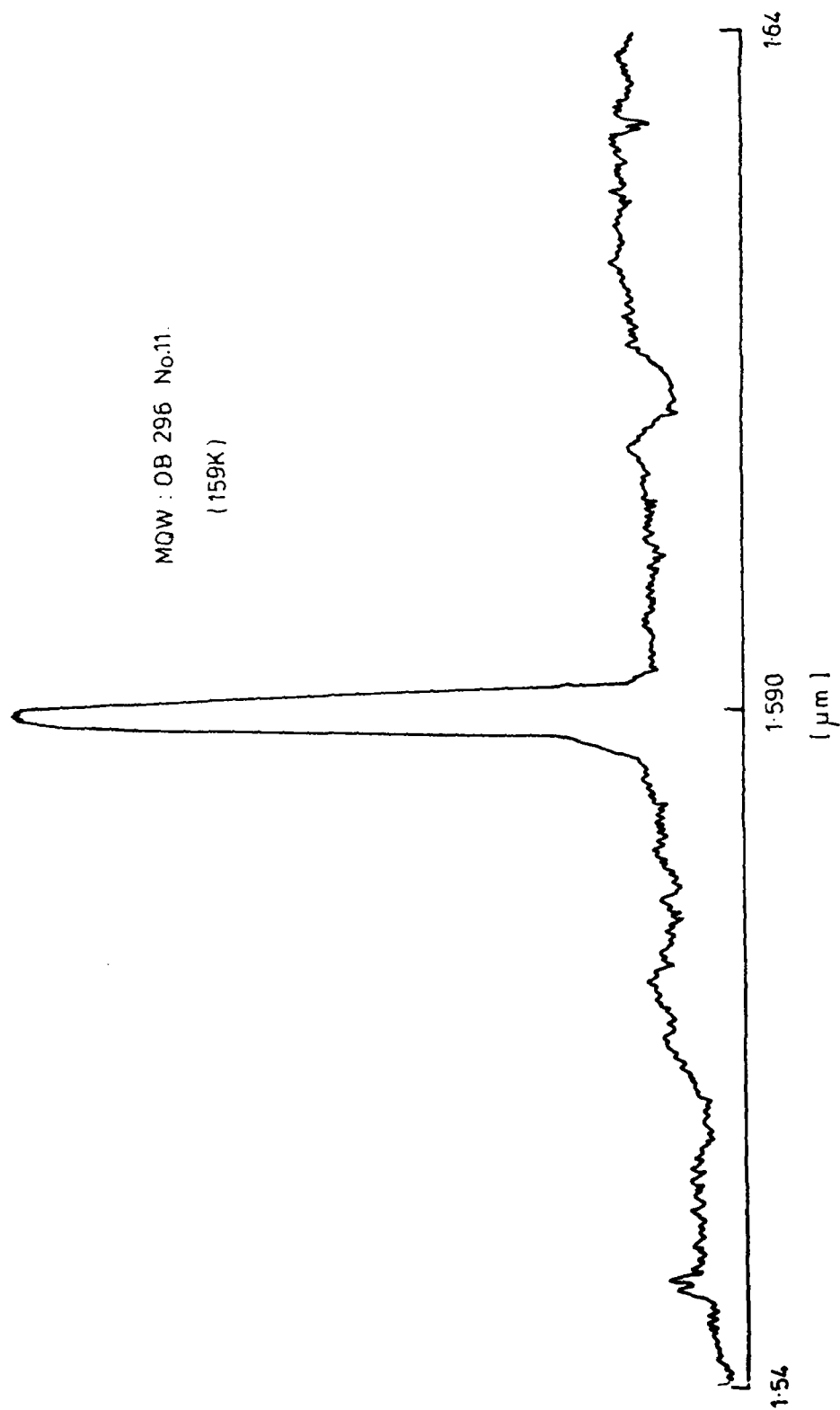


FIG.20 PULSE DRIVE SPECTRUM FOR AN  $\text{InGaAs/InP}$  MQW LASER (110 Å WELLS, 100 Å BARRIERS)



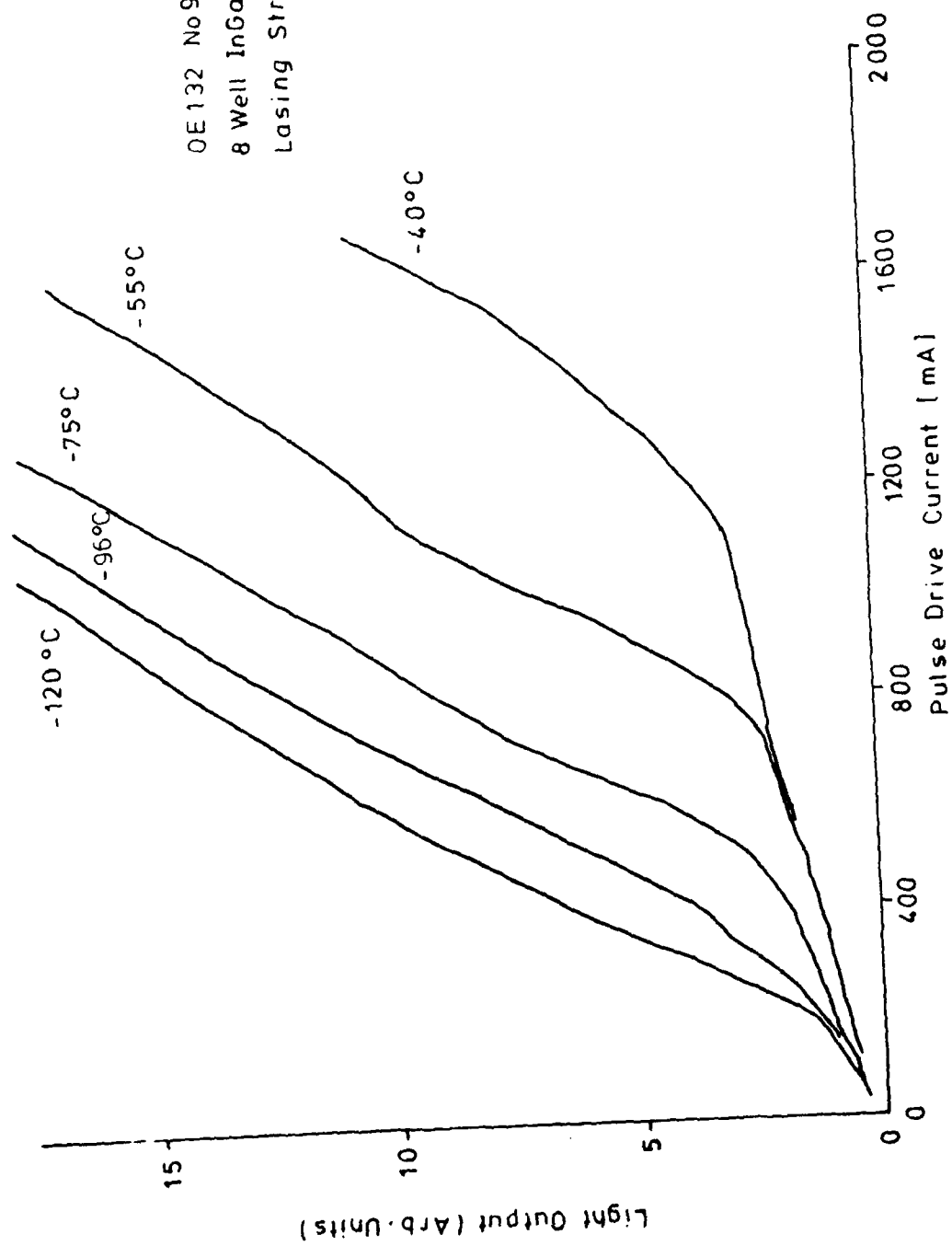


FIG. 21 LOW TEMPERATURE LASING CHARACTERISTICS.

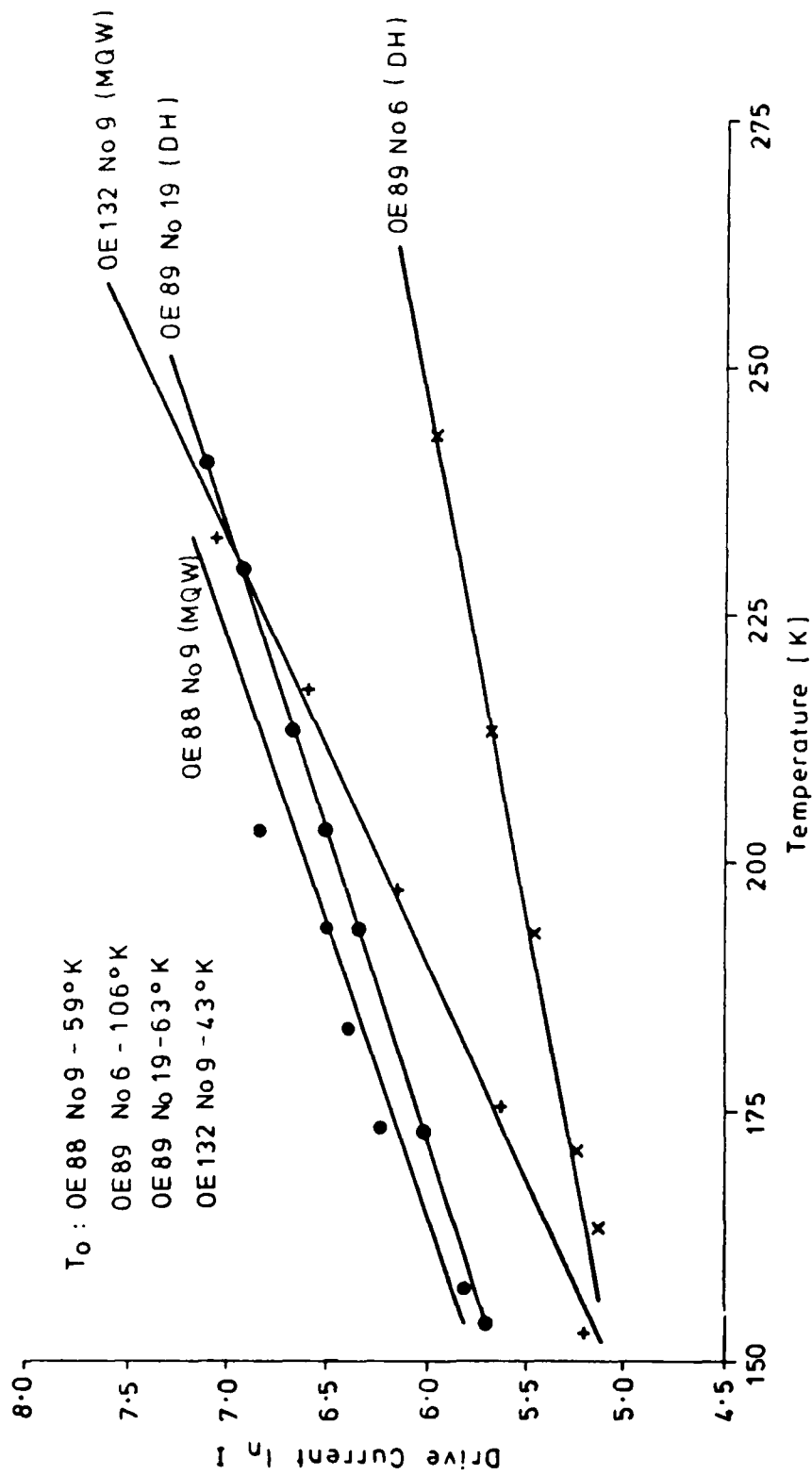


FIG.22 VARIATION OF LASING THRESHOLD OF DH AND MQW LASERS WITH TEMPERATURE.

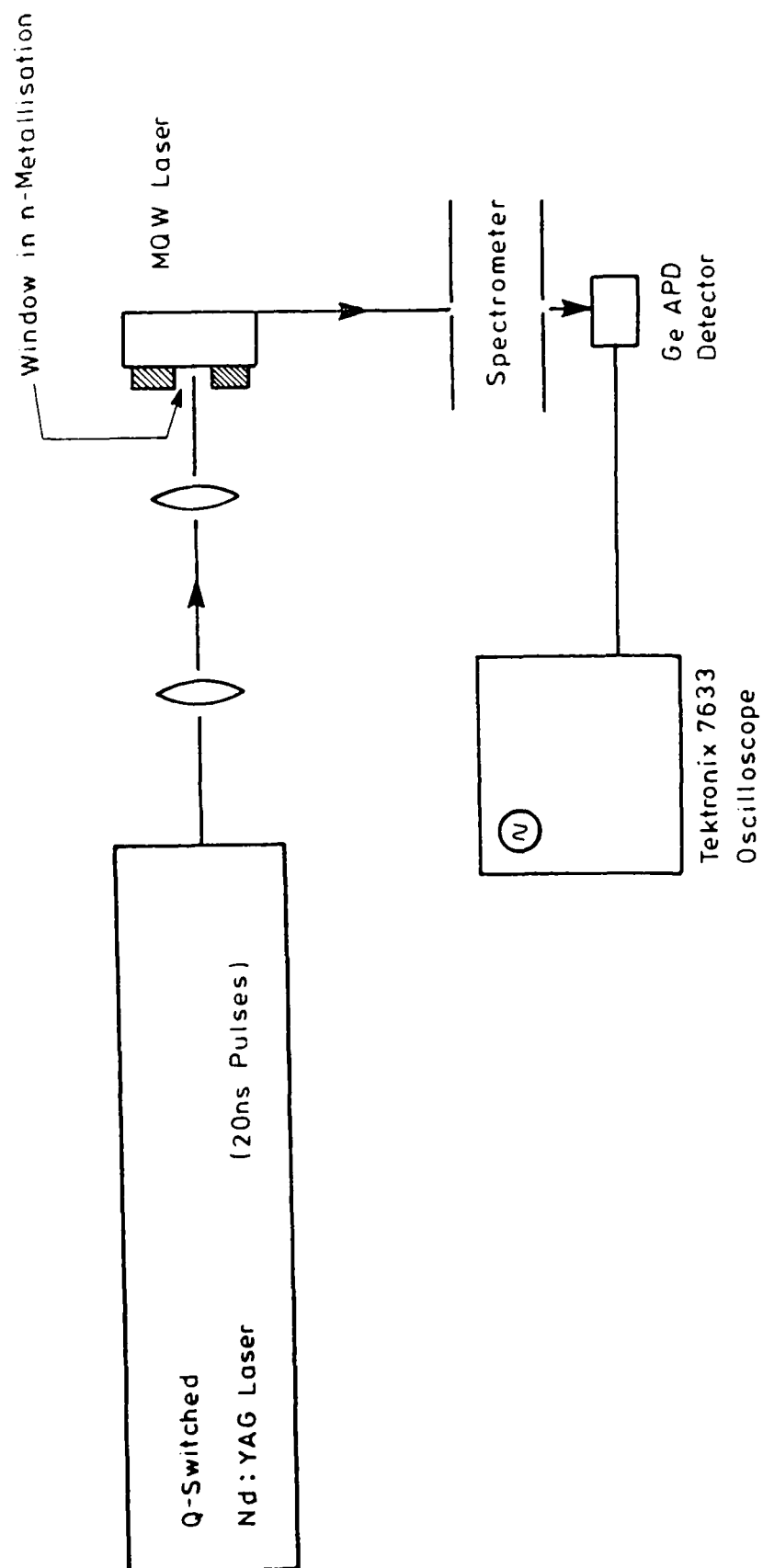
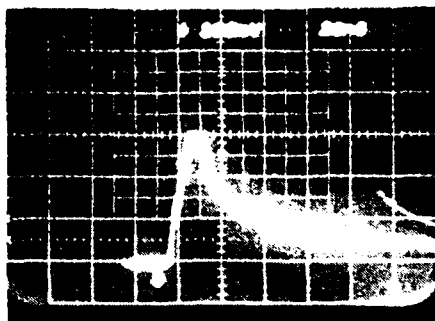
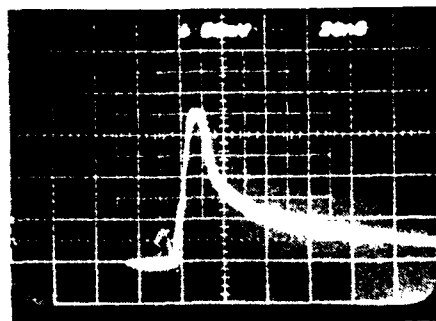


FIG.23 APPARATUS FOR OPTICALLY PUMPED LASING CHARACTERISATION.

$4I_0$

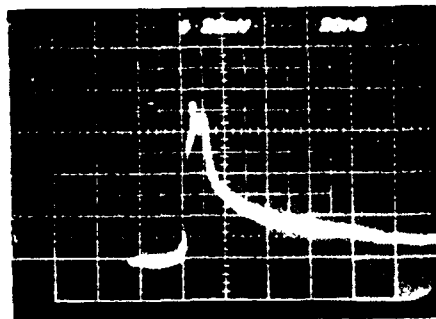


$3I_0$

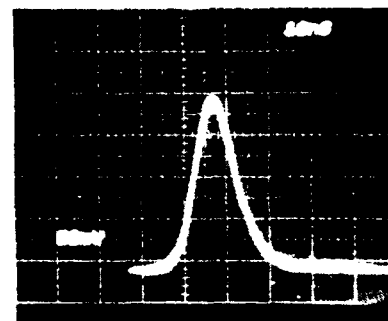
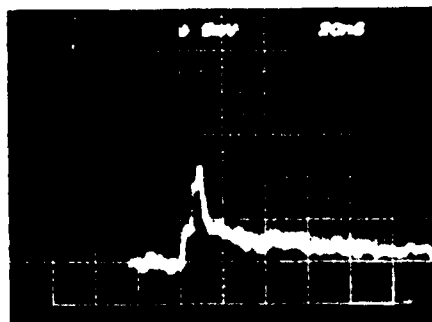


Optical Pump Power

$2I_0$



$I_0$



Nd-YAG Input Pulse

FIG. 24 SERIES OF TRACES SHOWING THE OPTICALLY PUMPED LASING ACTION FROM A 30 WELL GaInAs/ InP MQW LASER.

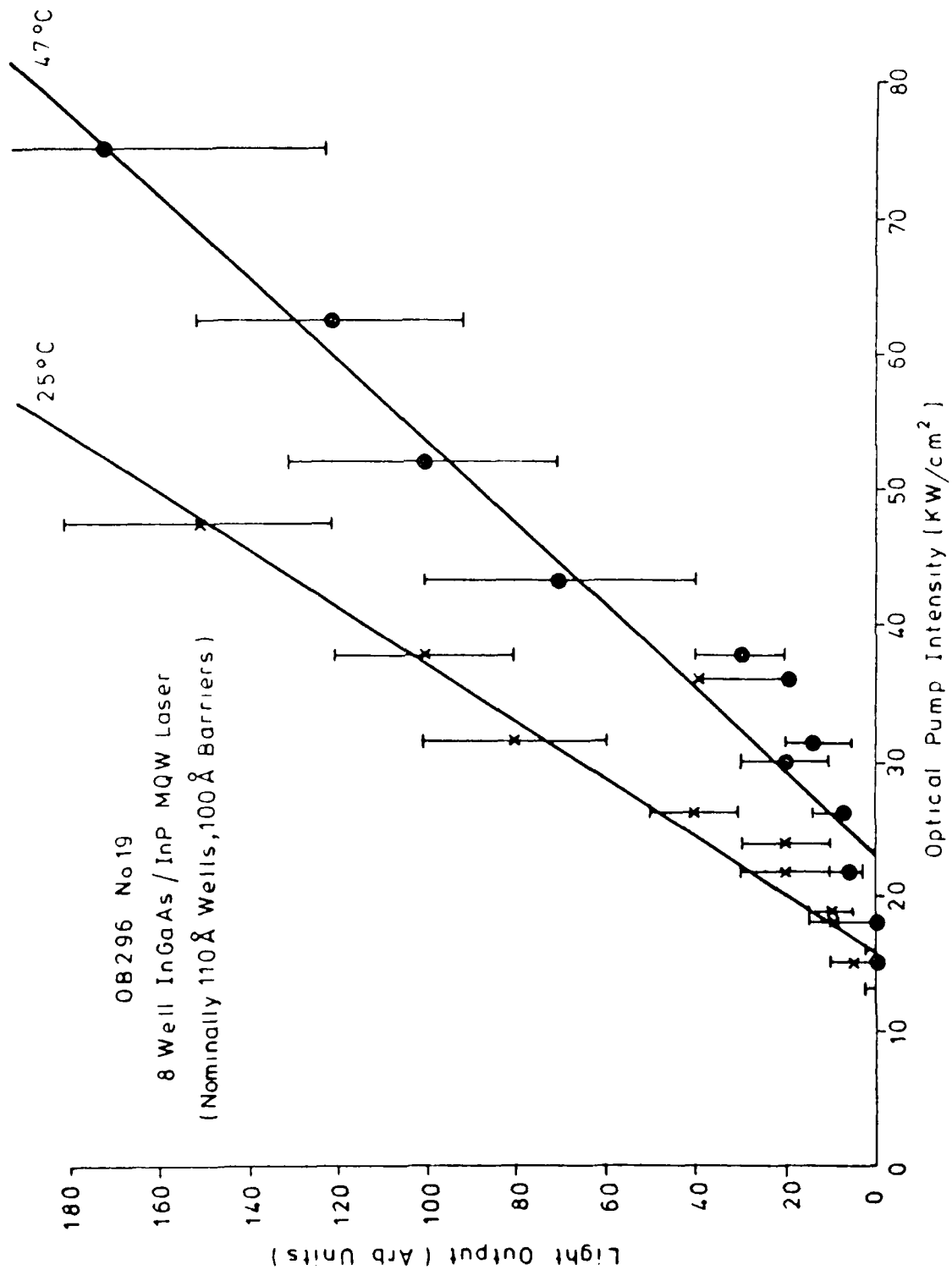


FIG.25 LIGHT OUTPUT vs OPTICAL PUMP POWER.

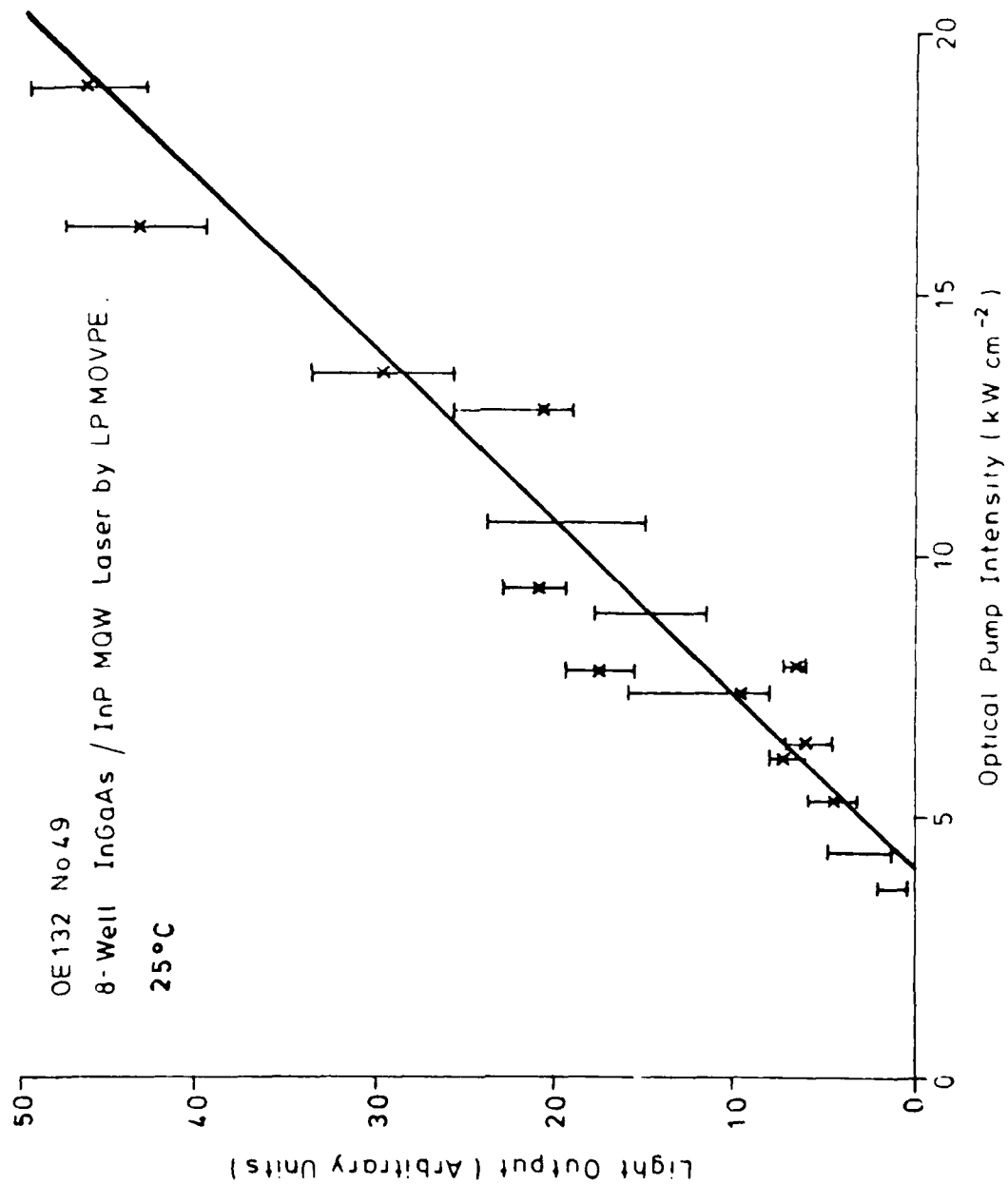


FIG.26 LIGHT OUTPUT vs OPTICAL PUMP POWER

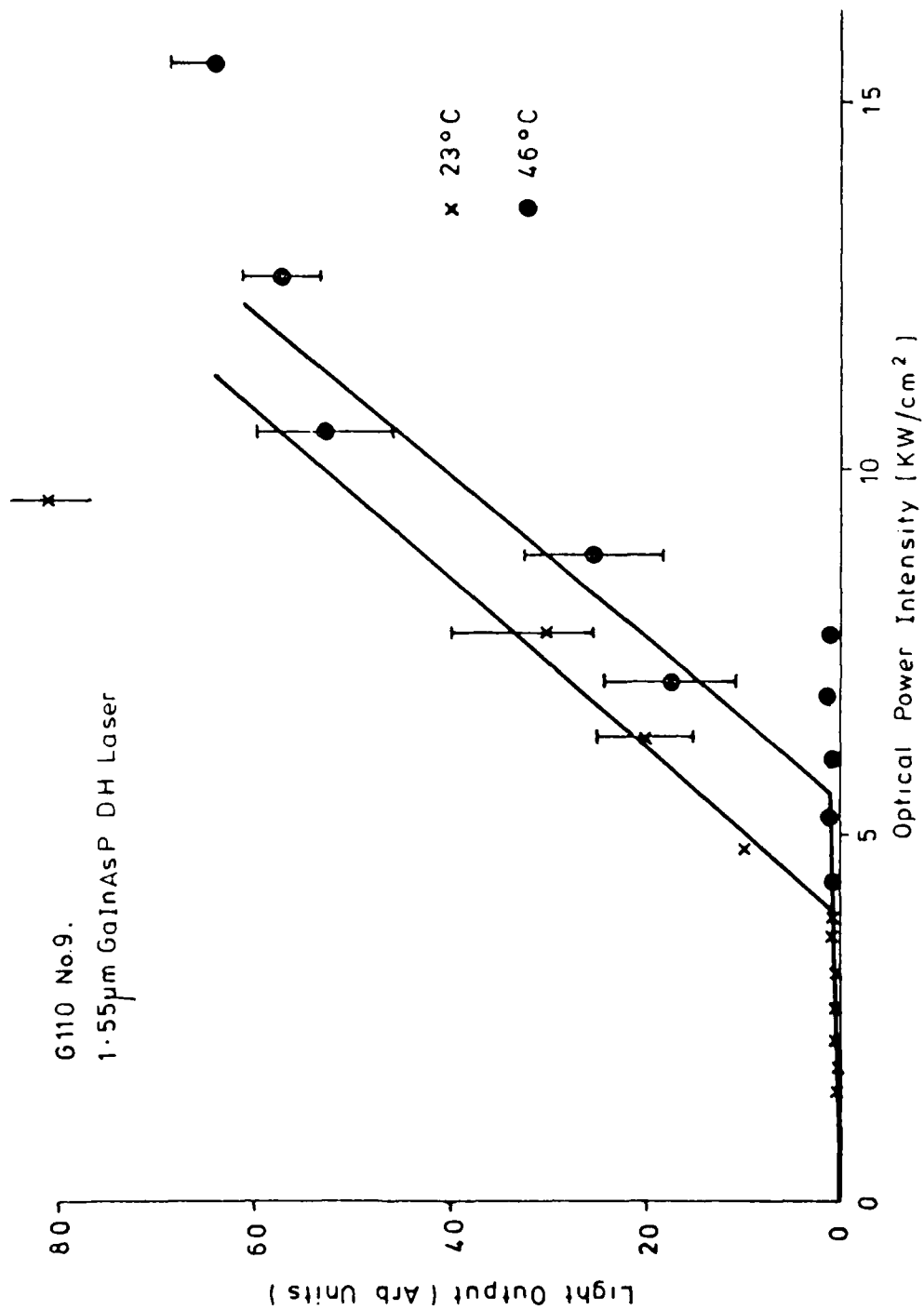


FIG.27 LIGHT OUTPUT vs OPTICAL PUMP POWER.

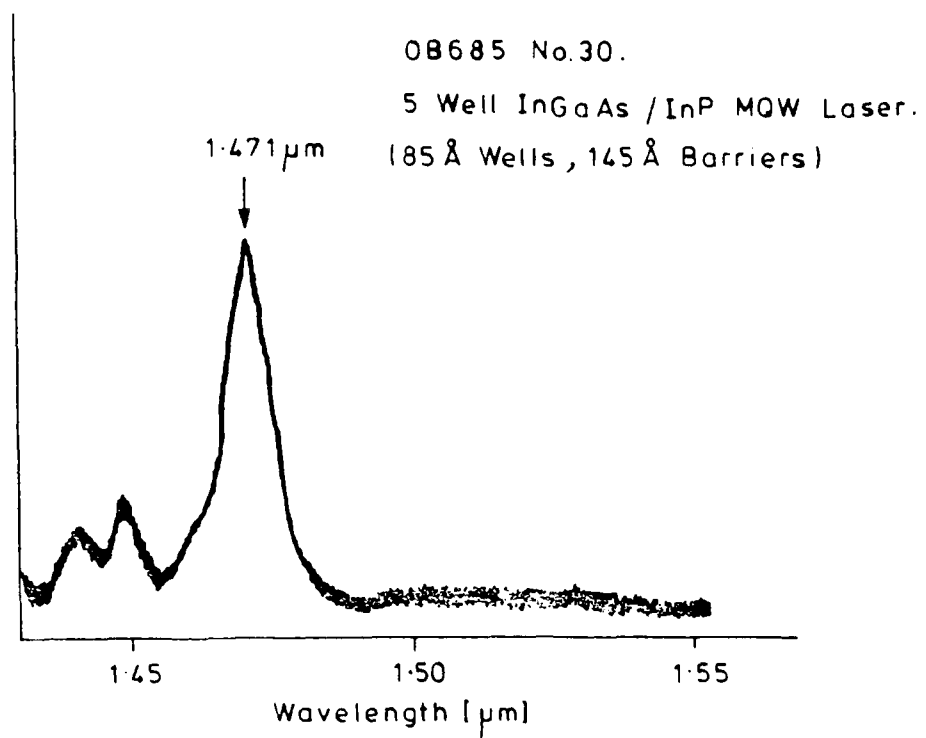


FIG. 28 OPTICALLY PUMPED LASING SPECTRUM.



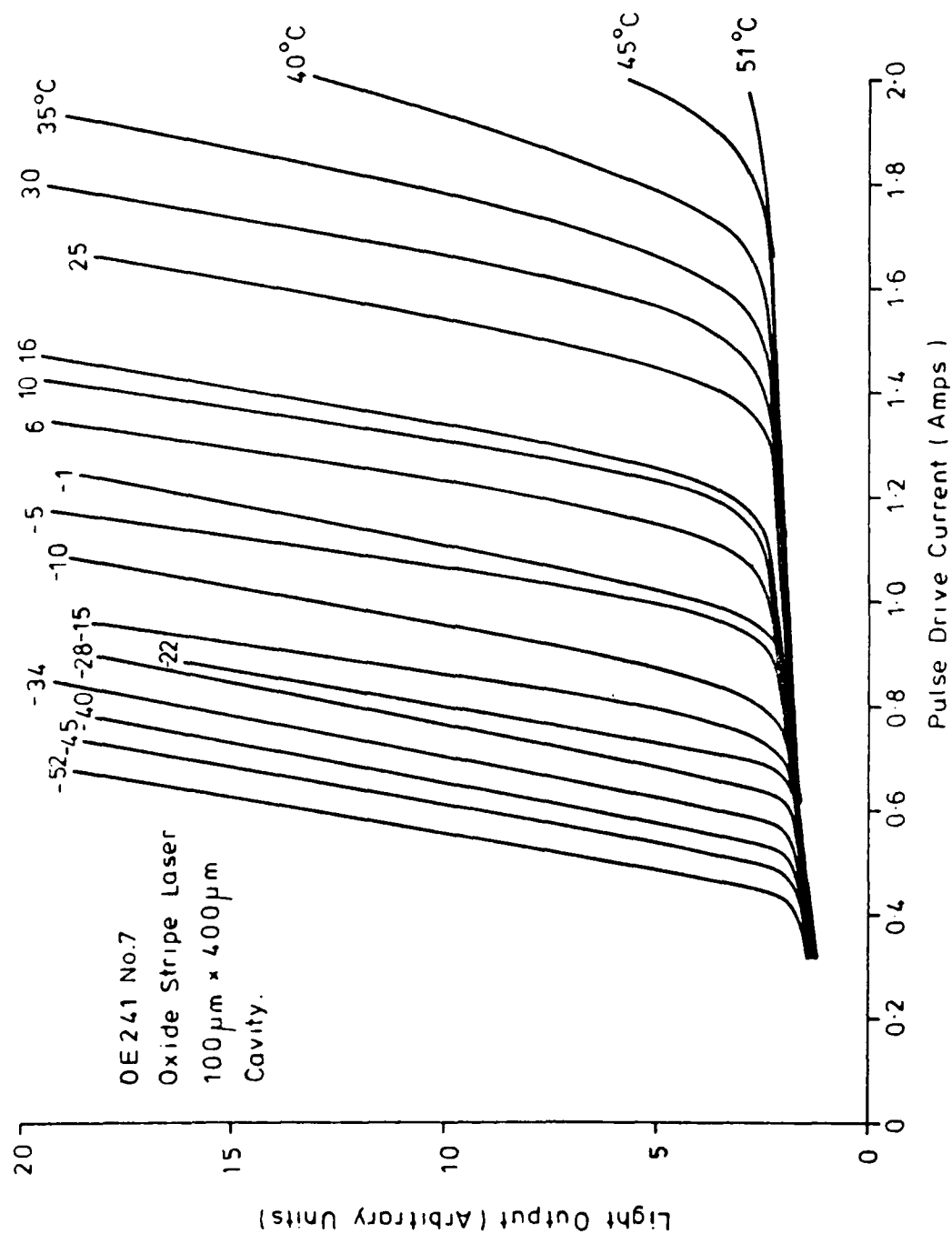


FIG.29 VARIATION OF LIGHT/CURRENT CHARACTERISTICS WITH TEMPERATURE  
FOR AN 8-WELL  $\text{InGaAs/InP}$  MQW OXIDE STRIPE LASER WITH THINNER  
BARRIERS (100 Å WELLS, 25 Å BARRIERS.)

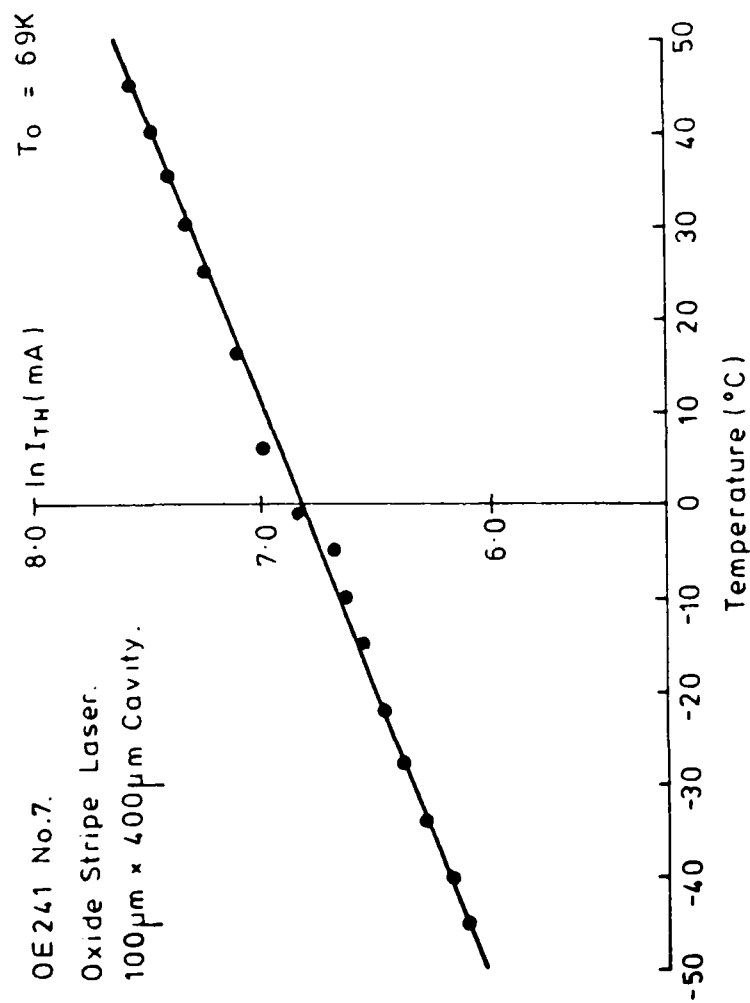


FIG. 30 VARIATION OF THRESHOLD CURRENT WITH TEMPERATURE FOR AN 8 - WELL  
InGaAs/InP MQW LASER WITH THINNER BARRIERS (~100Å WELLS, 25Å BARRIERS).

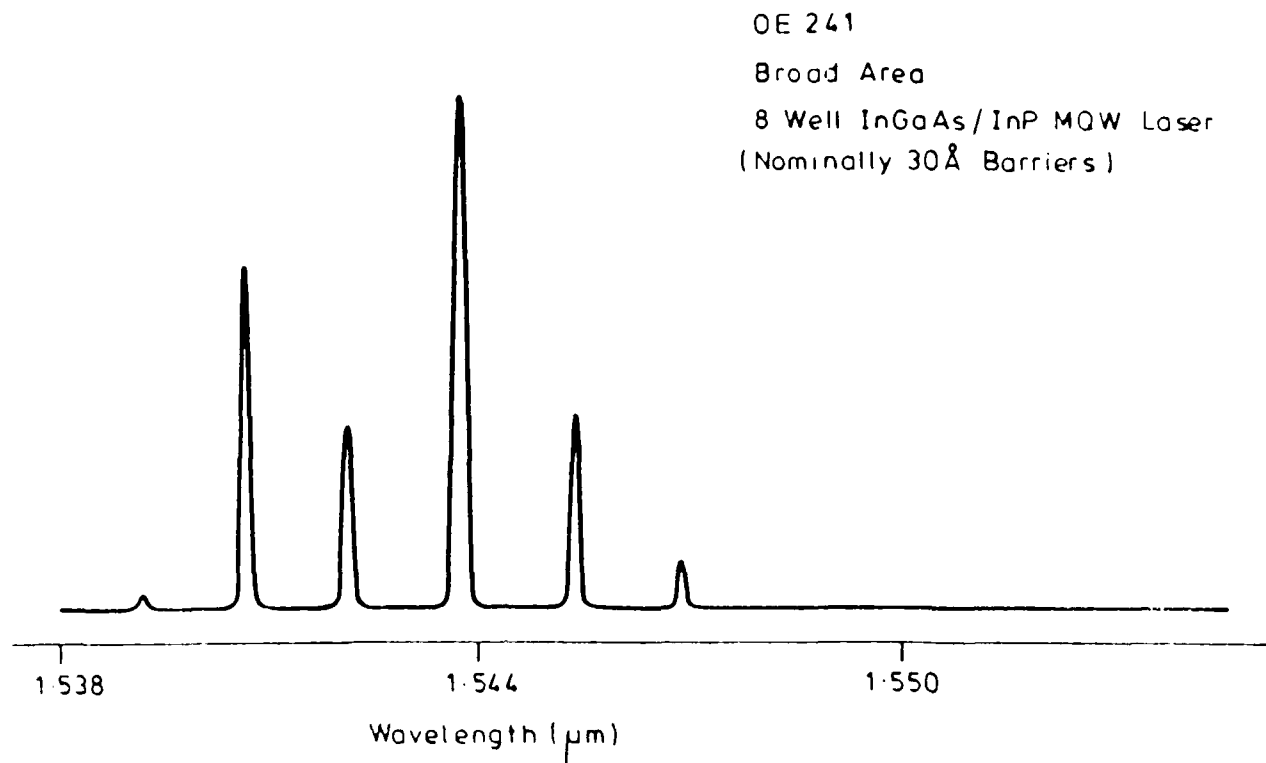


FIG 31 MQW LASER SPECTRUM FOR OXIDE STRIPE InGaAs/InP LASER  
WITH THINNER BARRIERS.

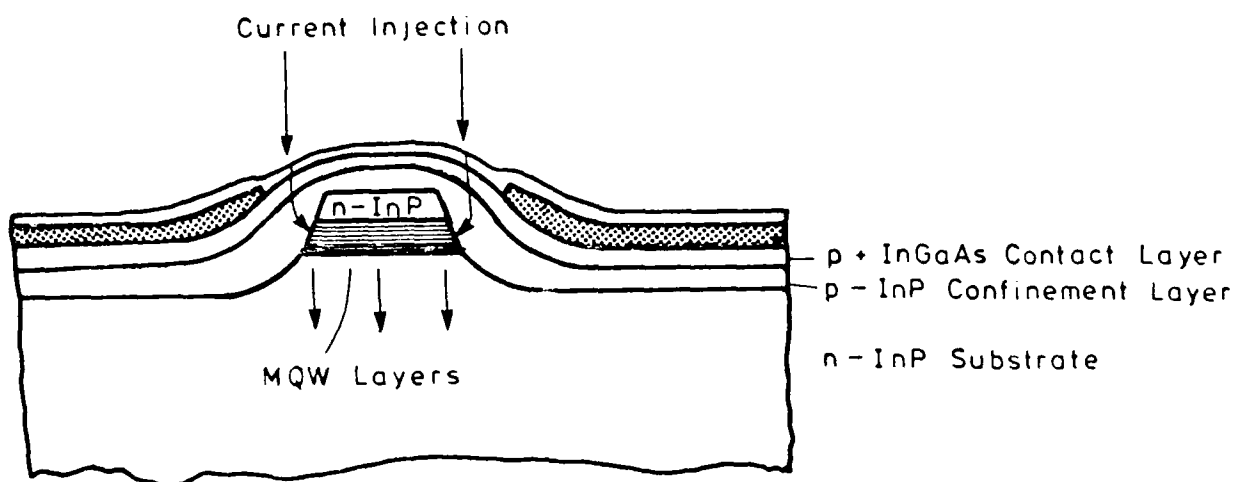


FIG. 3? TRANSVERSE BURIED STRIPE MQW LASER.

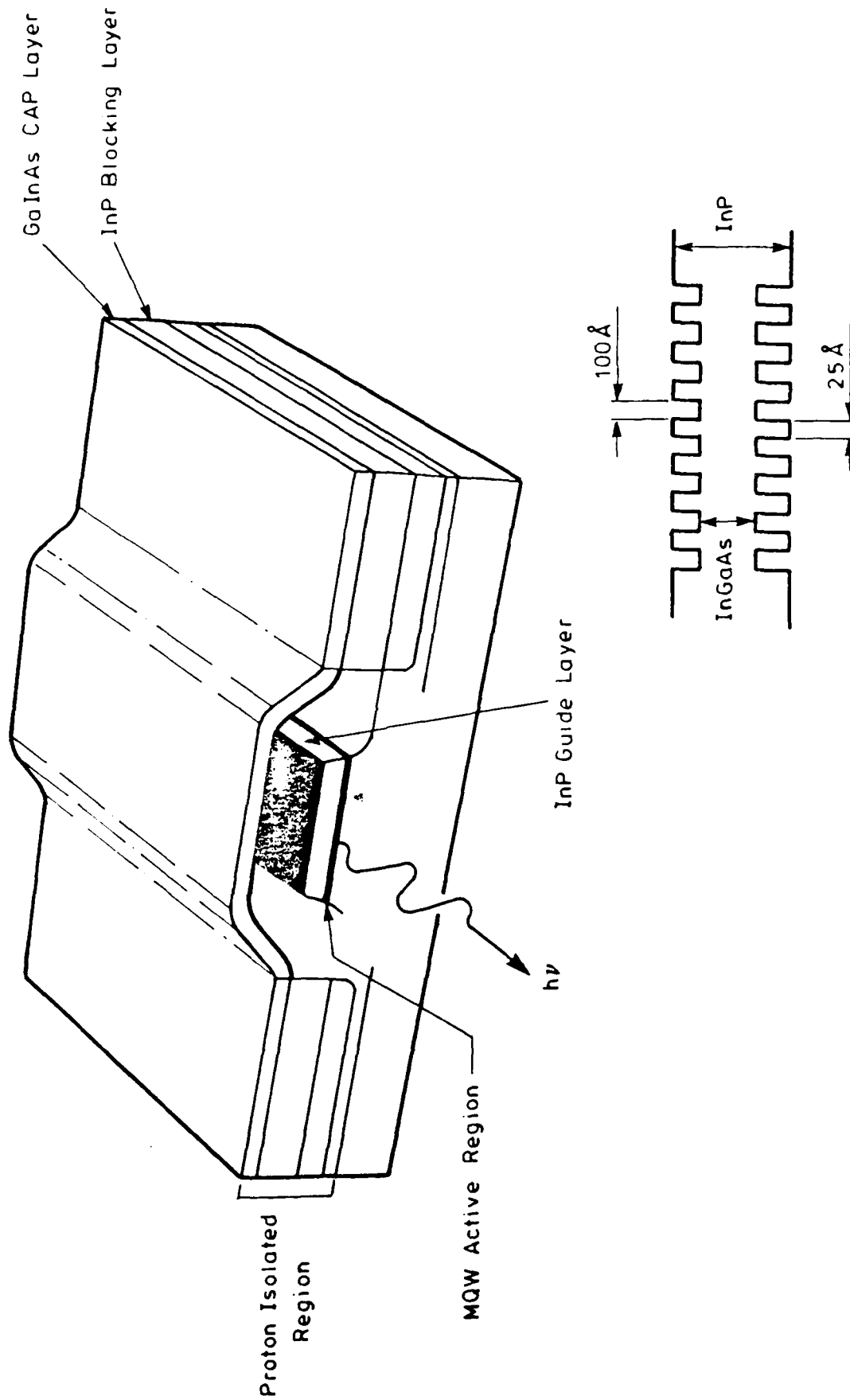


FIG.33 ALL MOVPE BURIED RIDGE InGaAs / InP MQW LASER

OE 241B No 53

InGaAs/InP MQW Laser at 21°C

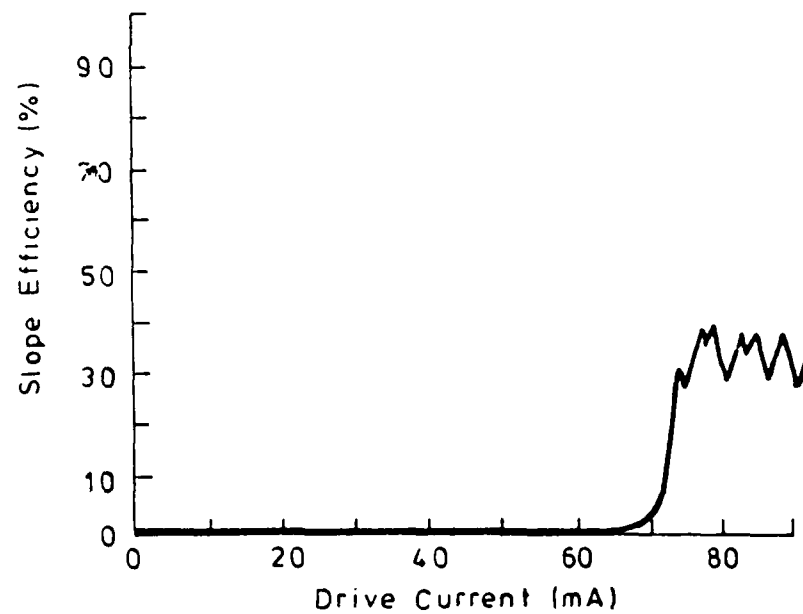
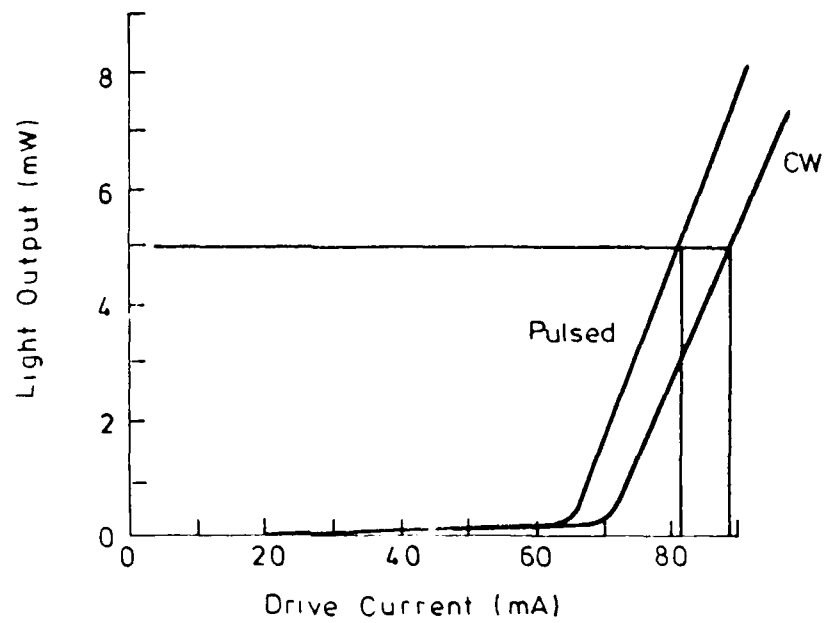


FIG. 34 CW AND PULSED LIGHT/CURRENT CHARACTERISTICS FOR BURIED RIDGE InGaAs/InP MQW LASER.

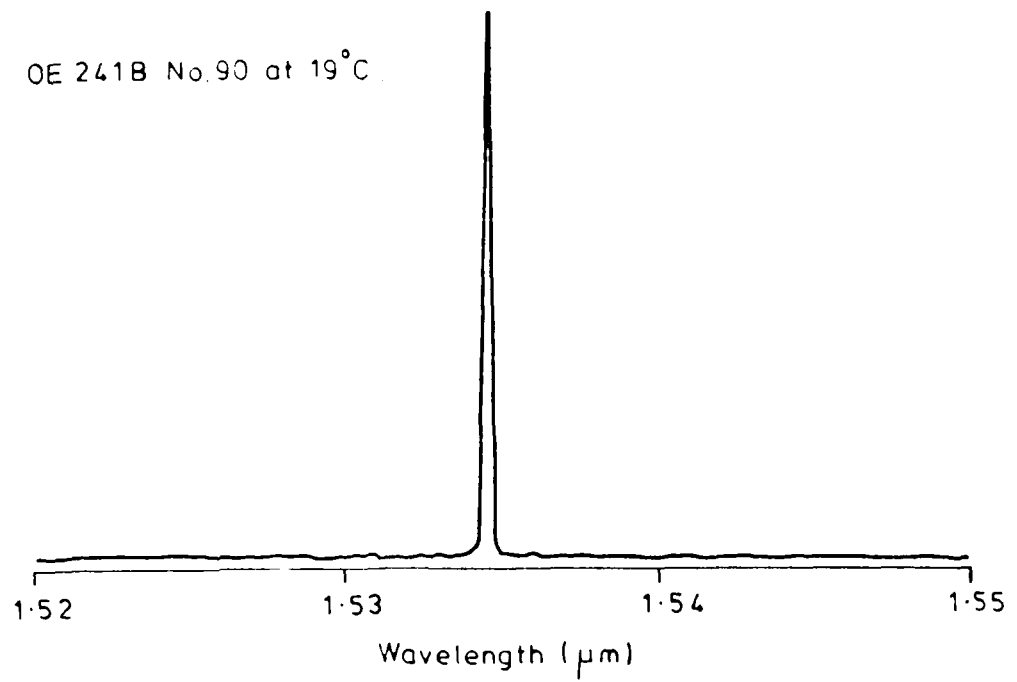


FIG.35 CW LASING SPECTRUM FOR BURIED RIDGE InGaAs/InP MQW LASER.

OE241B No.53  
@ 15°C.

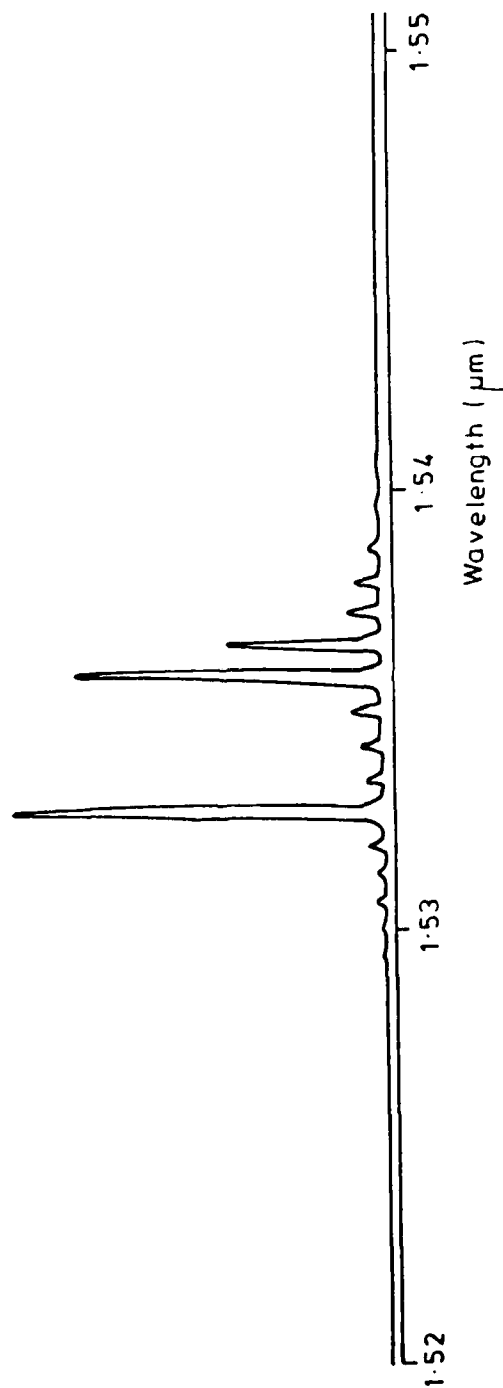


FIG. 36 LASING SPECTRUM OF BURIED RIDGE InGaAs / InP MQW LASER.



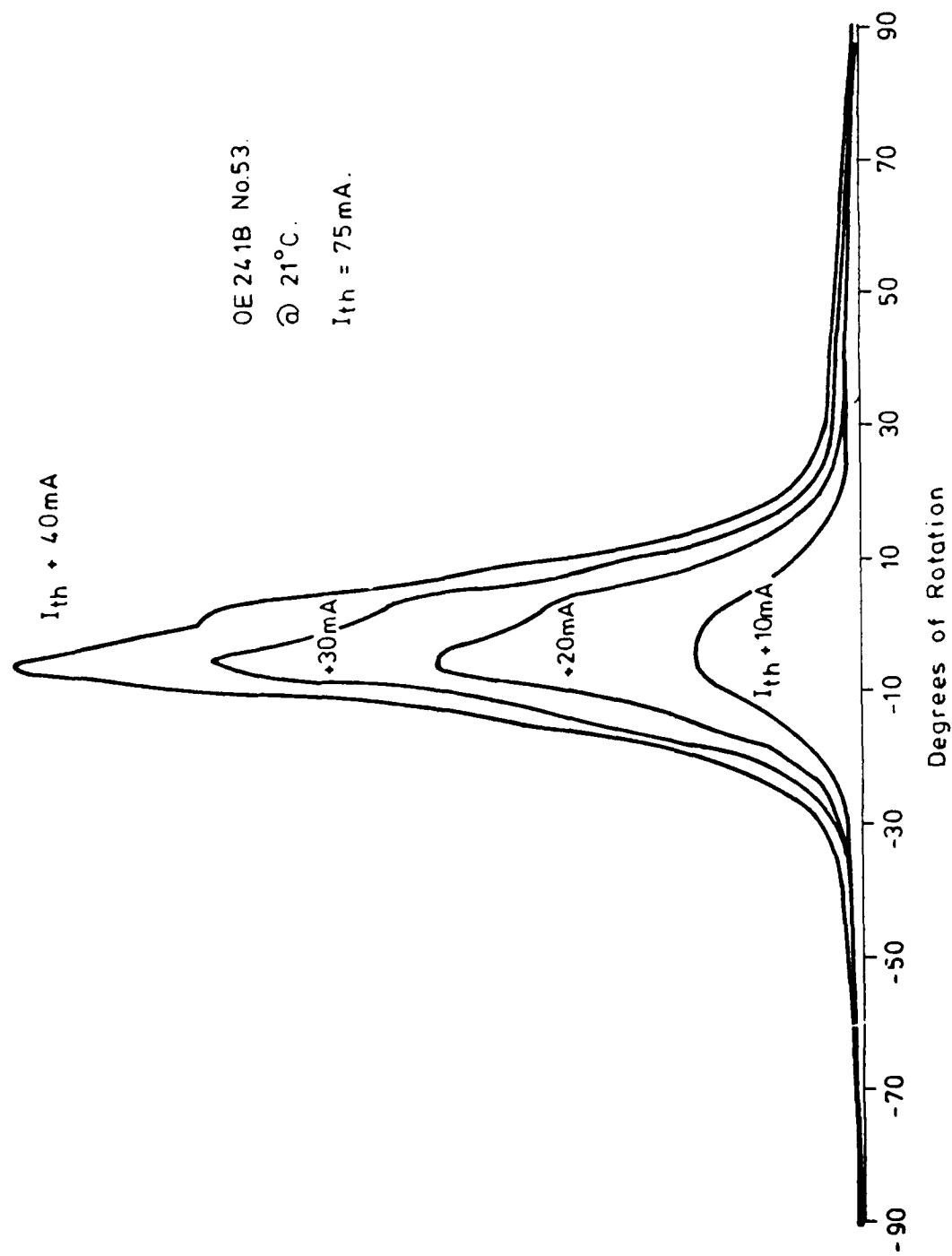


FIG.37 CW DRIVE FAR FIELD EMISSION IN PLANE OF ACTIVE LAYER FOR BURIED RIDGE InGaAs/InP MQW LASER.

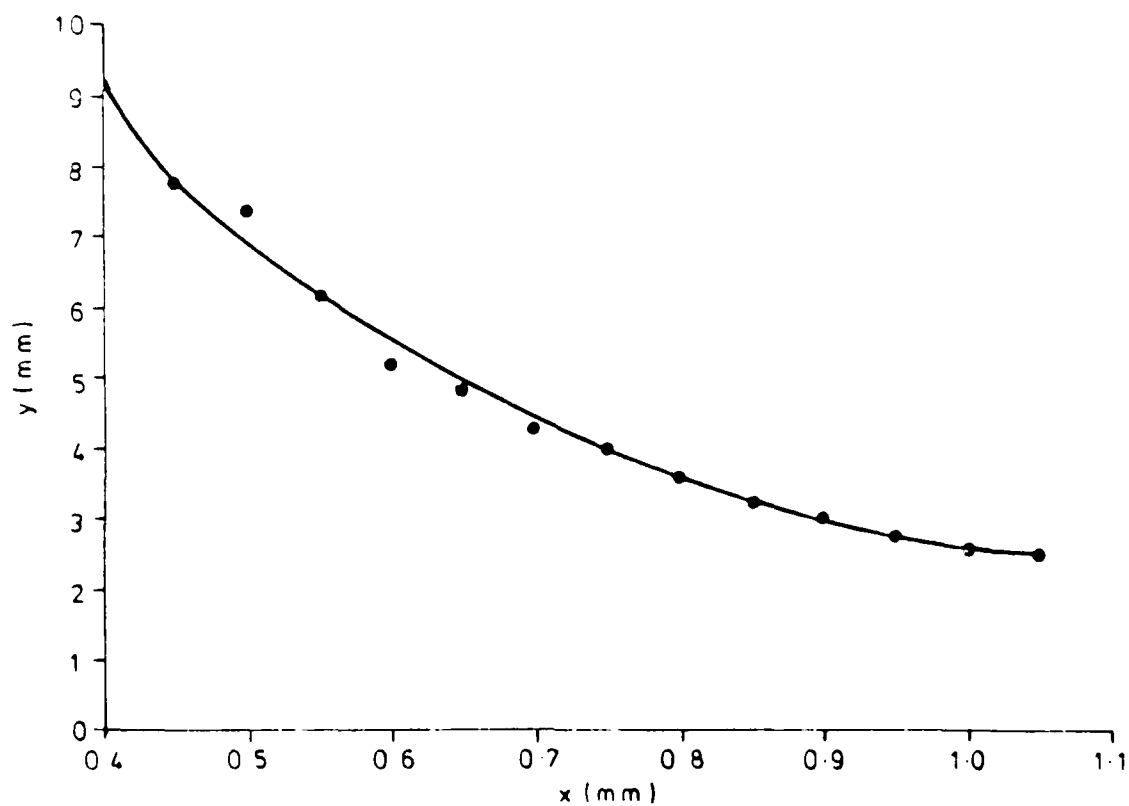
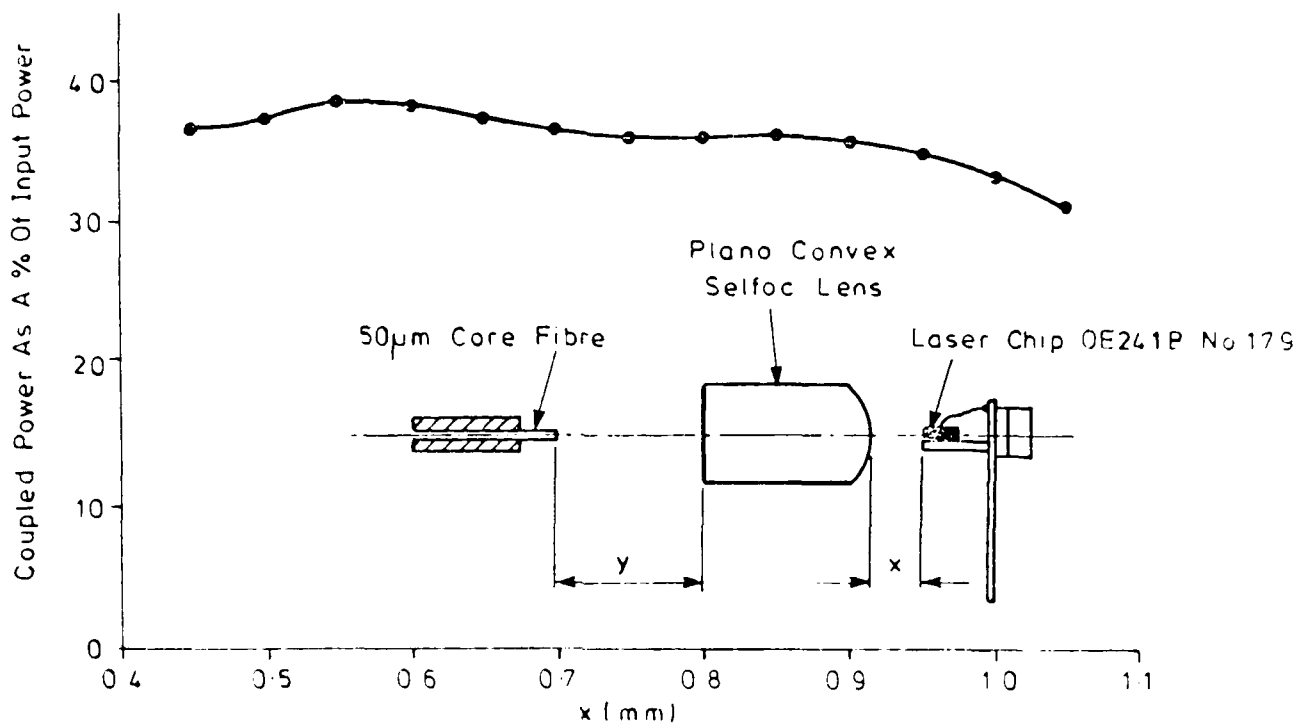


FIG 38 MQW LASER COUPLING EFFICIENCY INTO 50  $\mu\text{m}$  CORE FIBRE.

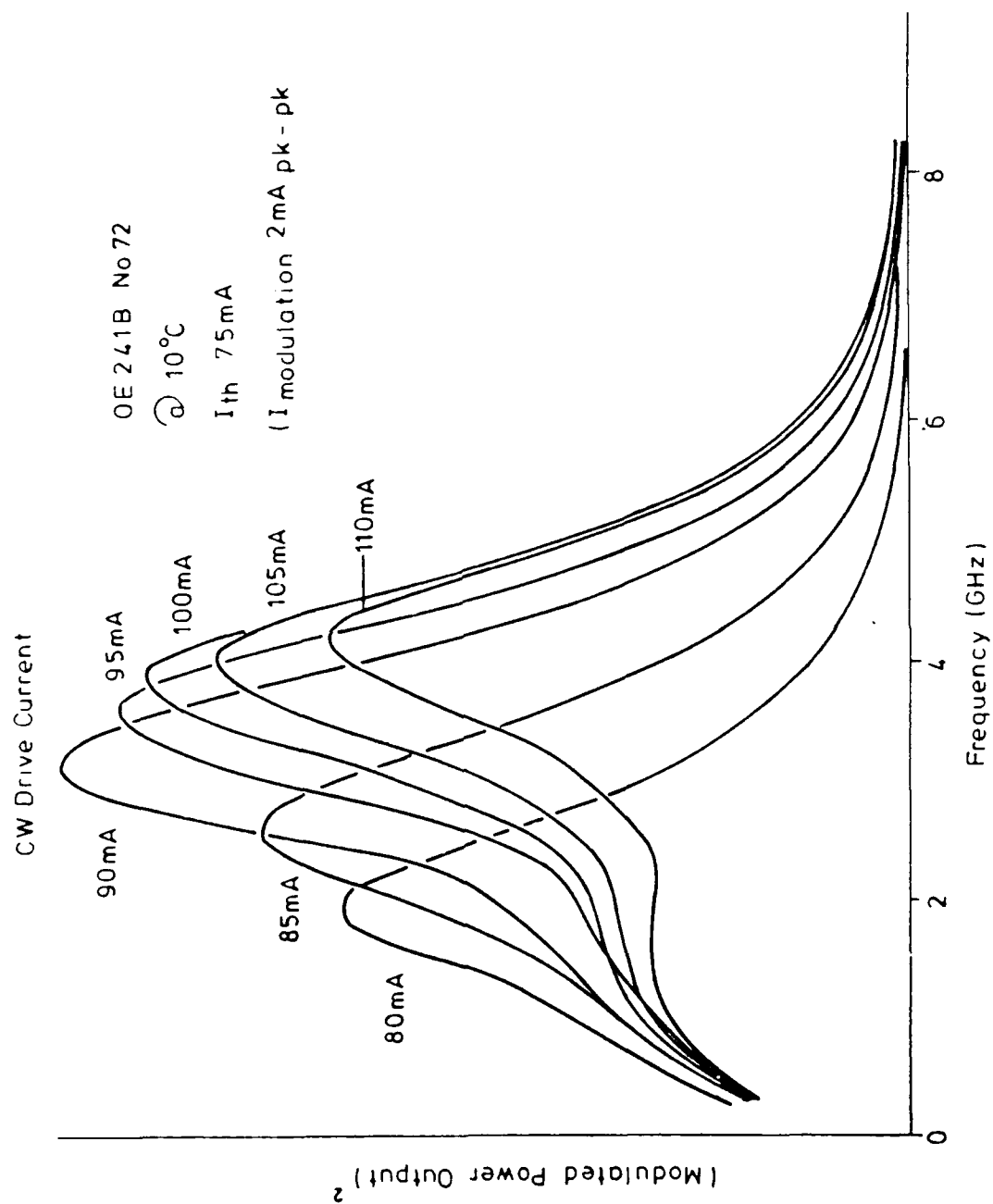


FIG. 39 SWEEP FREQUENCY RESPONSE FOR BURIED RIDGE InGaAs/InP MQW LASER.

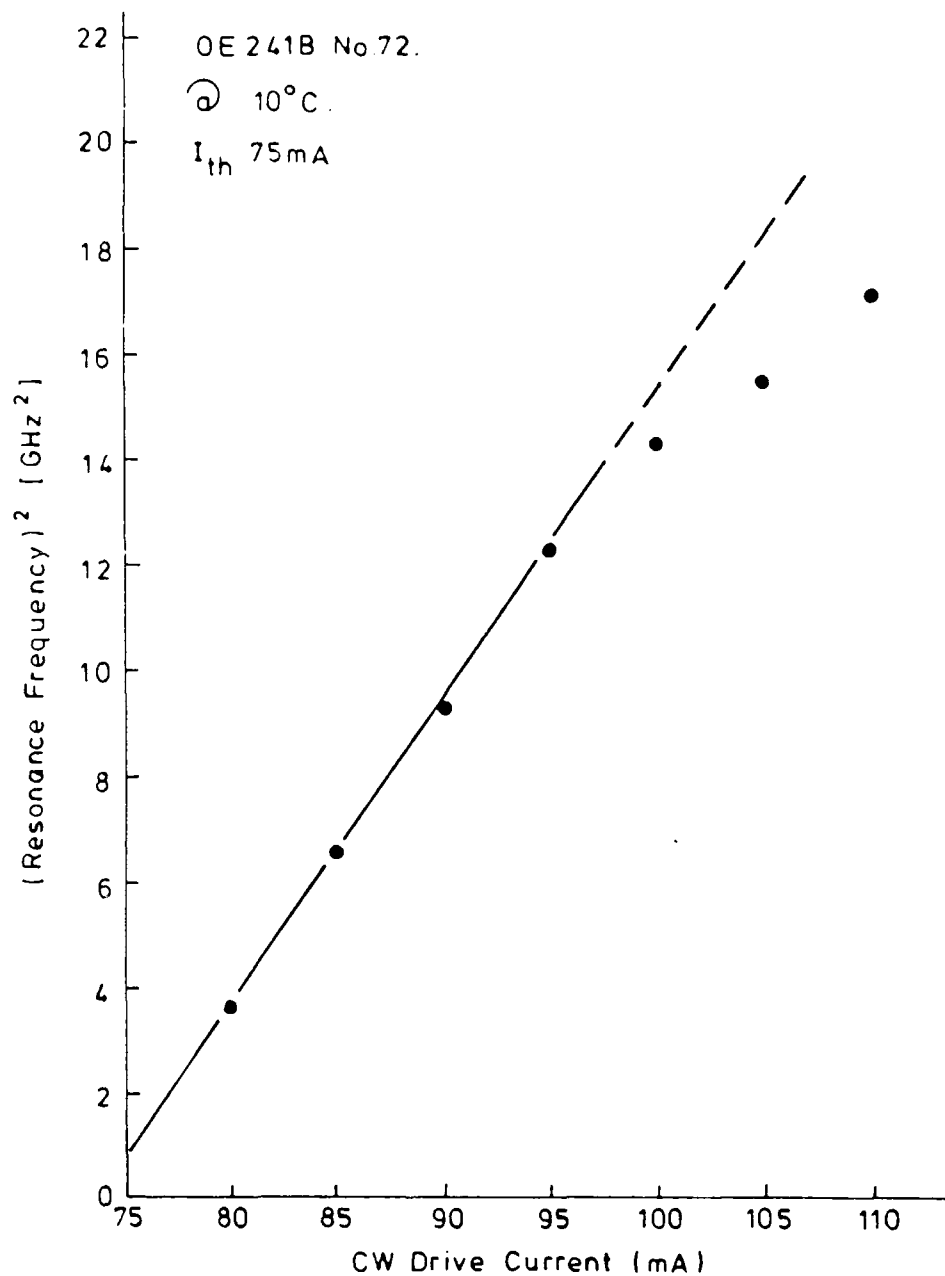


FIG.40 VARIATION OF RESONANCE FREQUENCY WITH MQW LASER DRIVE CURRENT.

OE 241B No. 23

@ 19°C

$I_{th}$  80mA

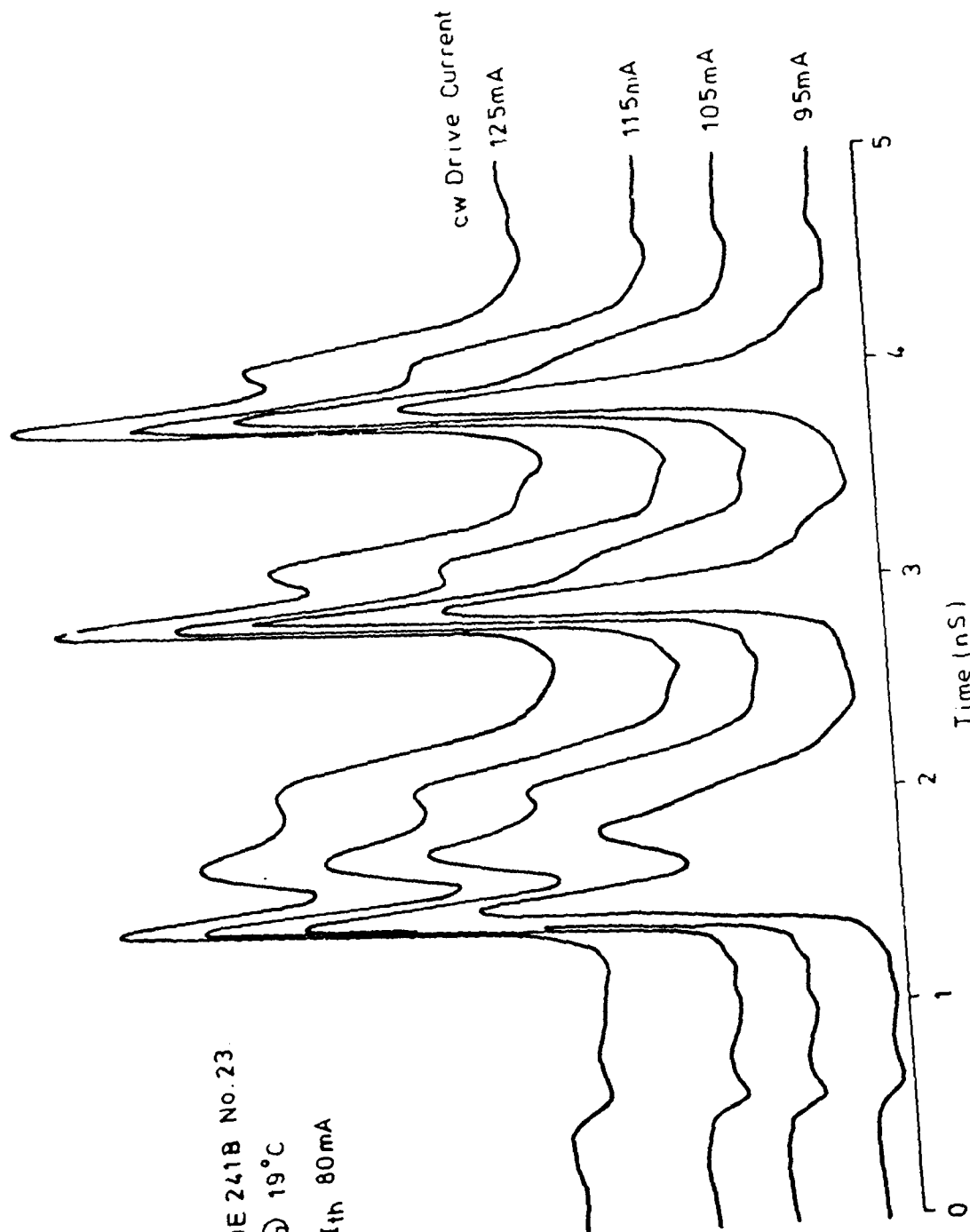


FIG. 41 2Gbit/s LARGE SIGNAL FREQUENCY RESPONSE FOR BURIED RIDGE InGaAs/InP MQW LASER.

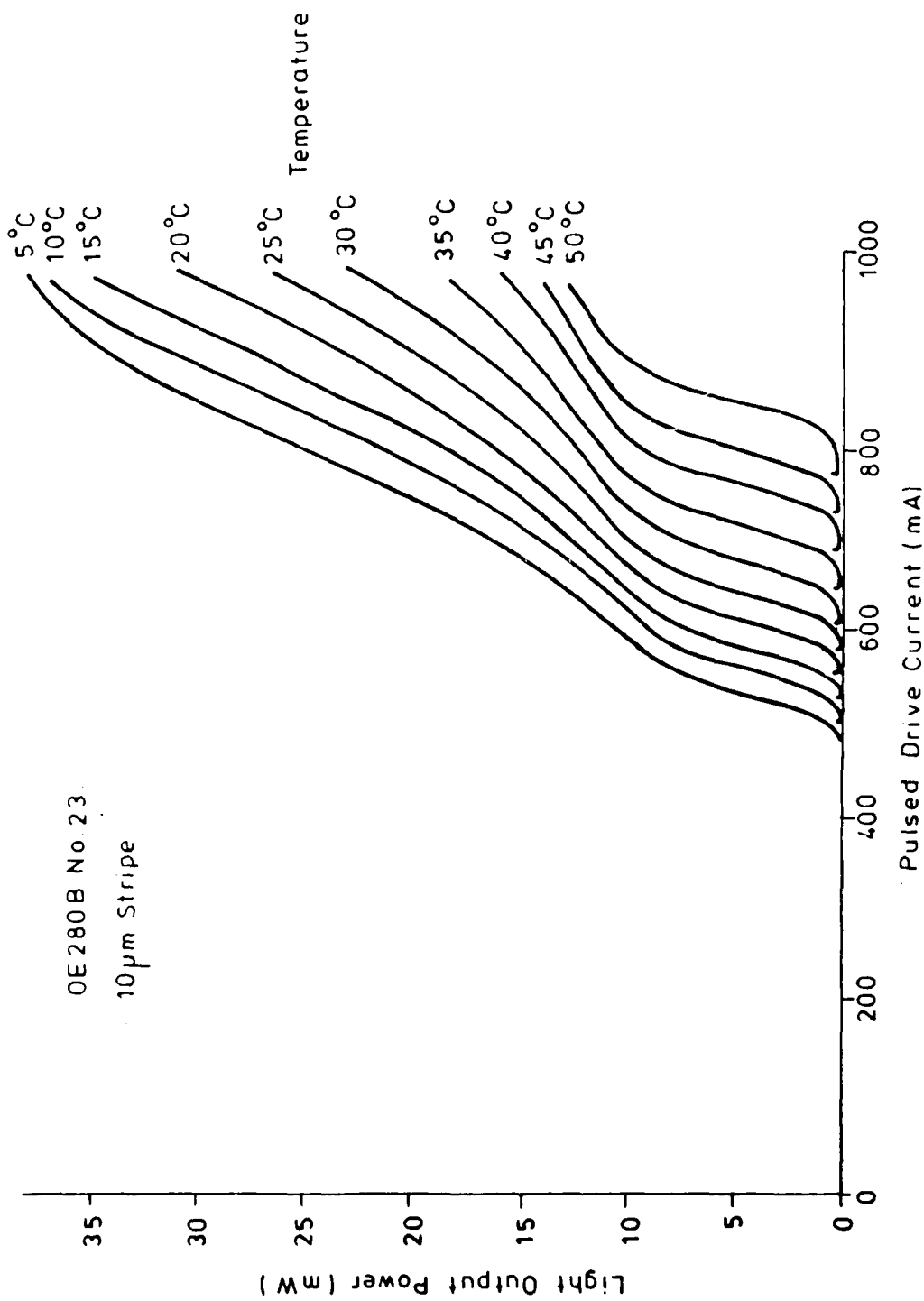


FIG.42 PULSED LIGHT/CURRENT CHARACTERISTICS OXIDE STRIPE GaAlInAs DH LASER.

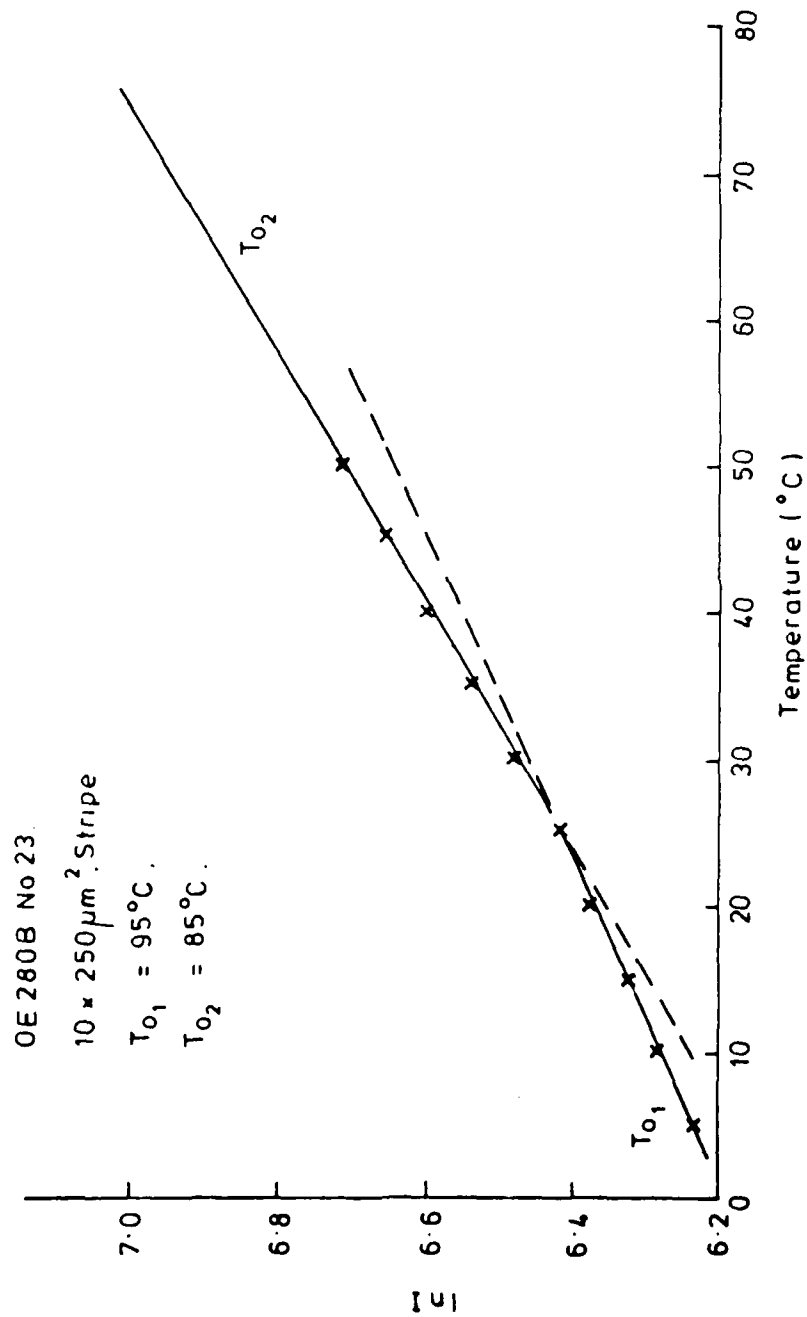


FIG.43 PLOT SHOWING  $T_0$  CHARACTERISTICS FOR OXIDE STRIPE GaAlInAs DH LASER.

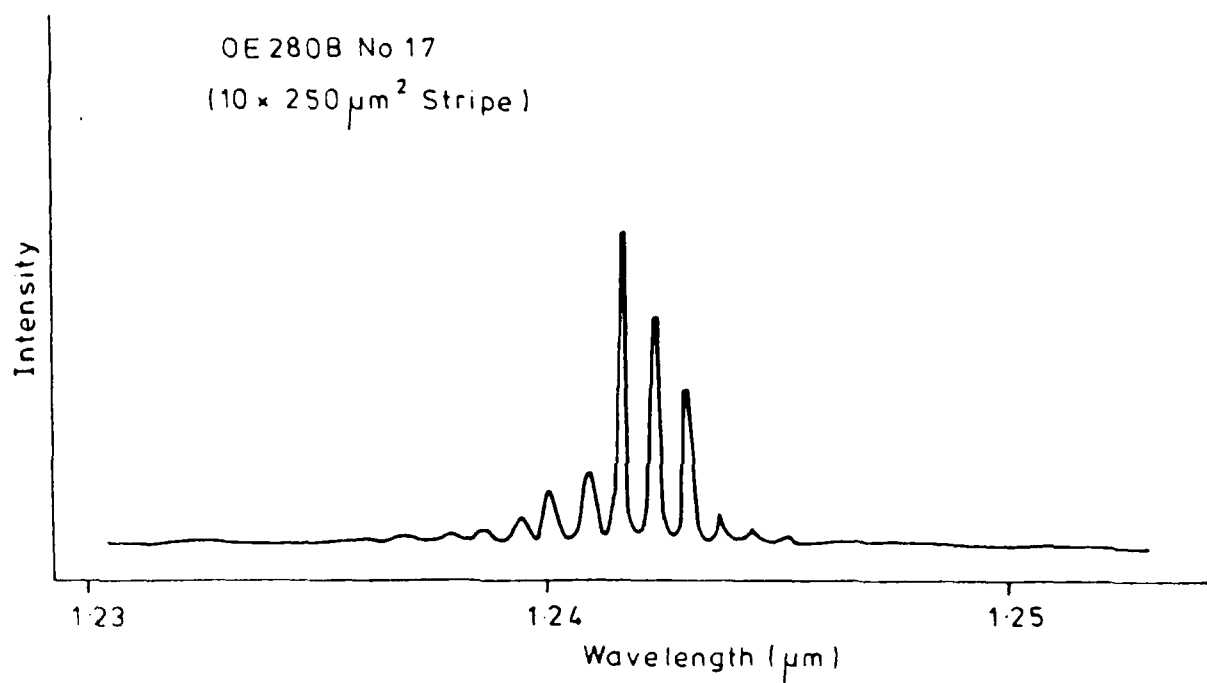


FIG.44 LASING SPECTRUM FOR GaAlInAs ACTIVE LAYER OXIDE STRIPE D H LASER.



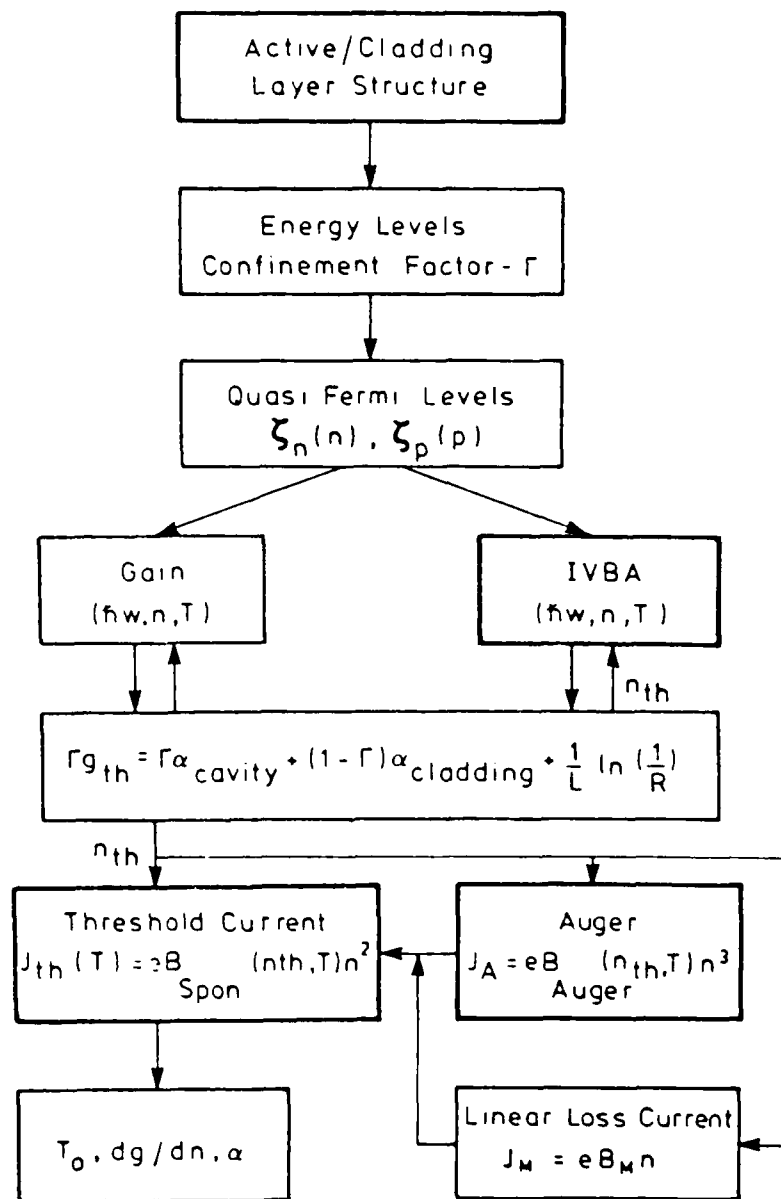


FIG 45

FLOW DIAGRAM FOR THE QUANTUM WELL LASER MODEL.

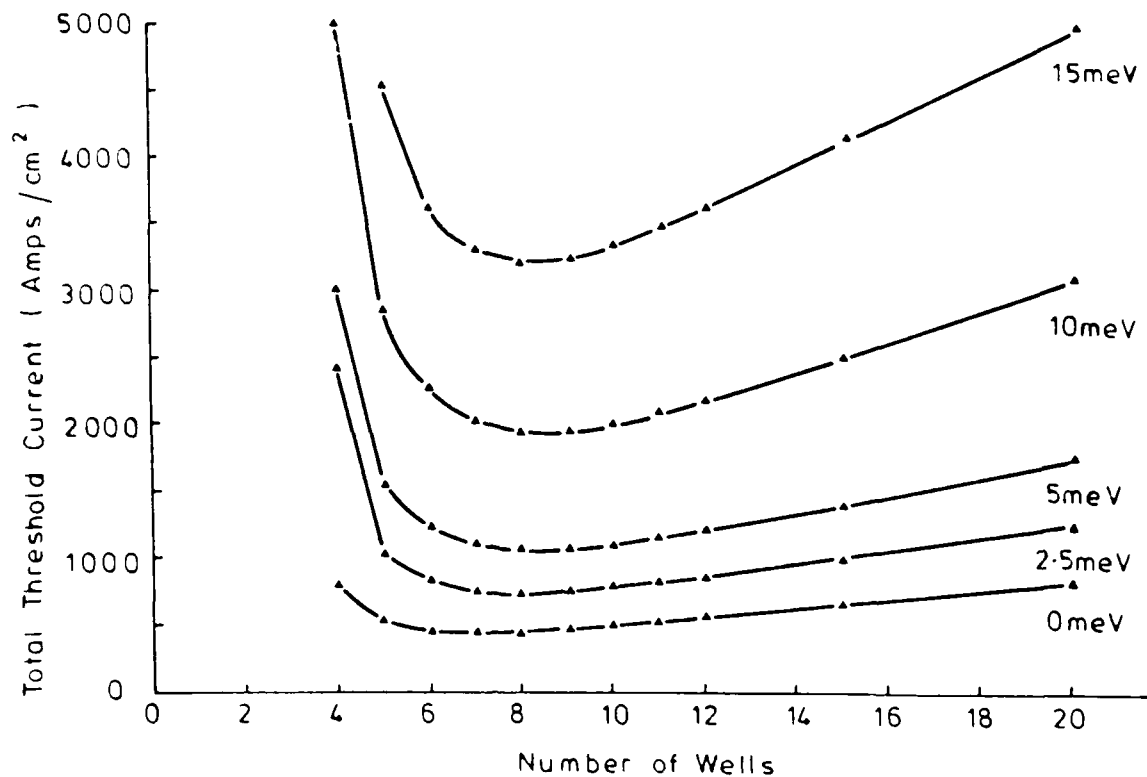


FIG. 46

TOTAL THRESHOLD CURRENT DENSITY FOR AN InGaAs/InP 110Å MQW LASER

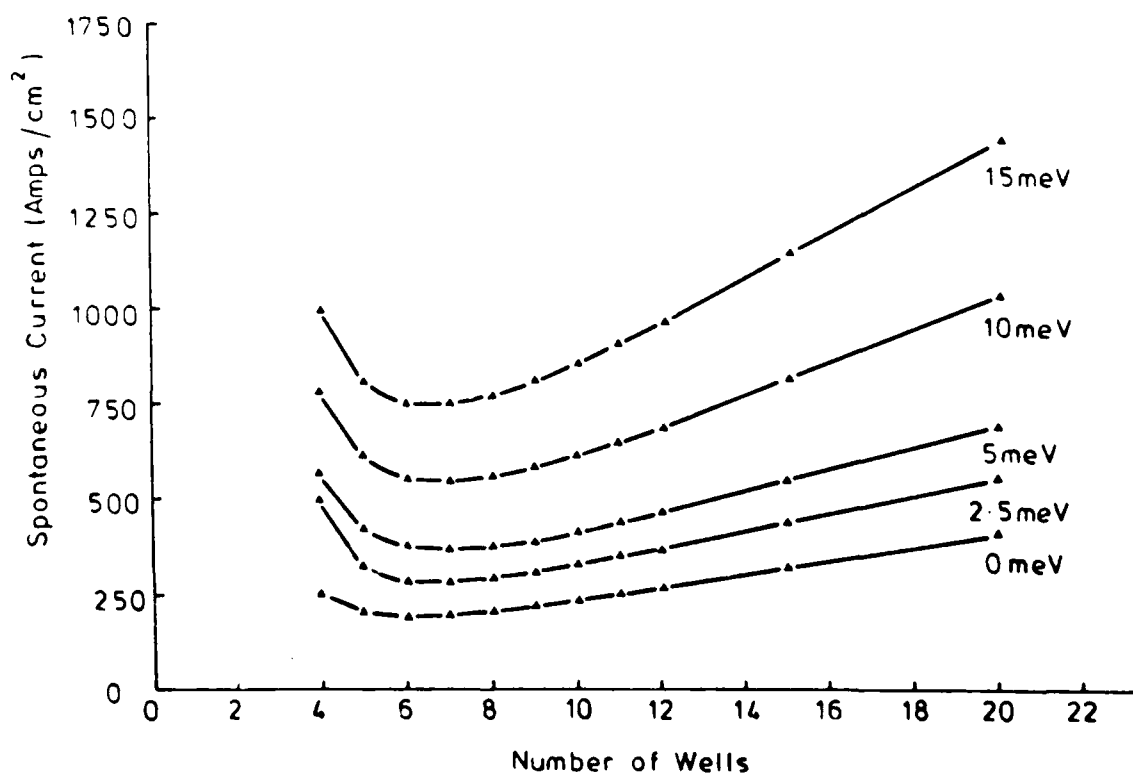


FIG. 47

SPONTANEOUS CURRENT DENSITY AT THRESHOLD FOR AN InGaAs/InP 110Å MQW LASER.

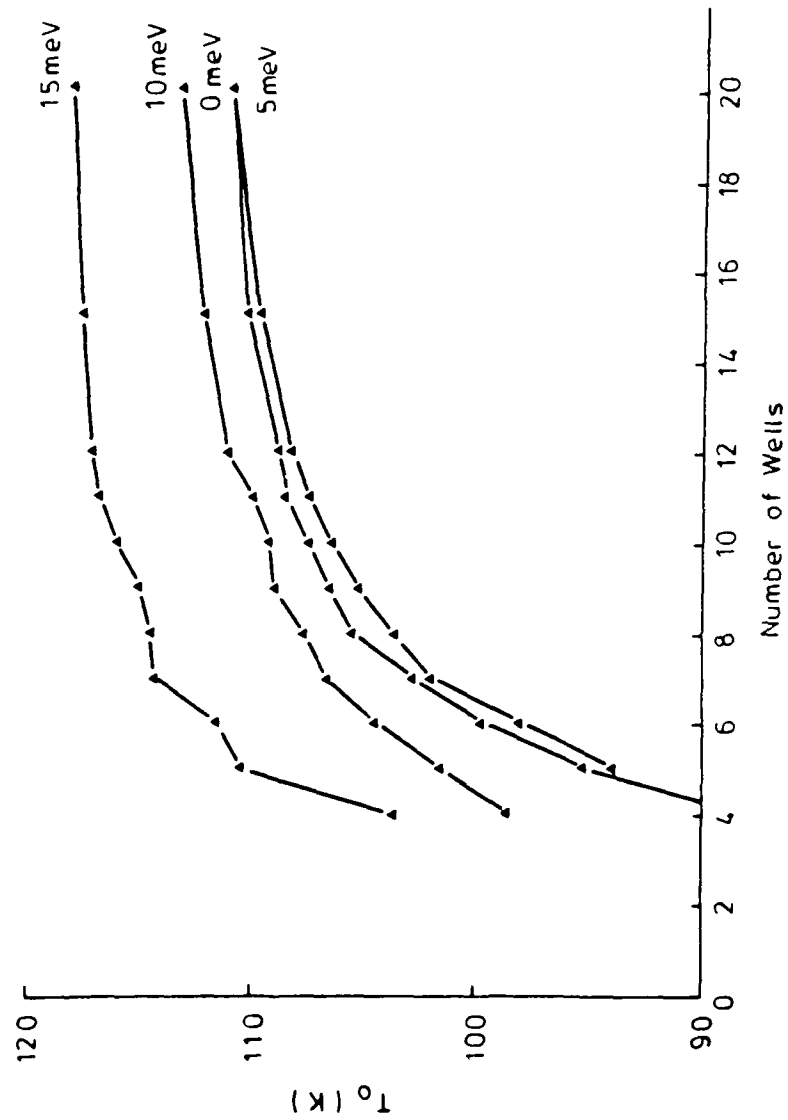


FIG. 48 TEMPERATURE SENSITIVITY AT 300K FOR AN InGaAs/InP 110Å MQW LASER

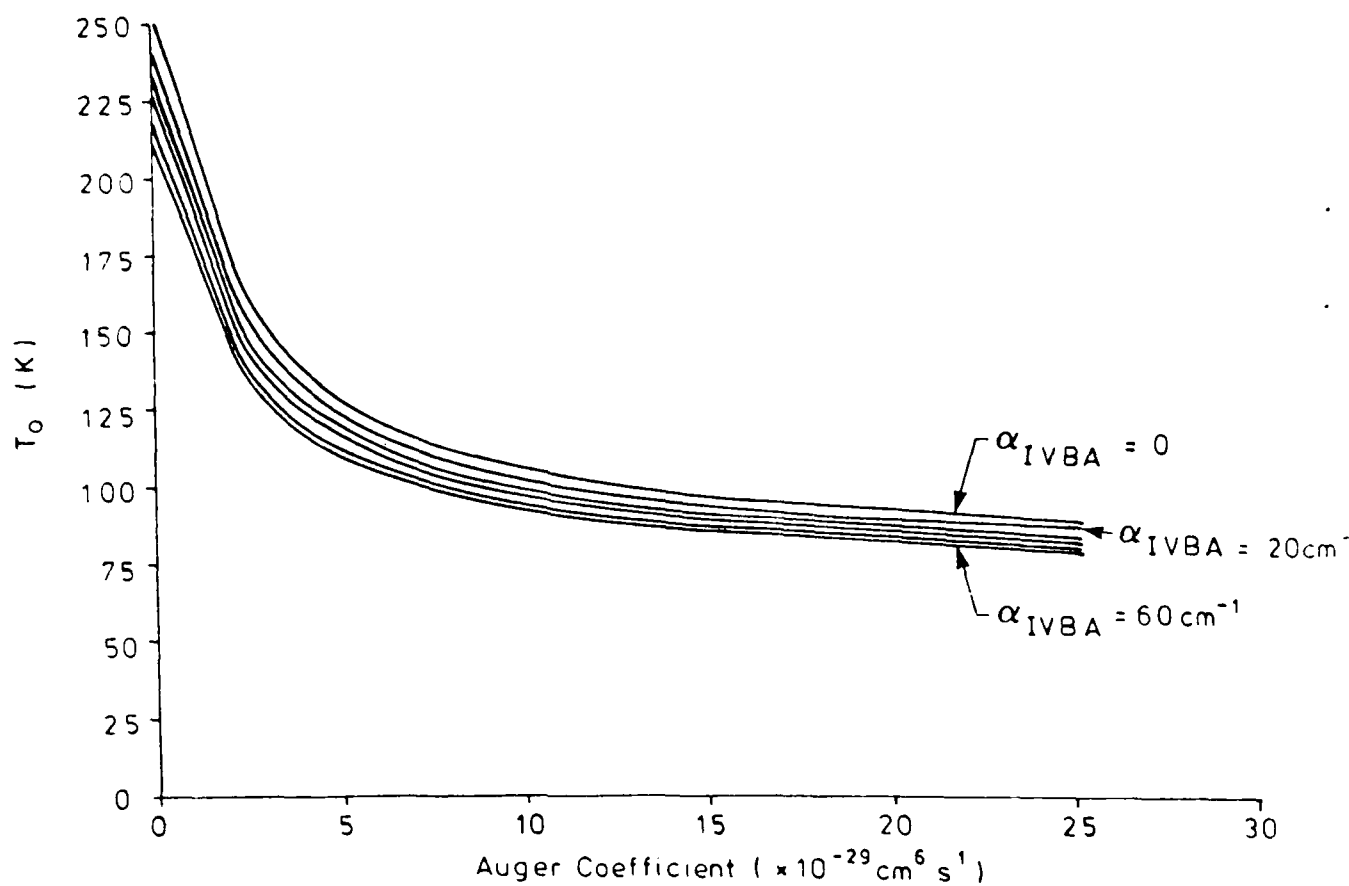


FIG 49 TEMPERATURE SENSITIVITY AT 300K FOR AN 8-WELL InGaAs/InP 110Å MQW LASER AS A FUNCTION OF IVBA AND AUGER LOSS RATES.

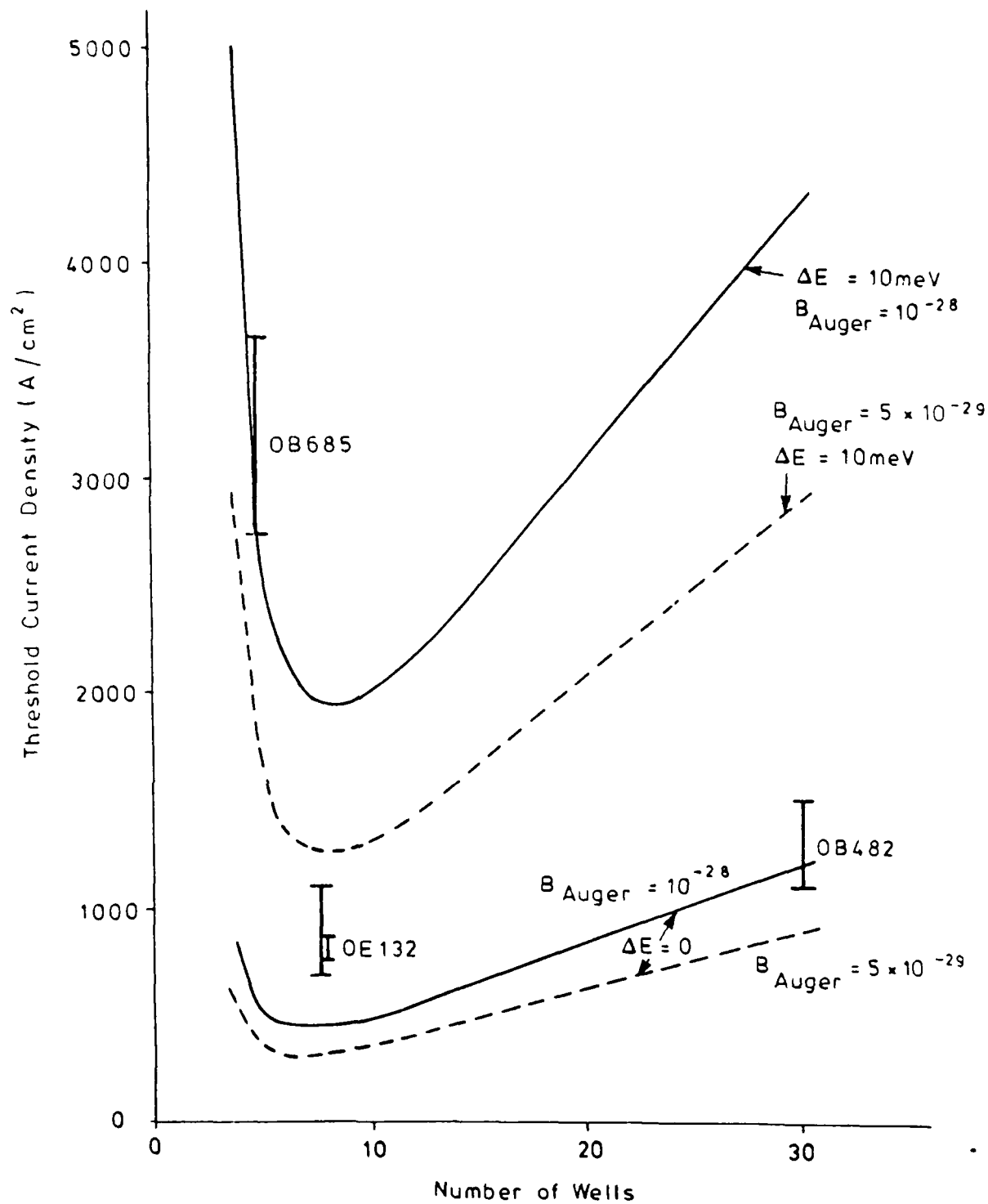


FIG. 50

A COMPARISON OF THEORETICAL AND EXPERIMENTAL LASING THRESHOLD CURRENT DENSITIES.

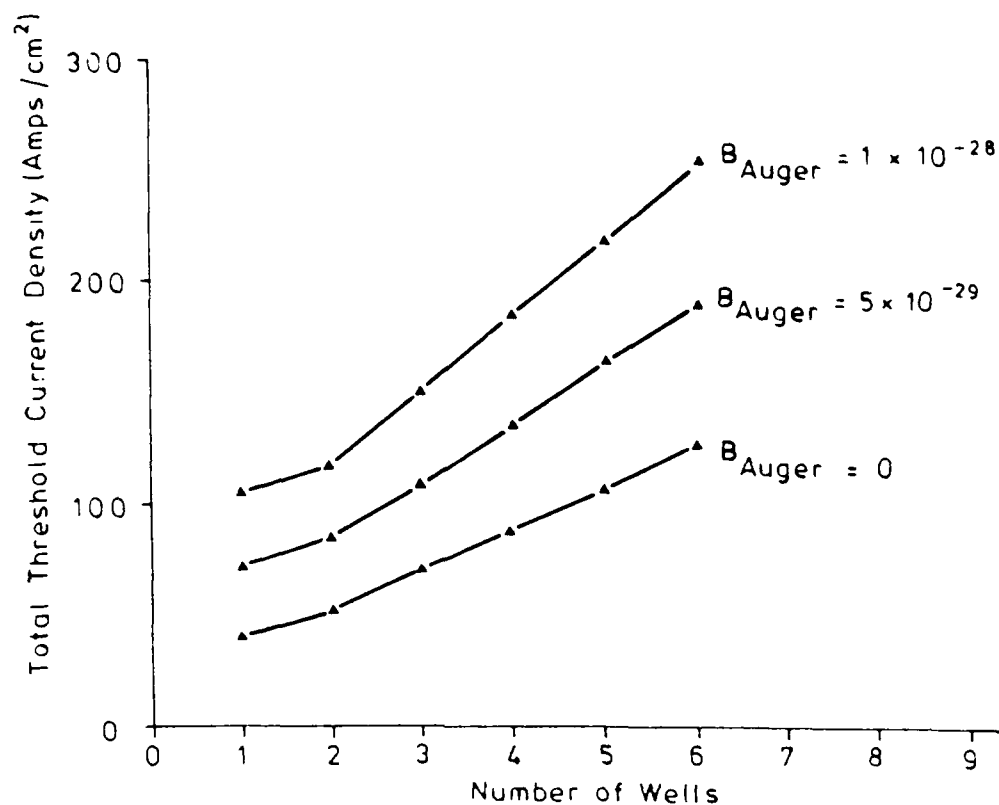


FIG. 51 THRESHOLD CURRENT DENSITY FOR MODIFIED InGaAs / InP STRUCTURES WITH HIGH REFLECTIVITY FACETS.

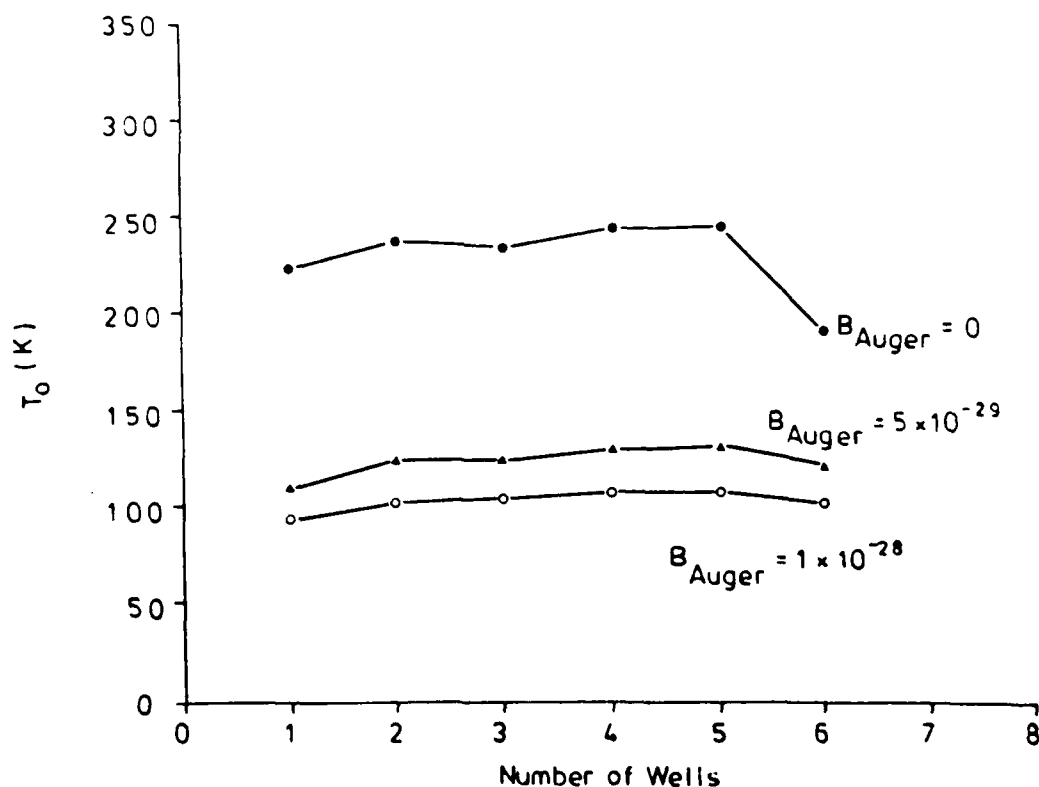
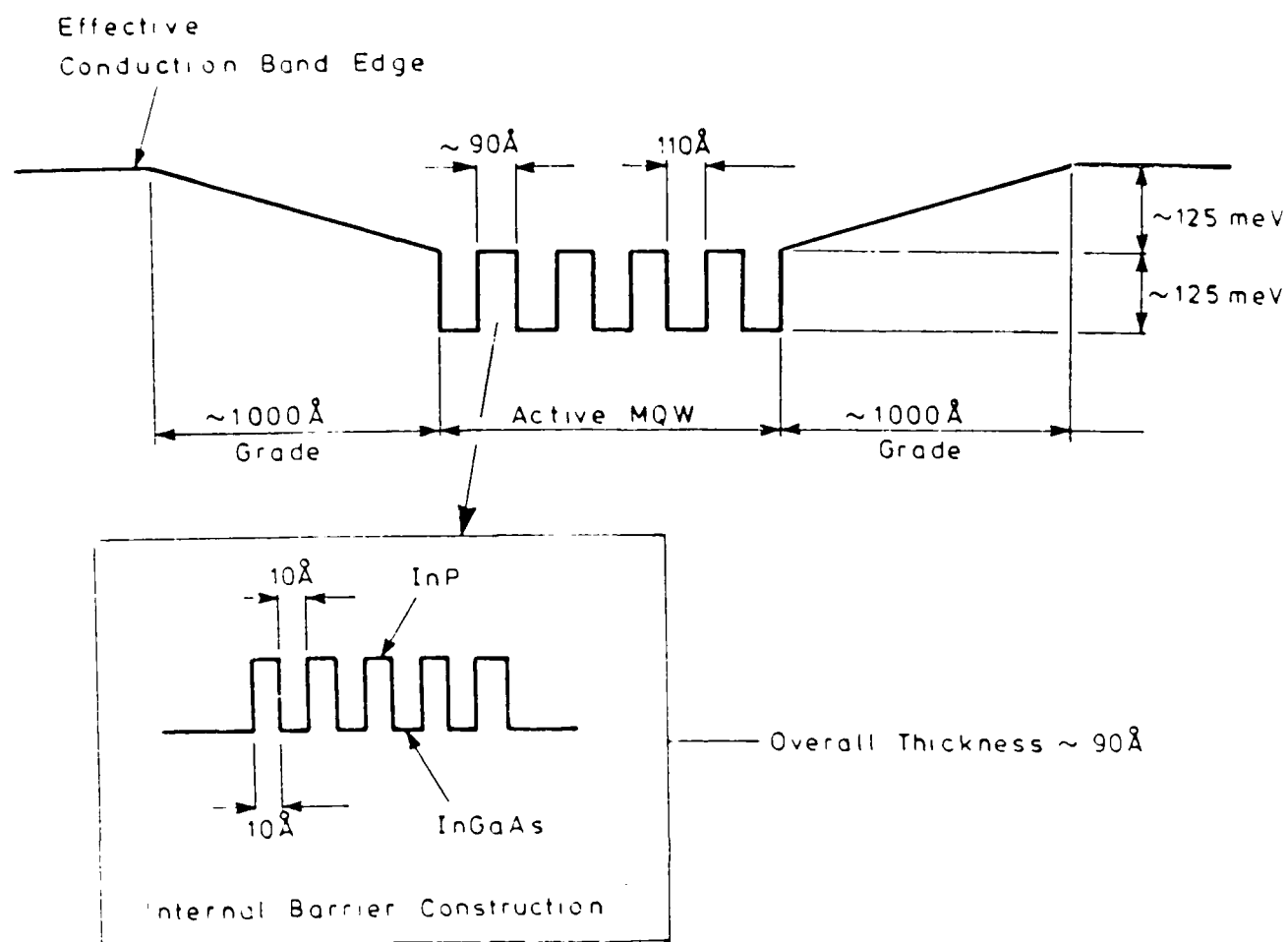


FIG. 52 TEMPERATURE SENSITIVITY FOR MODIFIED InGaAs / InP STRUCTURES WITH HIGH REFLECTIVITY FACETS.



$1000\text{\AA}$  Grade Composed of a Varying Well/Barrier Ratio Superlattice of  $50\text{\AA}$  Period.

InGaAs	5 $\text{\AA}$		6 $\text{\AA}$		7 $\text{\AA}$		25 $\text{\AA}$
InP		45 $\text{\AA}$		44 $\text{\AA}$		25 $\text{\AA}$	

FIG. 53 A GRIN-SCH MQW InGaAs:InP LASER DESIGN.

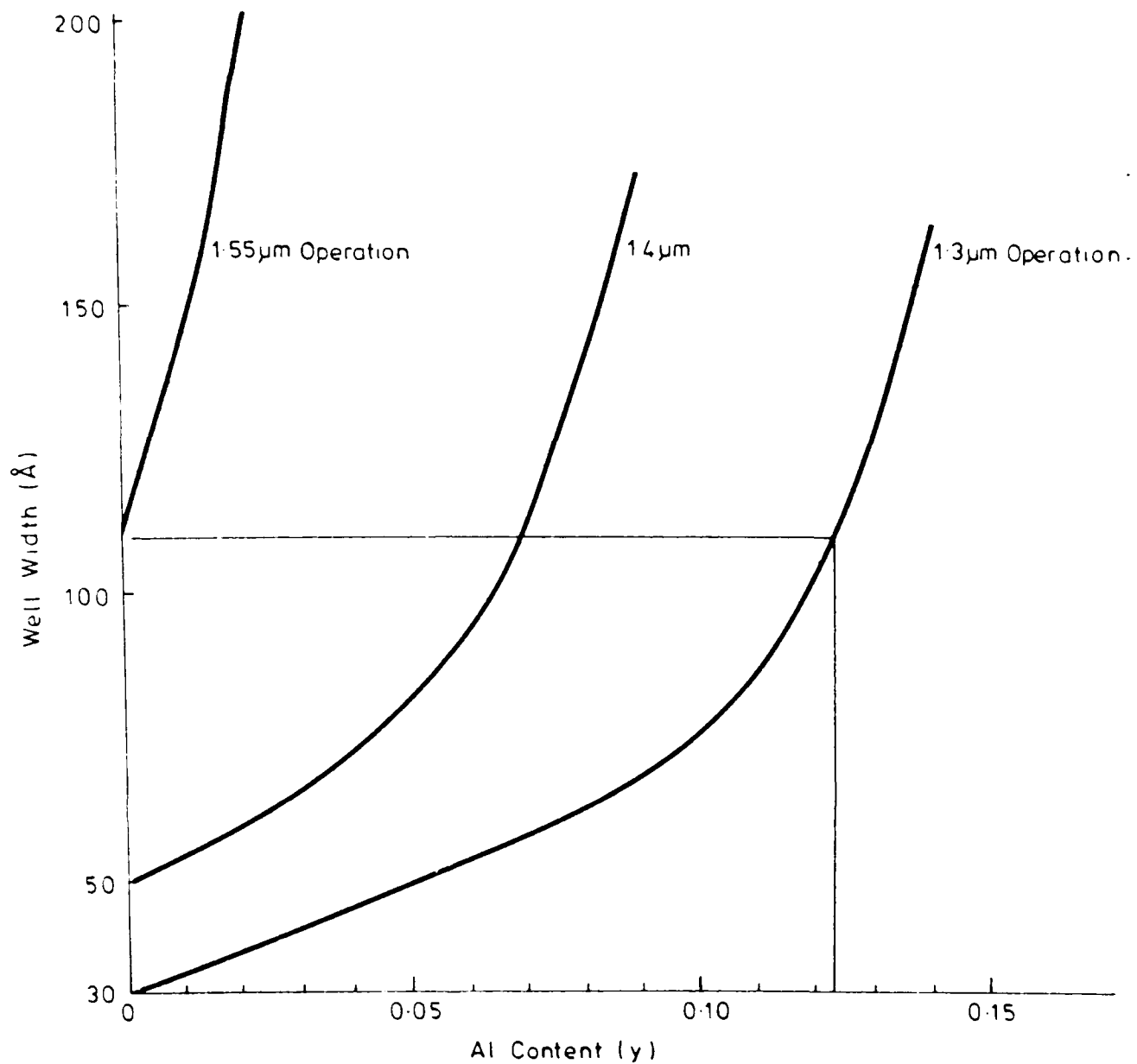


FIG. 54 CONSTANT EMISSION WAVELENGTH CONTOURS IN THE 1.3 - 1.55μm RANGE FOR AlGaInAs QUANTUM WELLS.



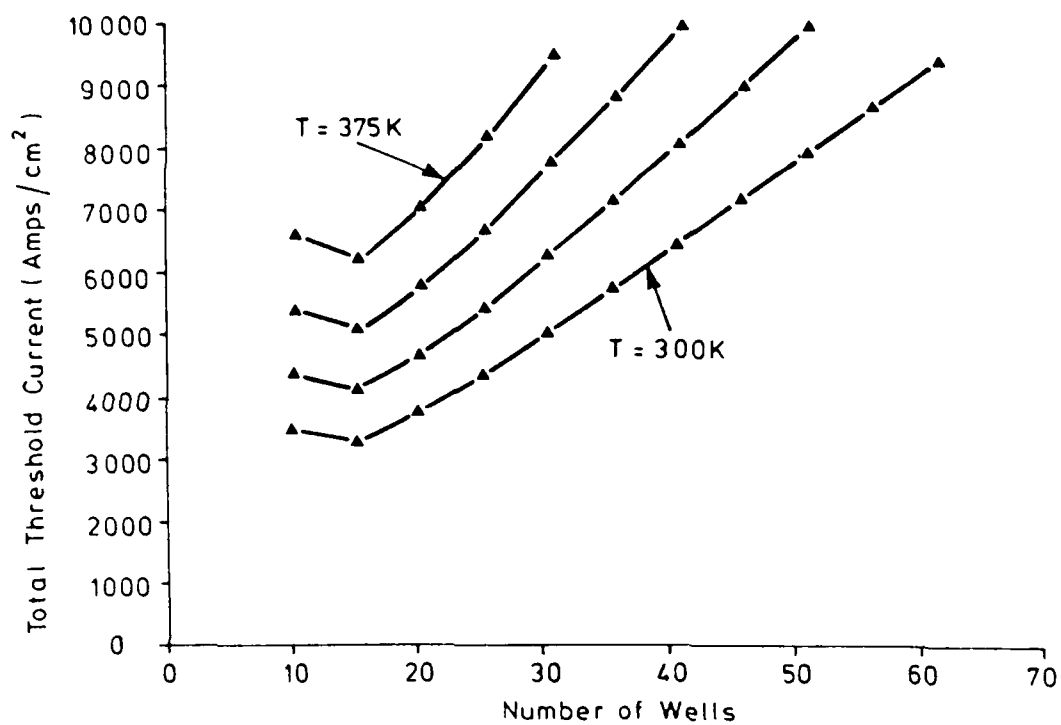


FIG. 55 CALCULATED TOTAL THRESHOLD CURRENT DENSITY FOR  
1.3μm MQW LASERS.

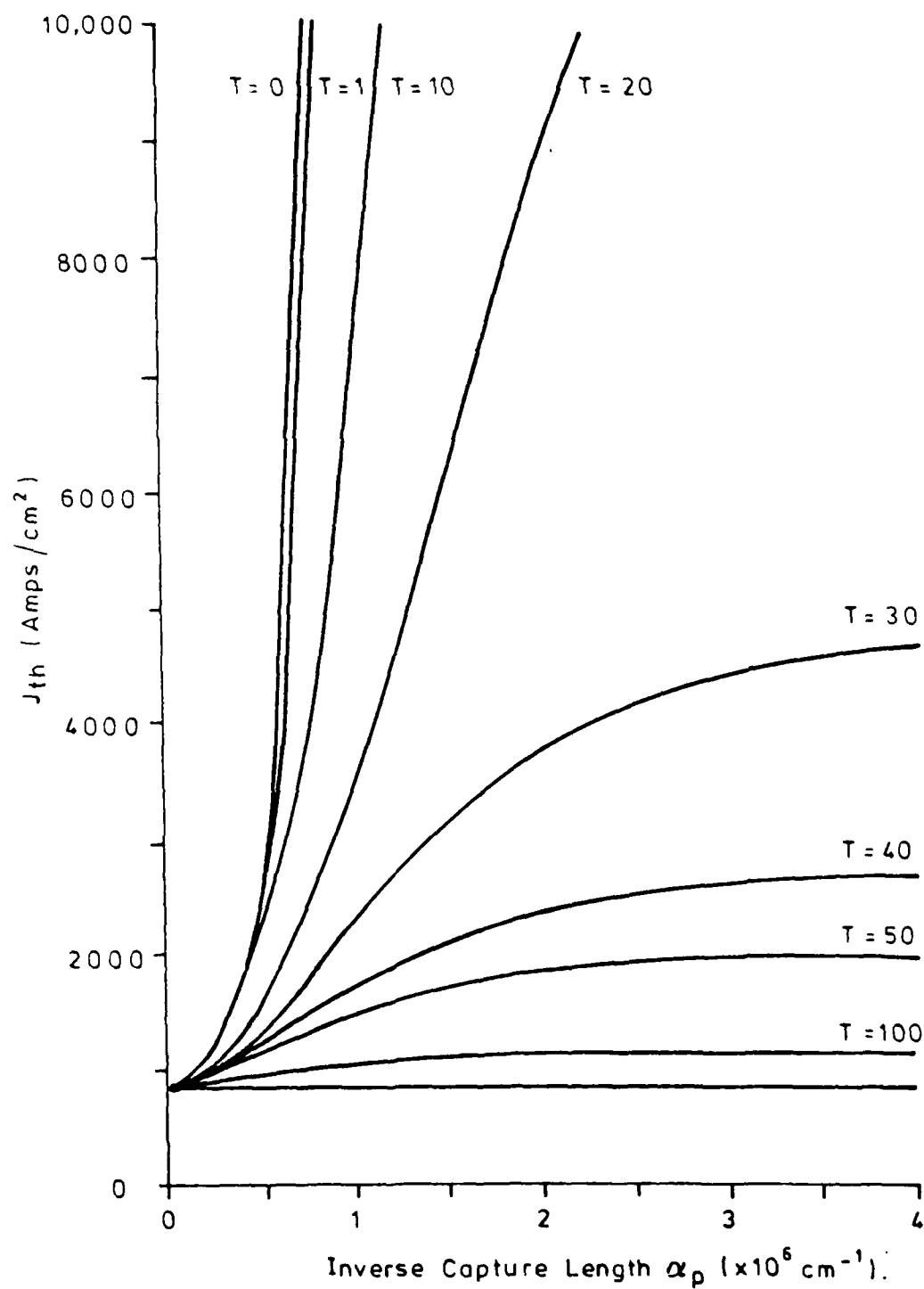


FIG.56

PREDICTED THRESHOLD CURRENT DENSITY FOR AN  
 $8 \times 110 \text{ \AA}$  MQW LASER.  $T \times 10^{-8} \text{ s}^{-1}$  IS THE INVERSE  
 TUNNELLING TIME.

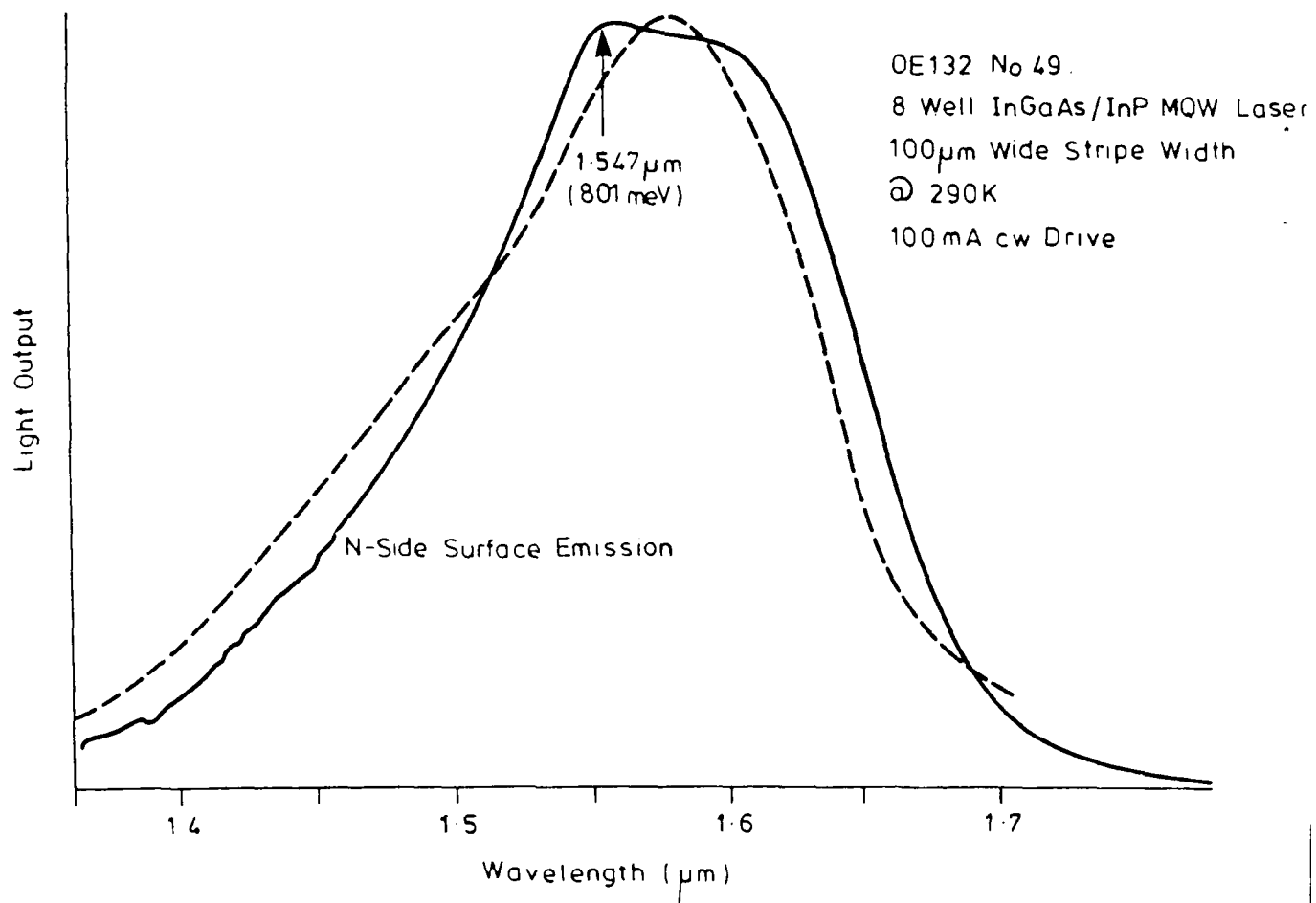


FIG. 58 THEORETICAL ELECTROLUMINESCENCE SPECTRUM (---) FOR  $\Delta E = 15 \text{ meV}$   
AND  $N = 5 \times 10^{17} \text{ cm}^{-3}$   
COMPARED WITH THE N-SIDE SURFACE EMISSION (—).

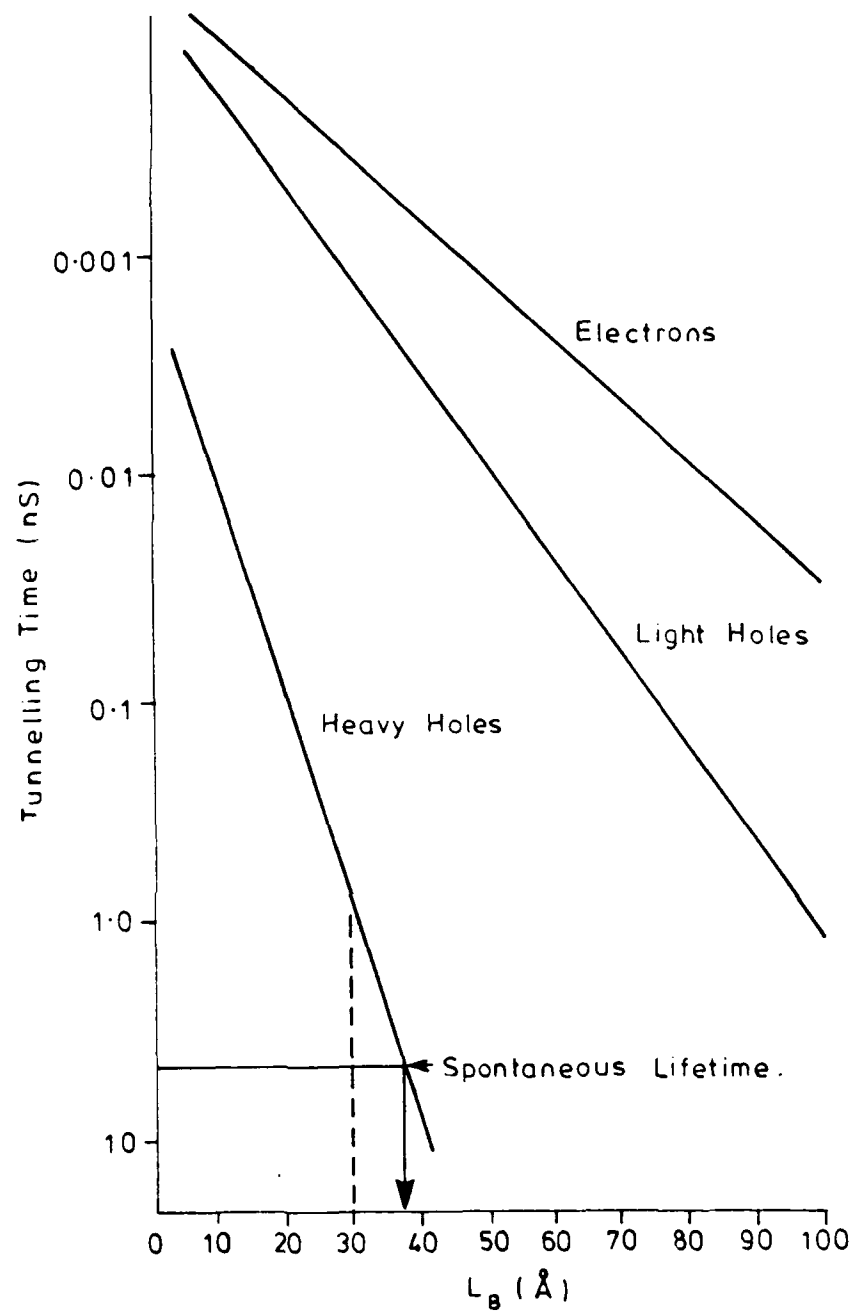


FIG. 57 TUNNELLING TIME FOR A DOUBLE WELL SYSTEM AS A FUNCTION OF BARRIER THICKNESS.

RESEARCH AND DEVELOPMENT FOR LASER SOURCES BASED ON  
QUANTUM WELL STRUCTURES FABRICATED IN THE InP ALLOY SYSTEM

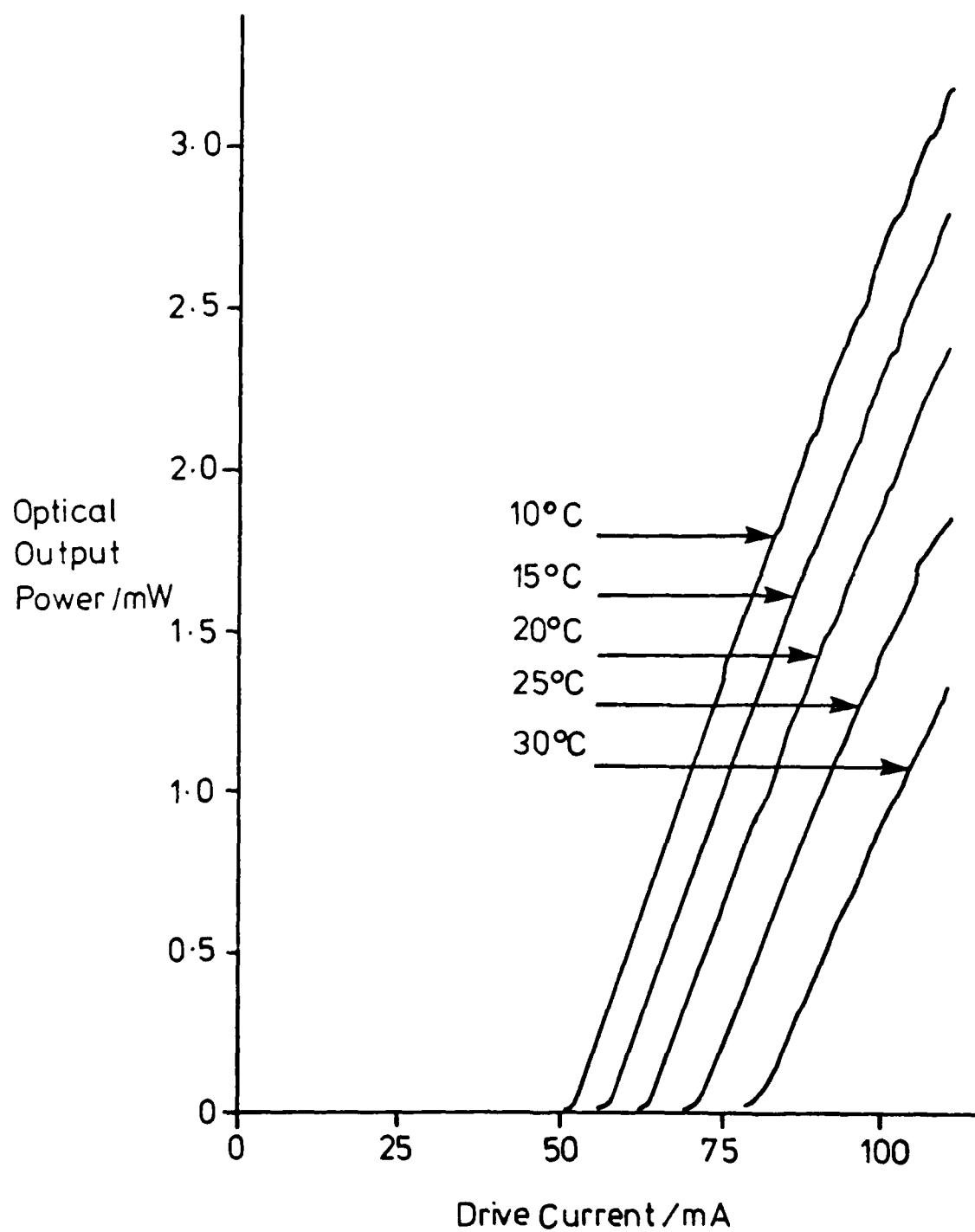
Project No. F.19628-85-C-0172

APPENDIX 1

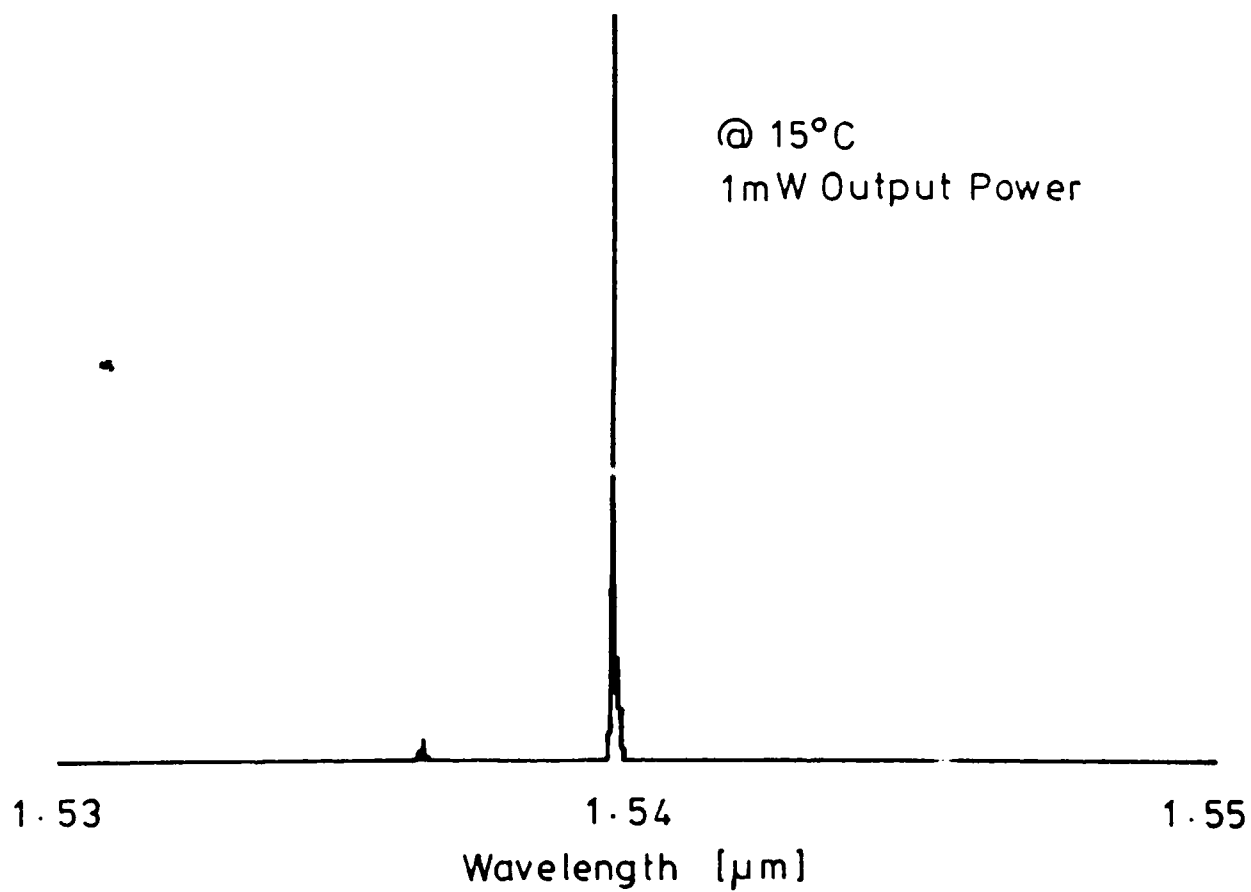
CHARACTERISTICS OF  
MQW LASER DELIVERABLES

Plus Additional GaAlInAs DH Devices.

Buried Ridge In Ga As /Inp MQW Laser Module LD 4227#014

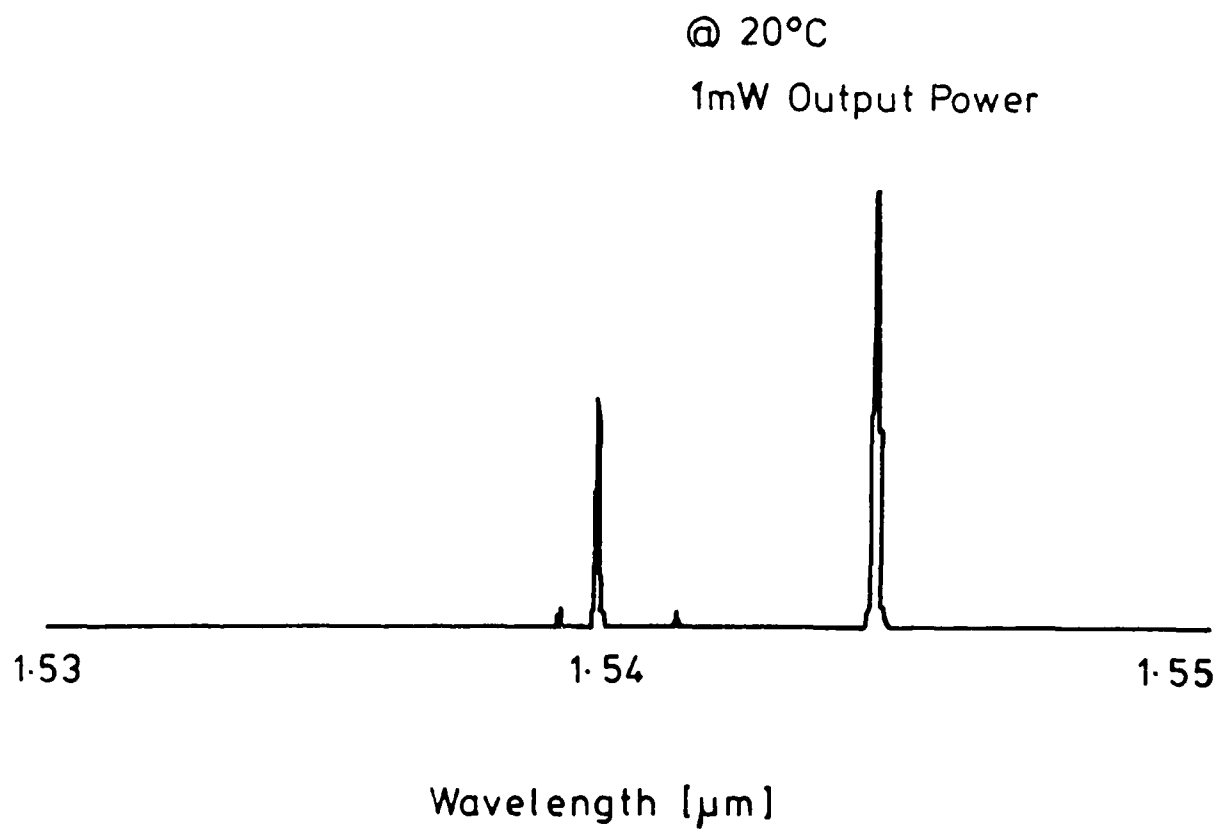


Buried Ridge  
In Ga As / InP MQW Laser Module LD 4227<sup>#</sup>014  
SPECTRAL CHARACTERISTICS



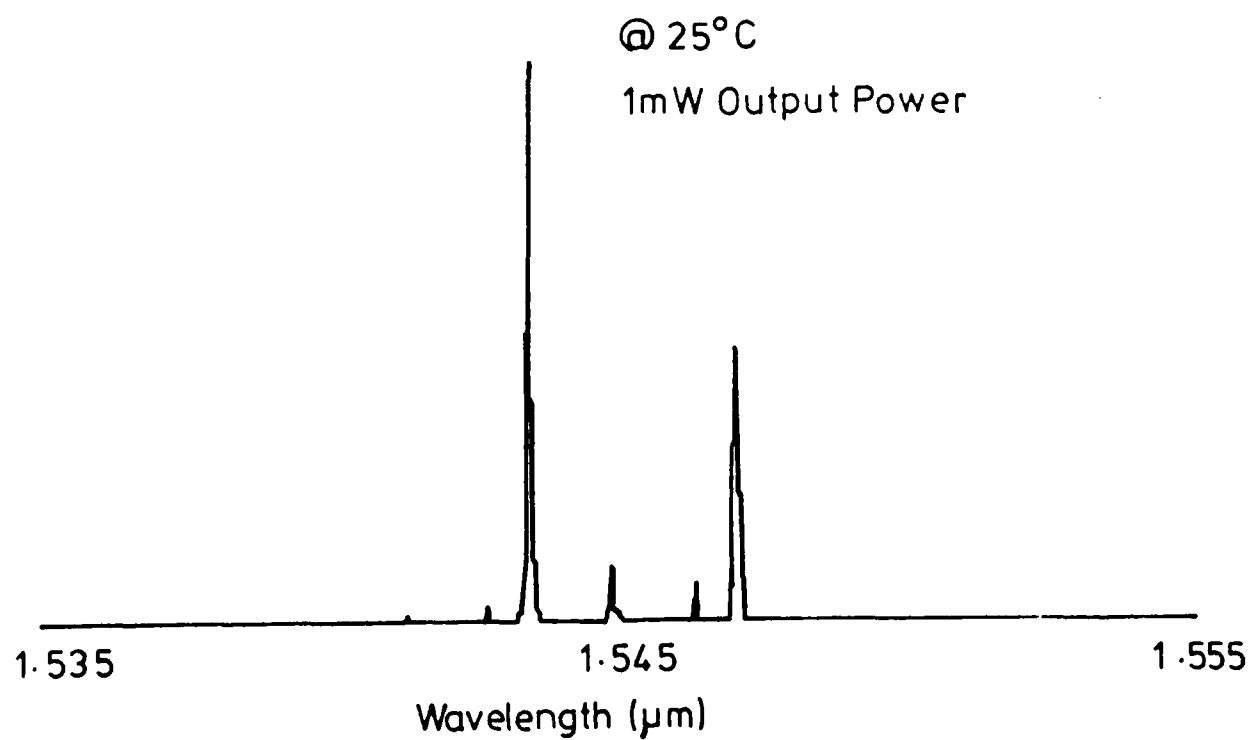
Buried Ridge  
In Ga As/ InP MQW Laser Module LD4227#014

SPECTRAL CHARACTERISTICS

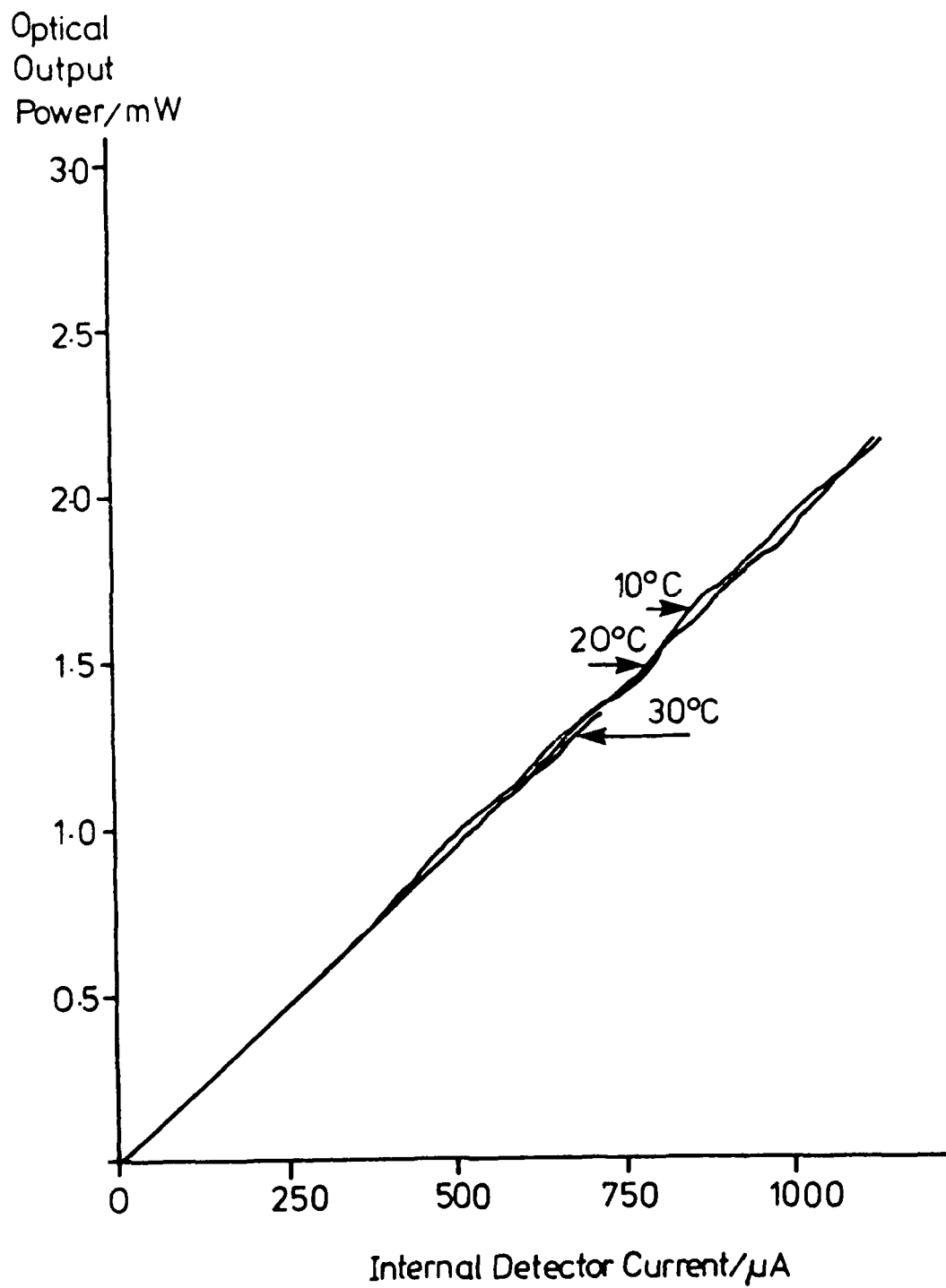


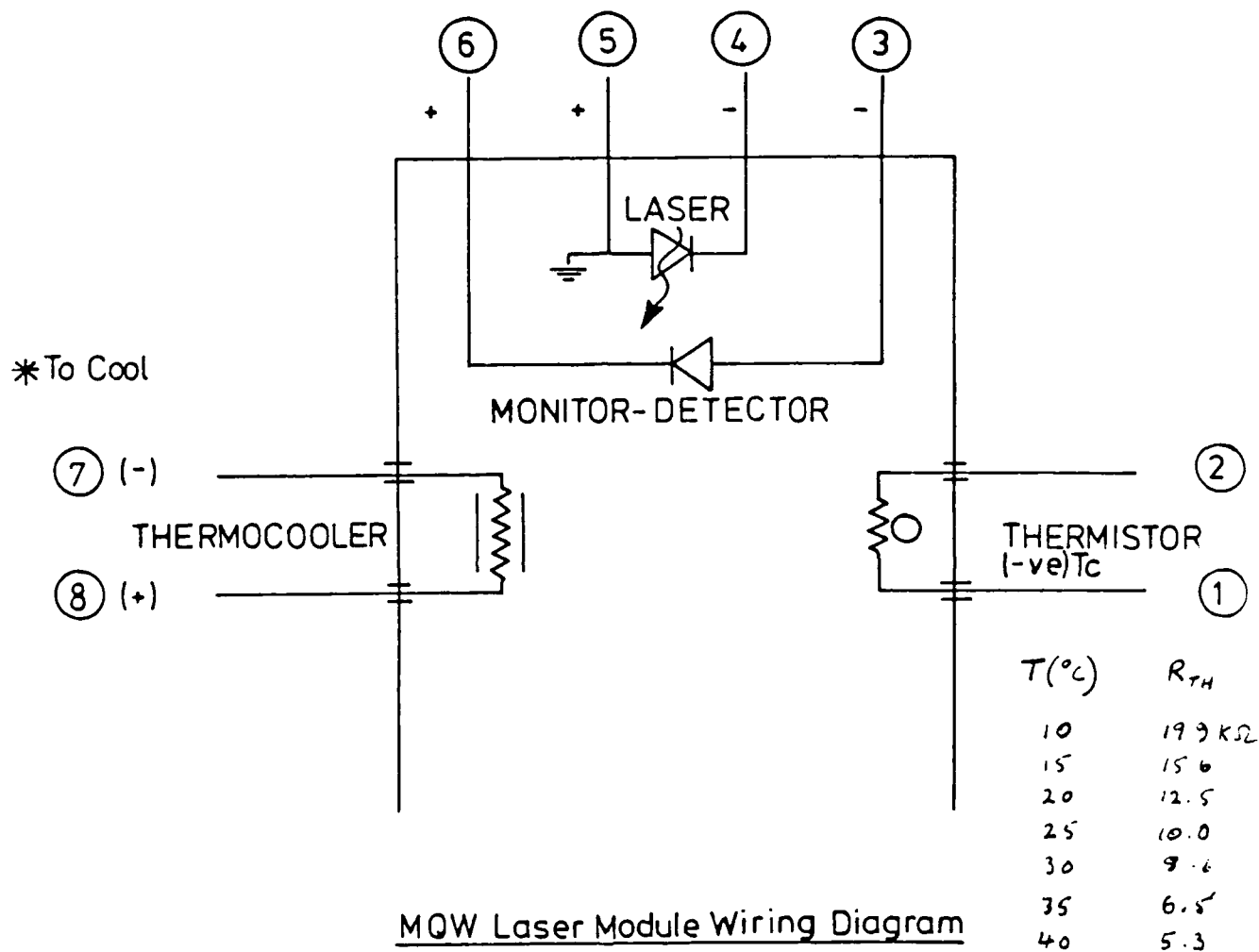


Buried Ridge  
In Ga As/InP MQW Laser Module LD4227#014  
SPECTRAL CHARACTERISTICS

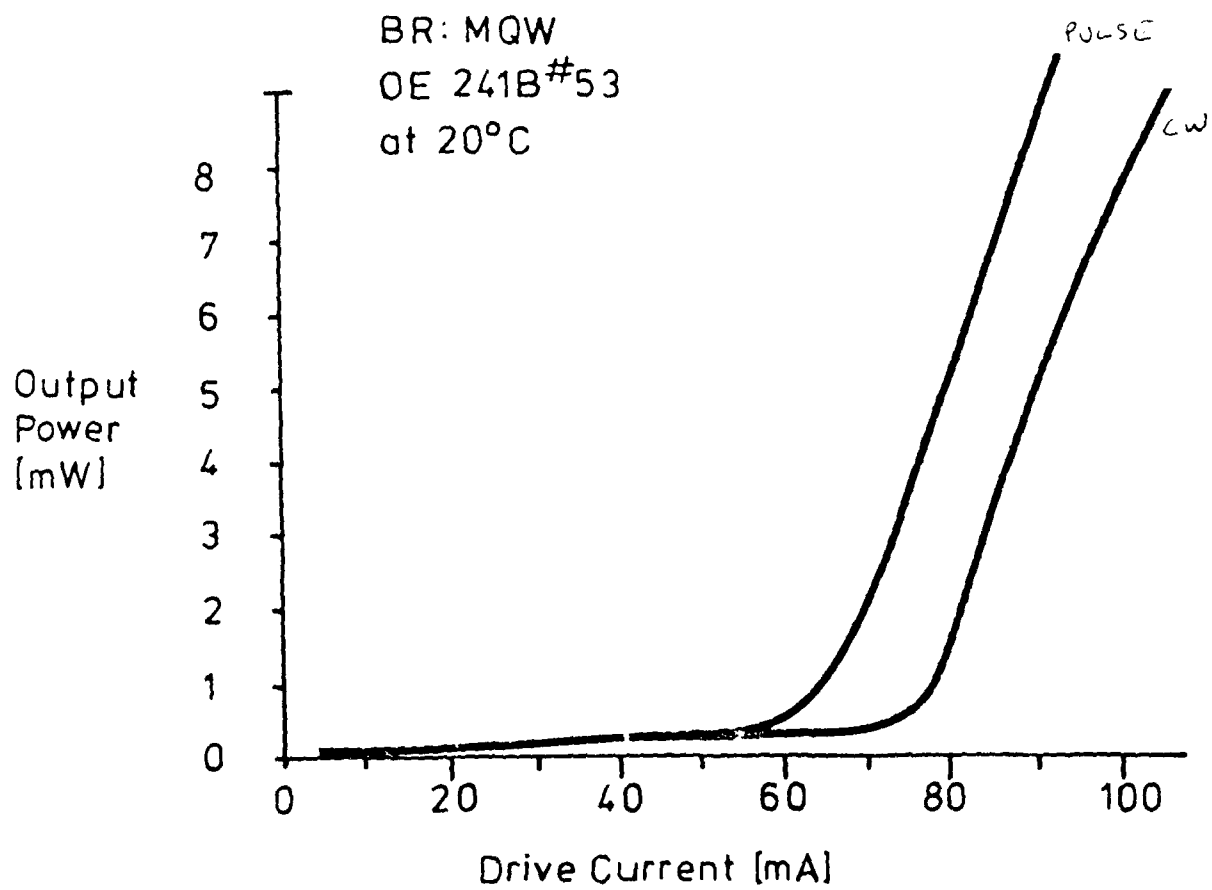


Buried Ridge InGaAs/InP MQW Laser Module LD 4227\*014

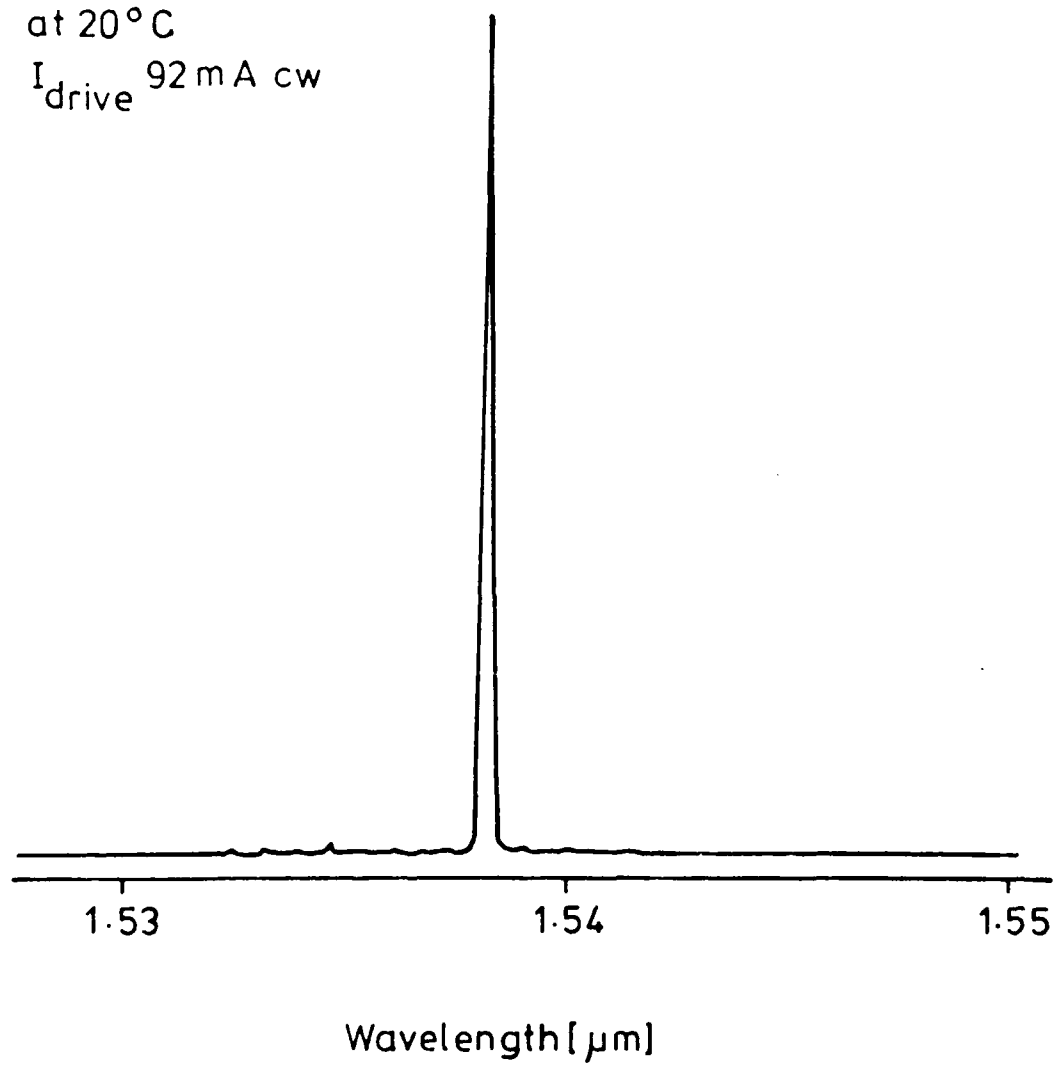




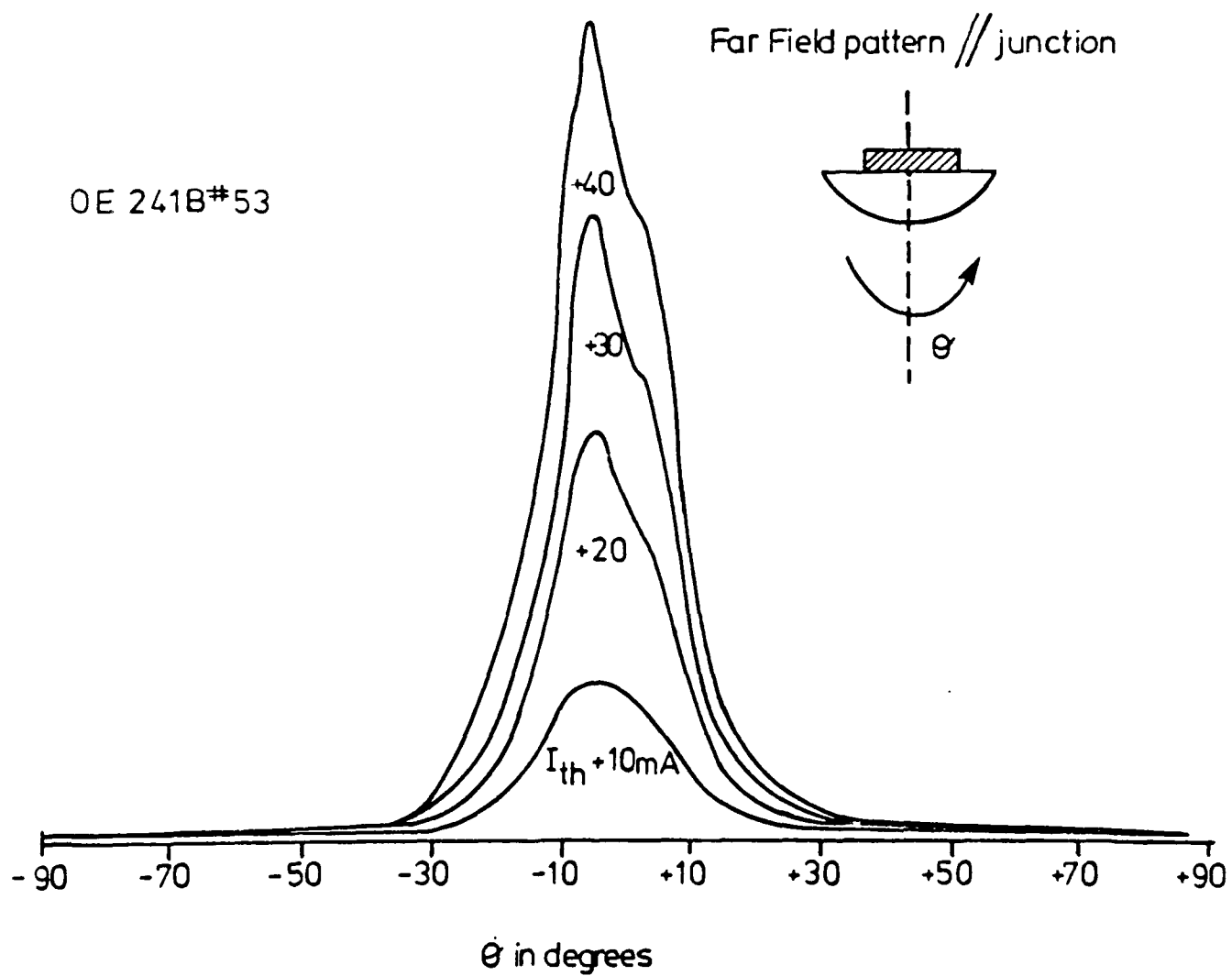
N.B. Ensure suitable external load (eg. 50 $\Omega$ ) is connected in series with laser diode prior to connecting power supply.

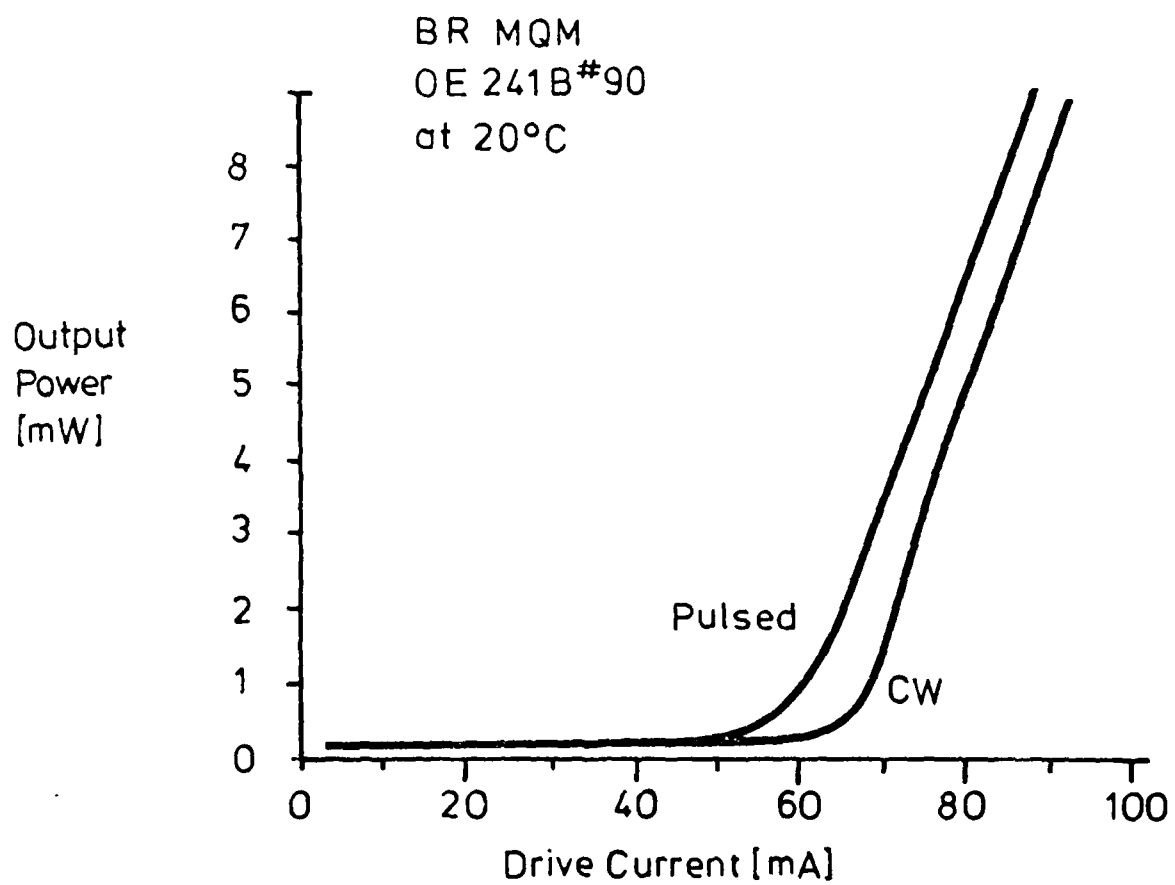


OE 241B<sup>#</sup>53  
at 20°C  
I<sub>drive</sub> 92 mA cw

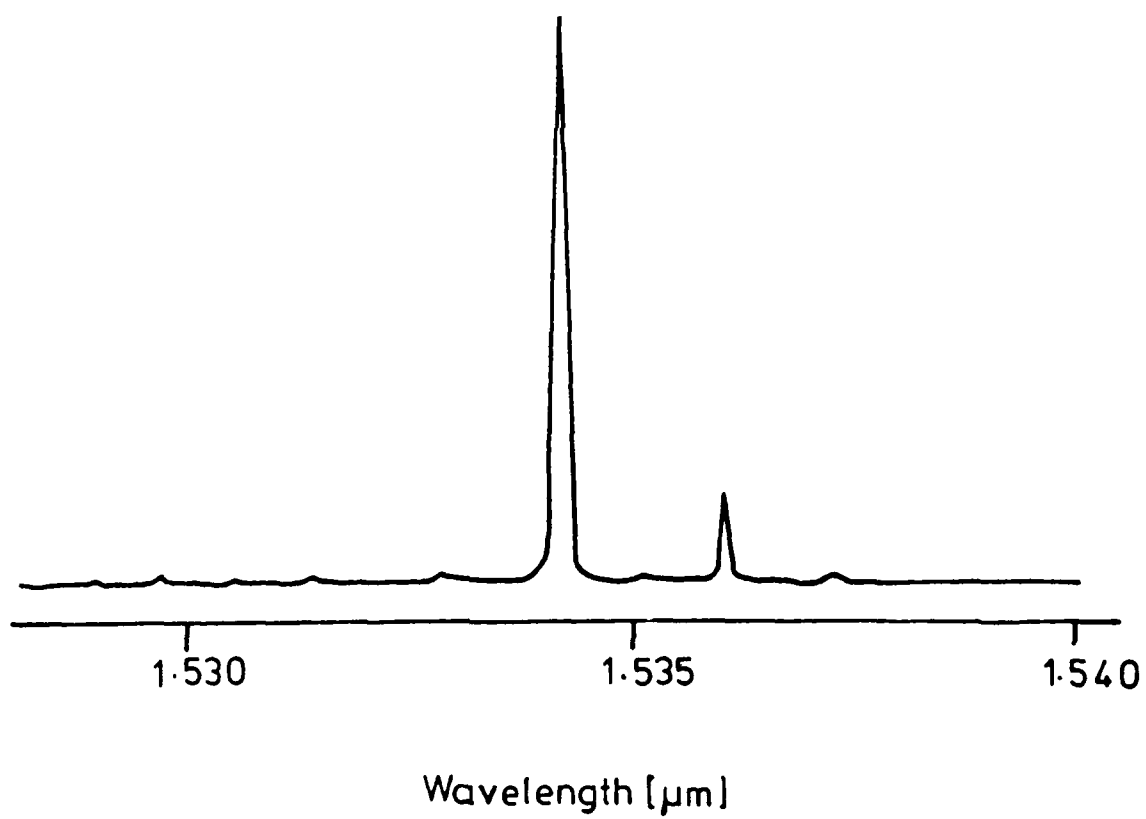


OE 241B#53

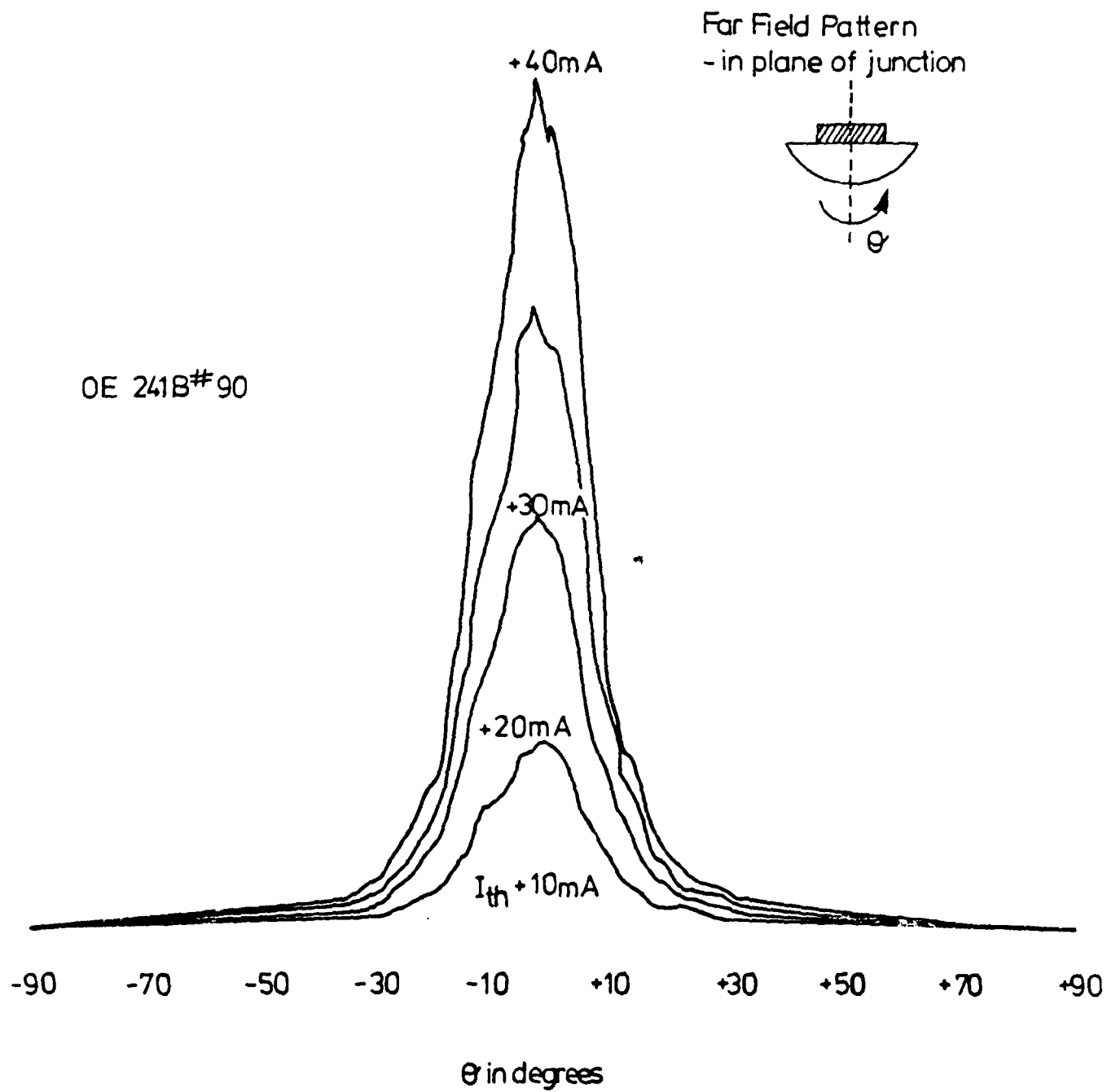


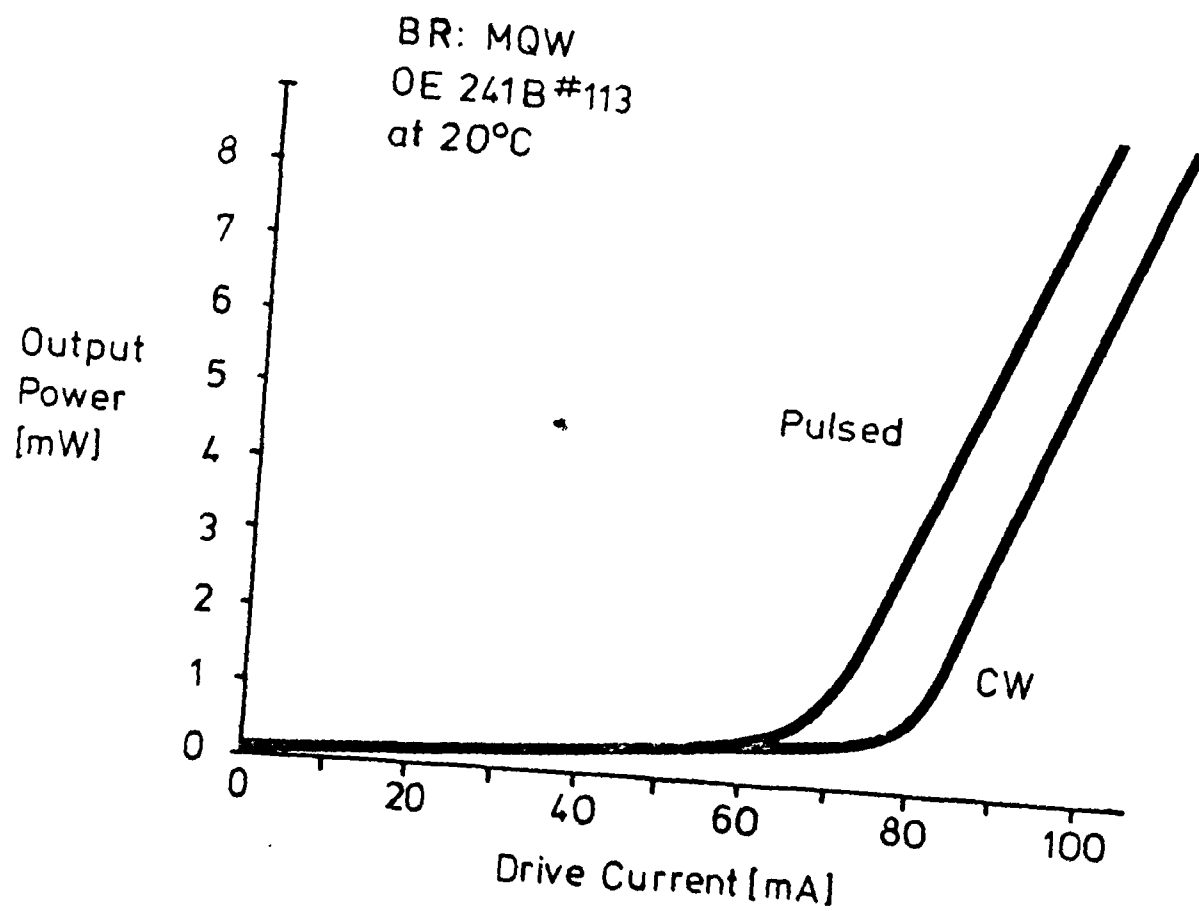


OE 241B#90  
at 20°C  
 $I_{\text{drive}}$  79 mA cw

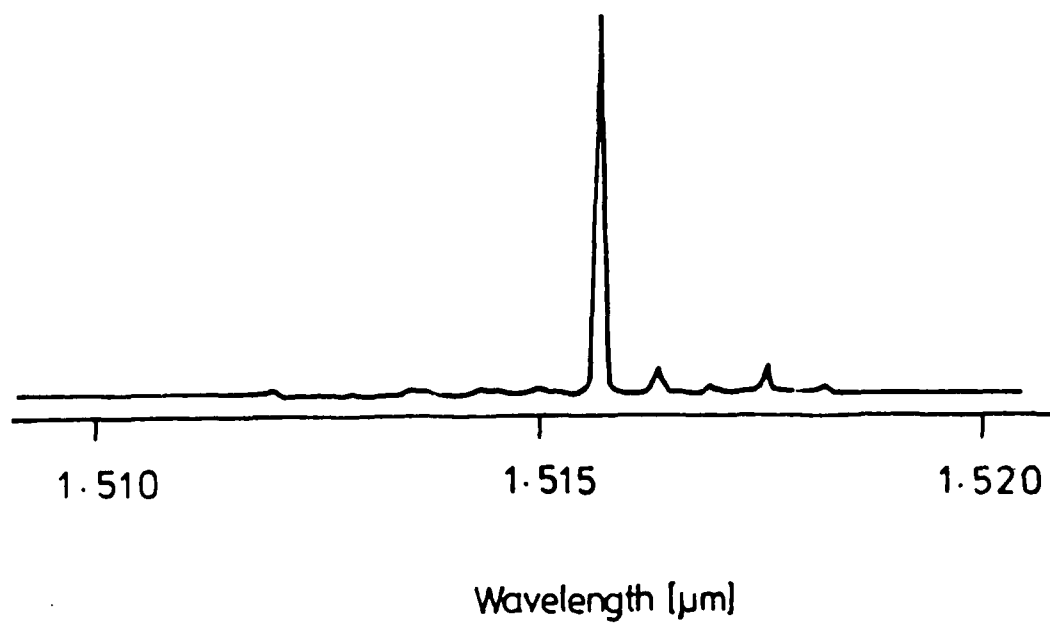




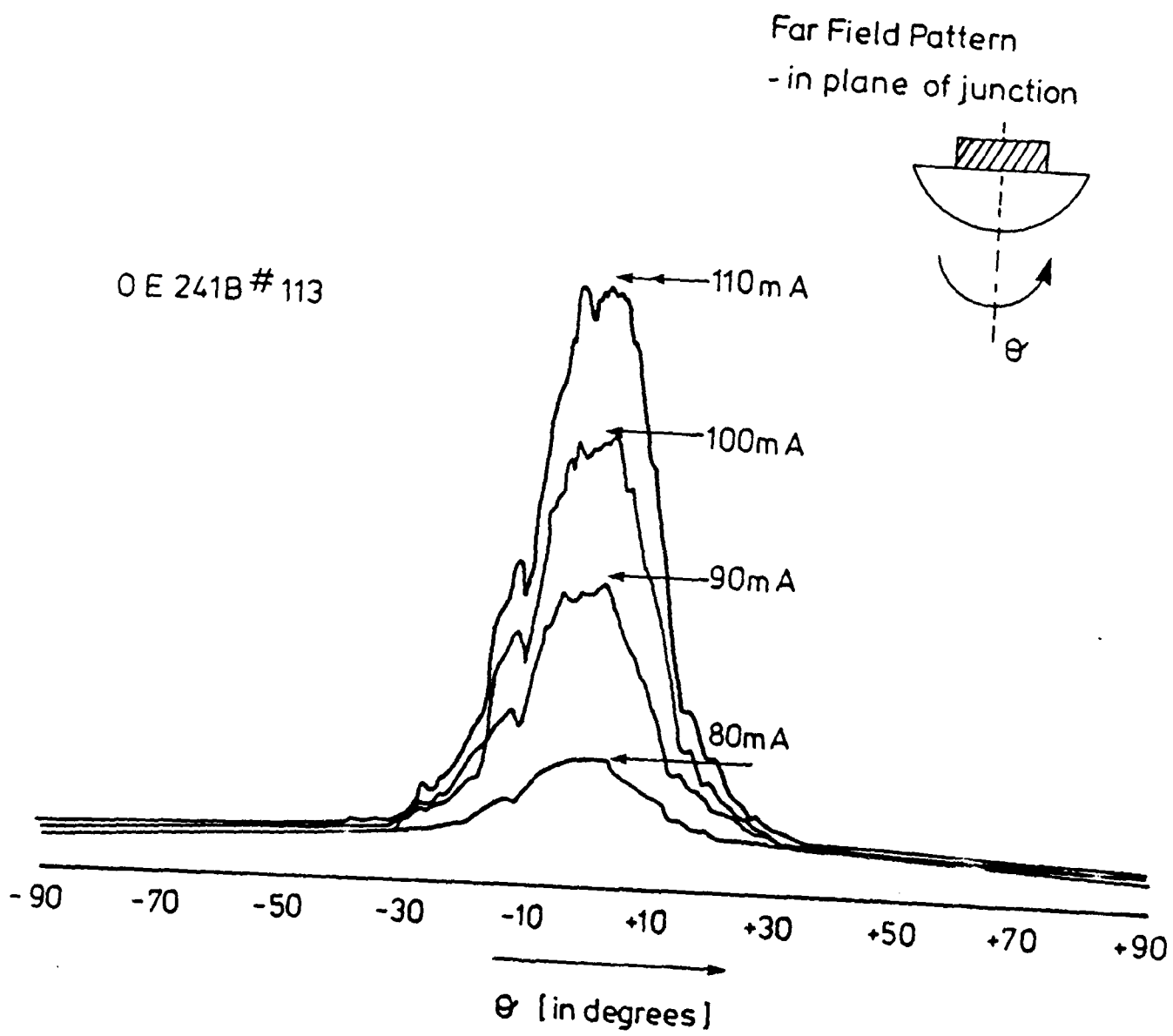


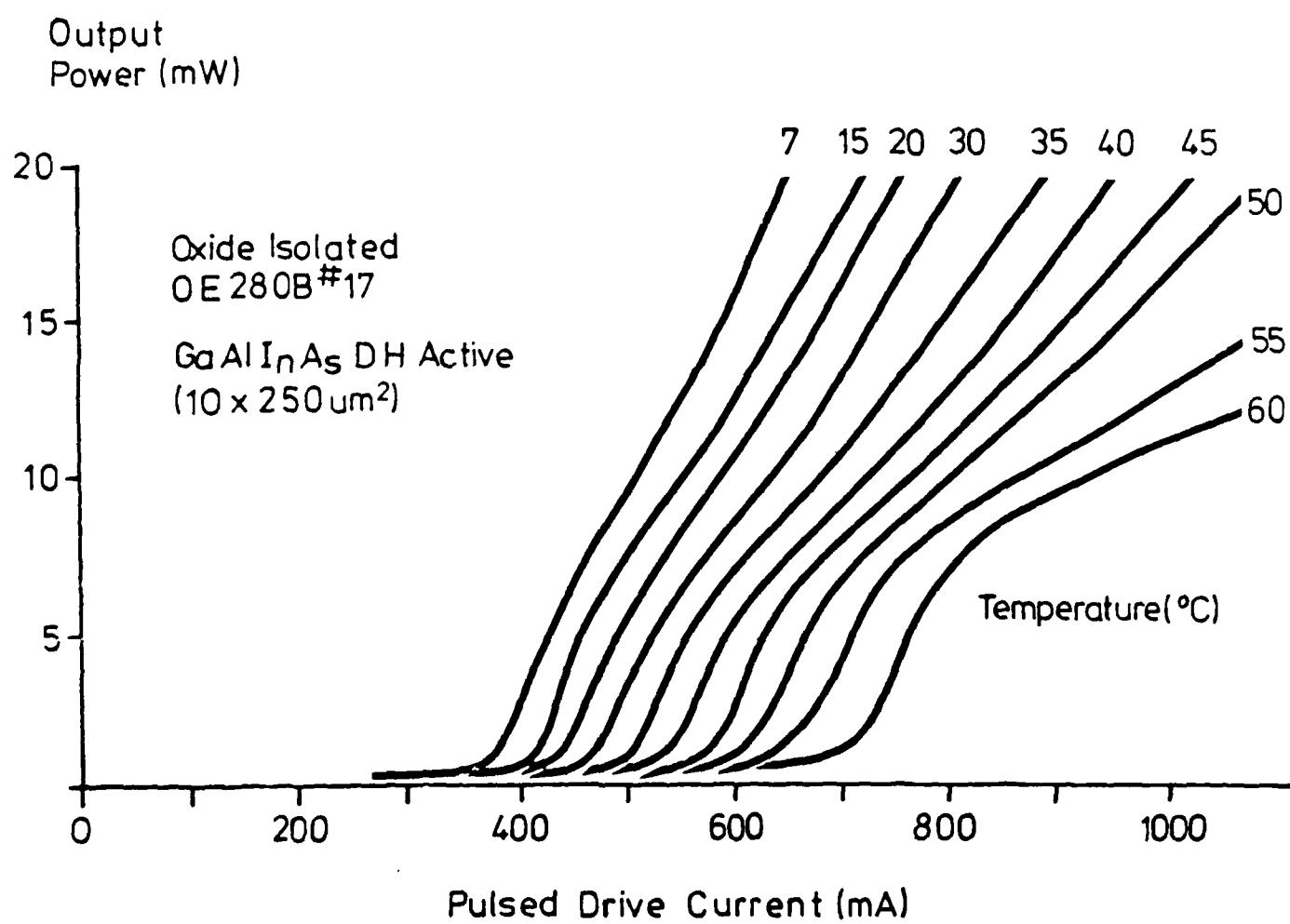


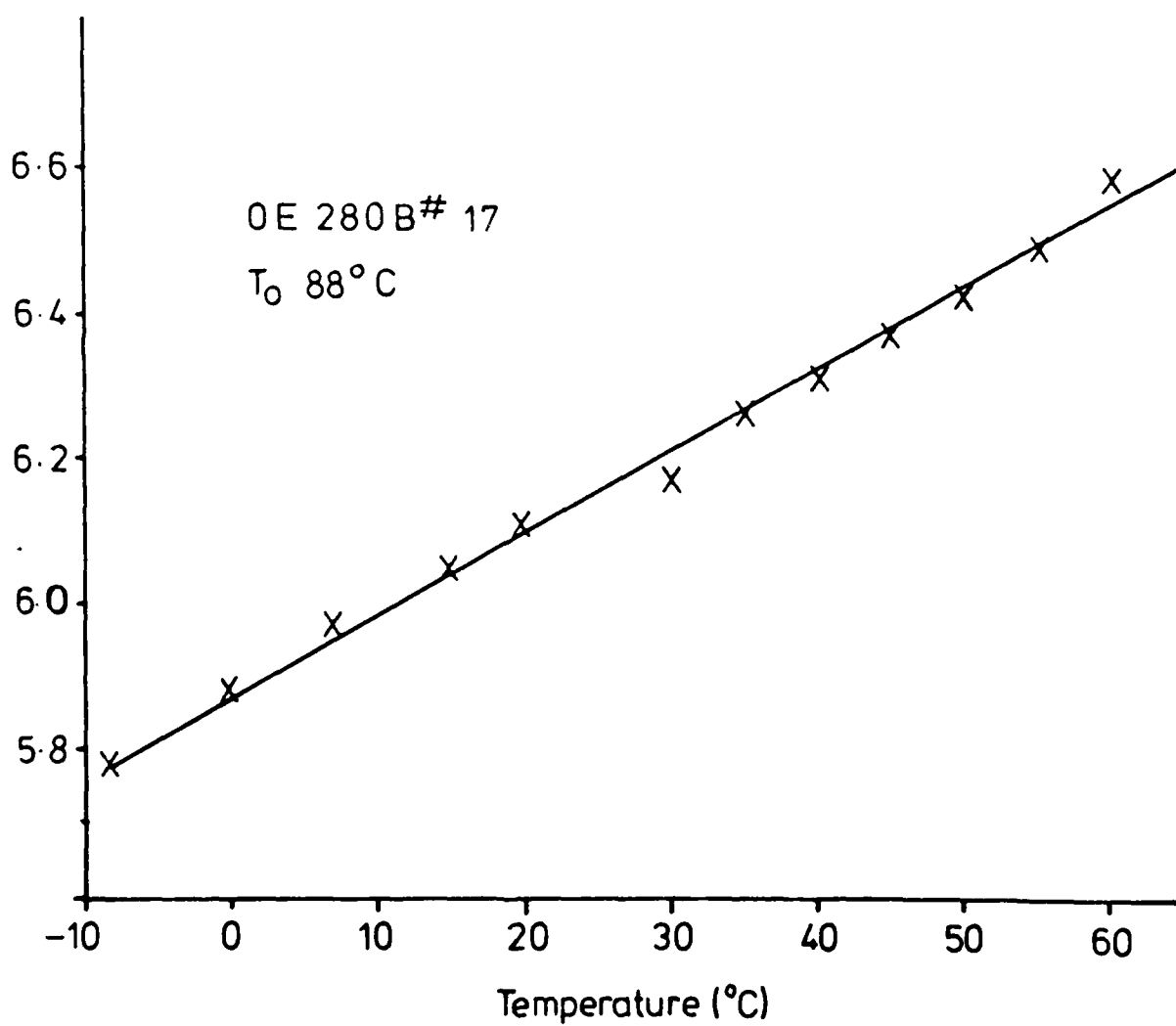
OE 241B<sup>#</sup>113  
at 20°C  
 $I_{\text{drive}}$  94 mA cw



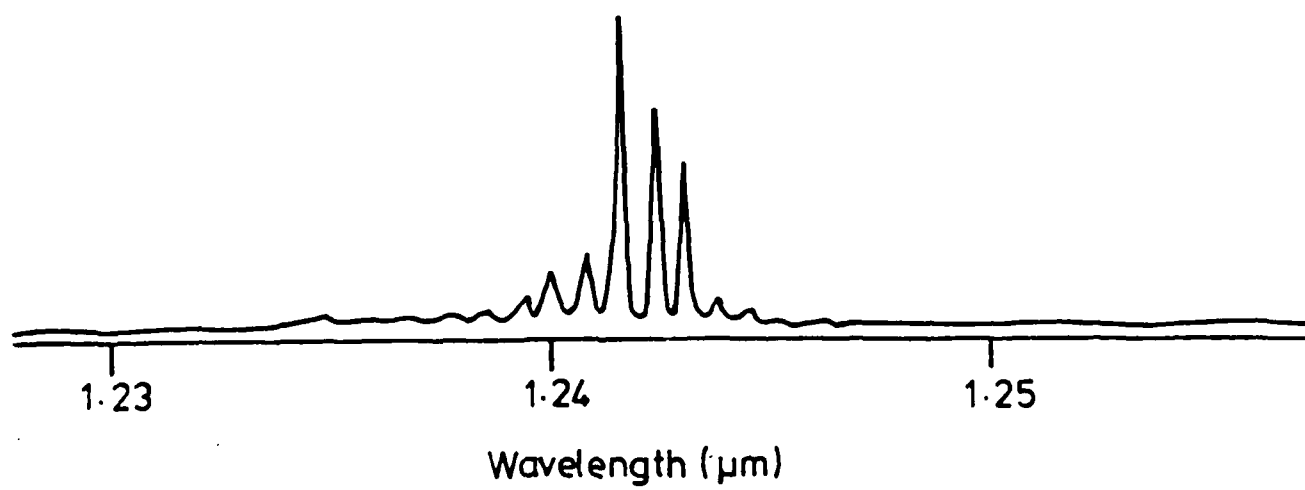
OE 241B # 113



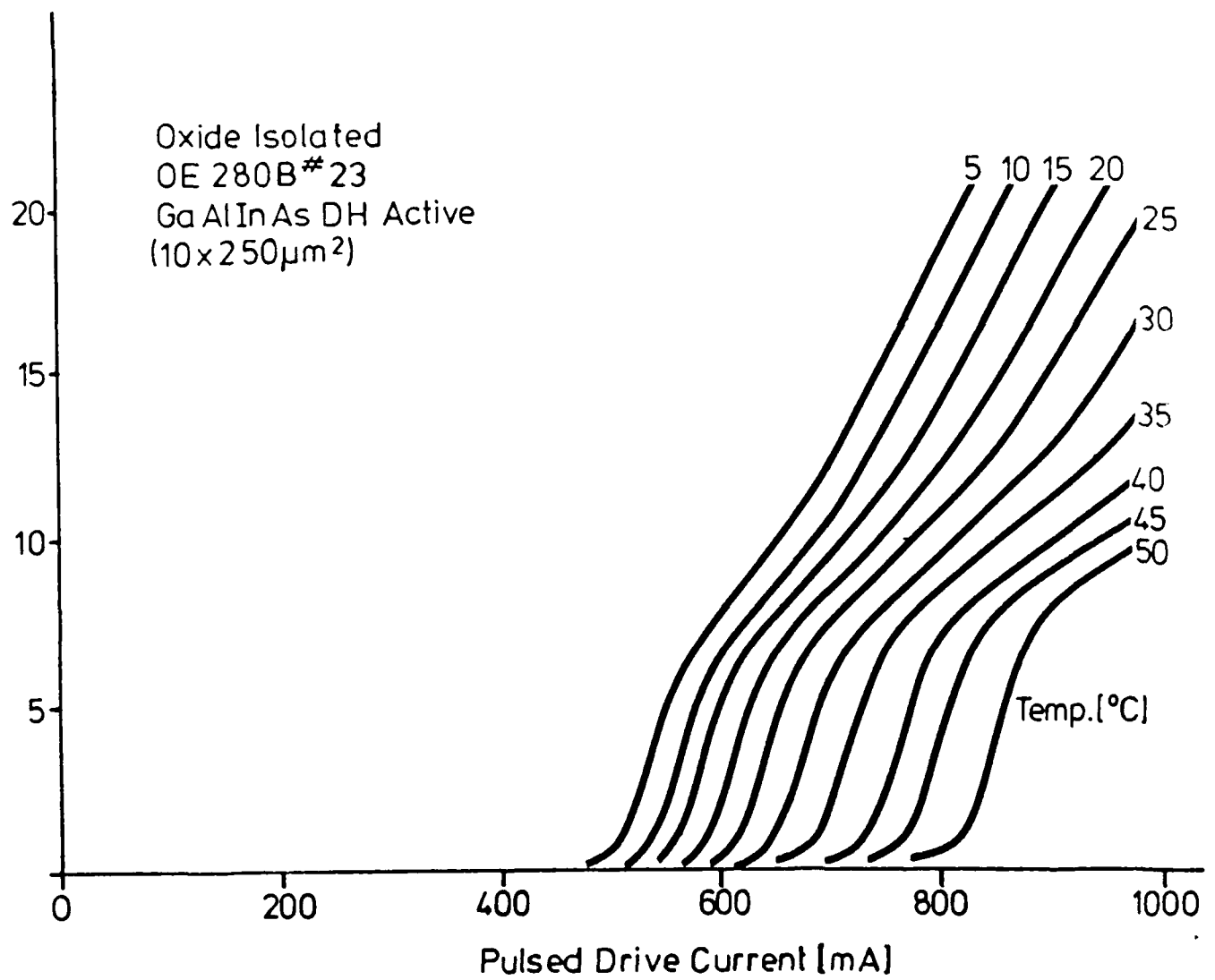




OE 280 B #17



Output  
Power [mW]

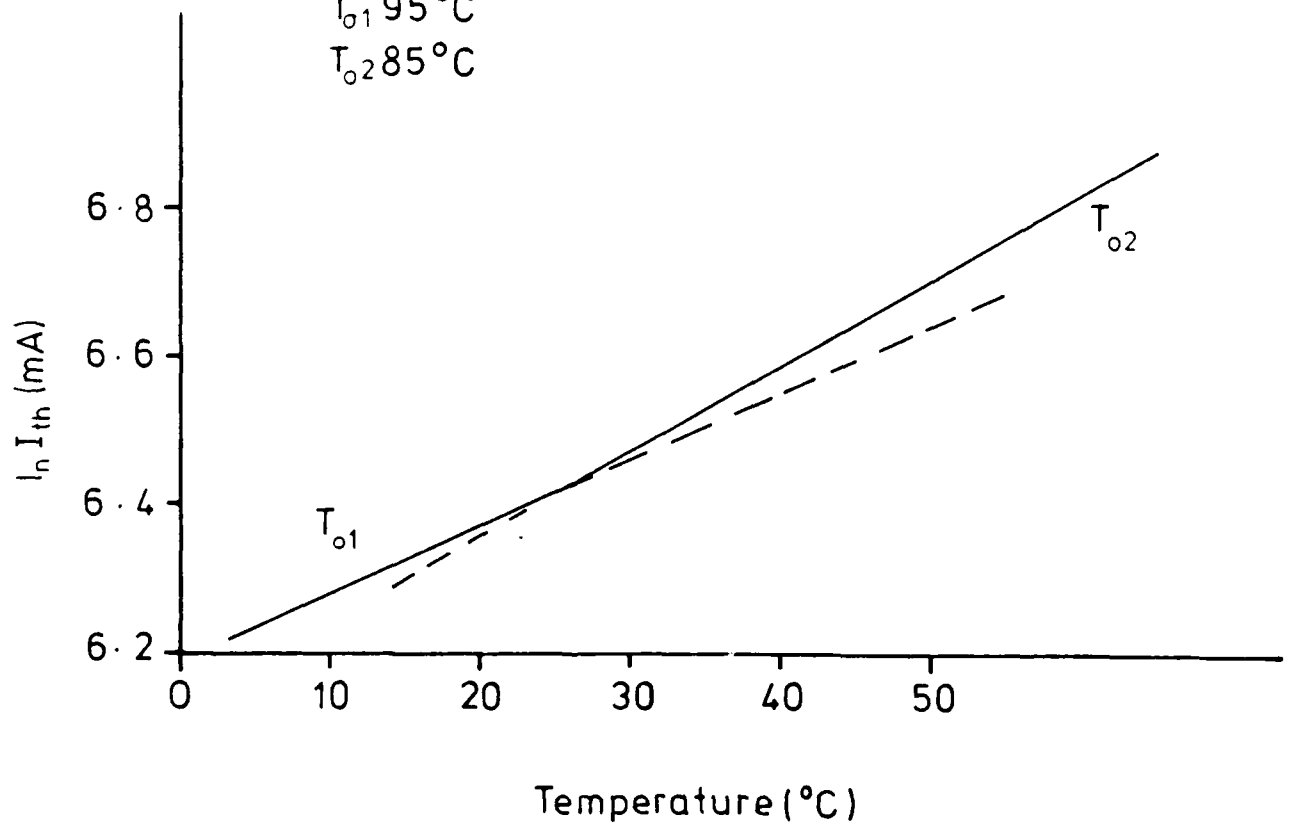




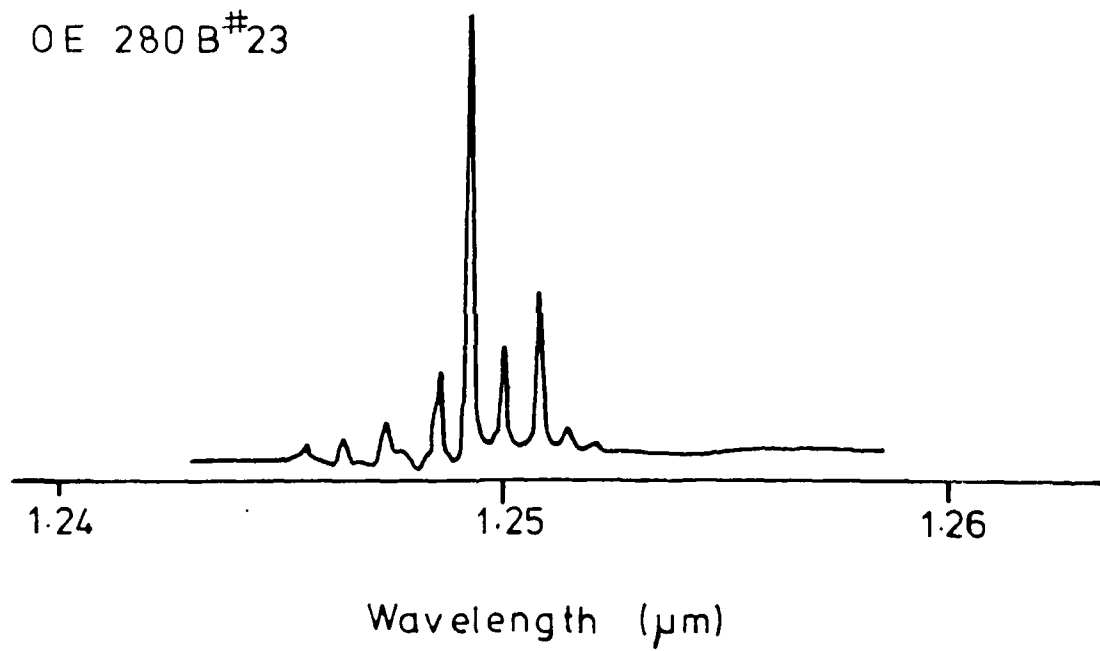
OE 280B#23

$T_{o1} 95^{\circ}\text{C}$

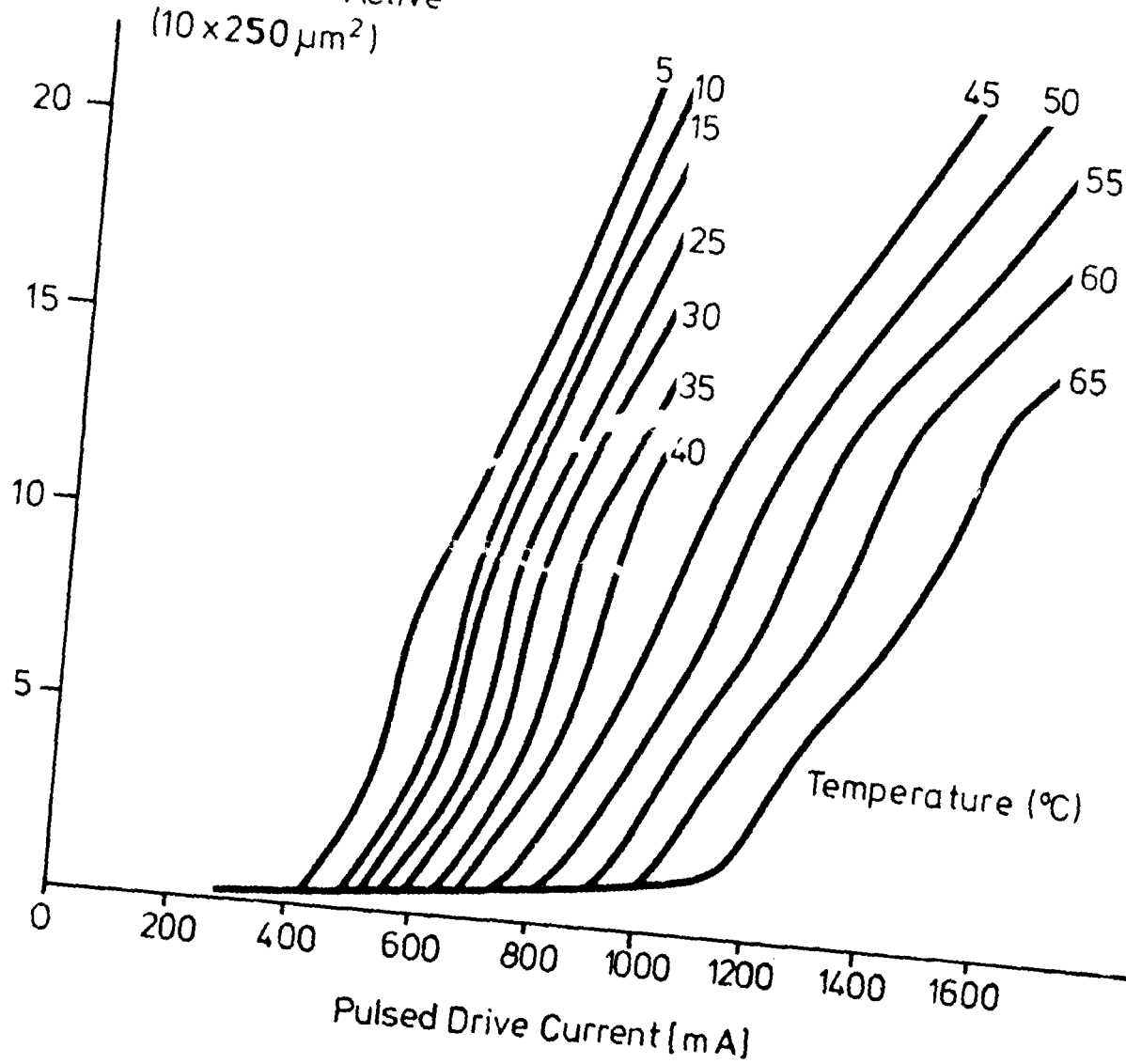
$T_{o2} 85^{\circ}\text{C}$

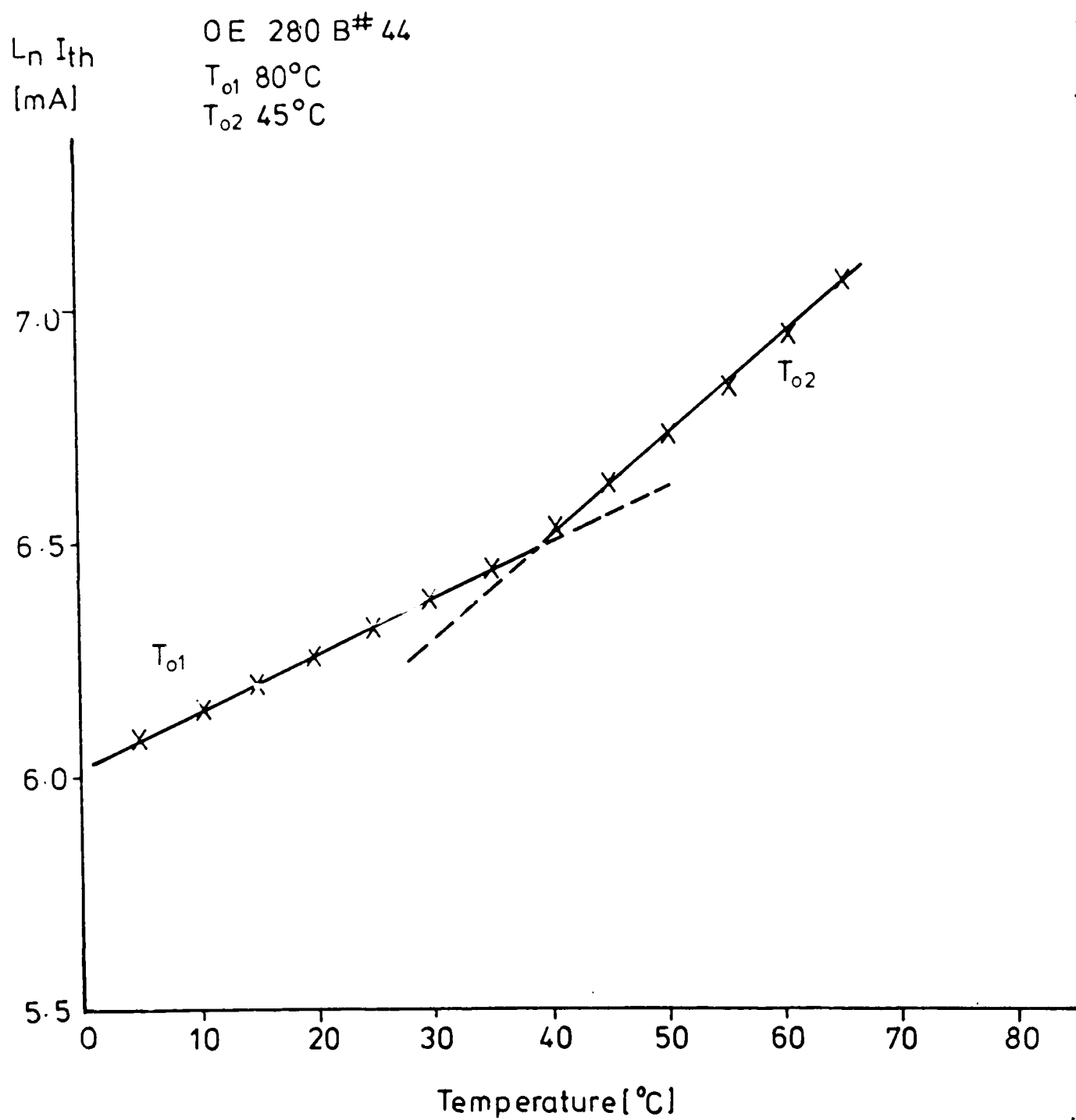


OE 280 B<sup>#</sup>23

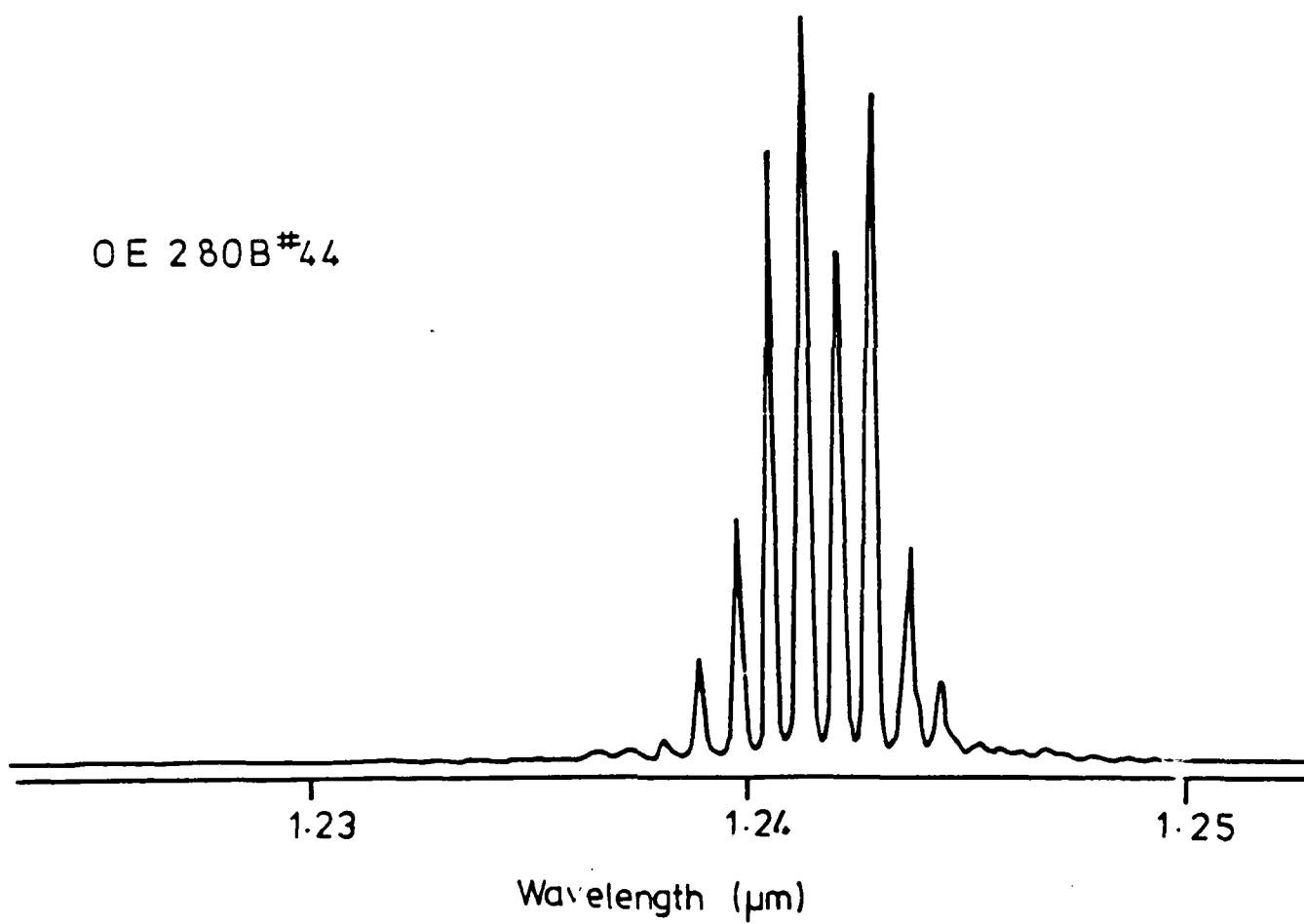


Oxide Isolated  
OE 280B#44  
GaAlInAs Active  
(10 x 250  $\mu\text{m}^2$ )

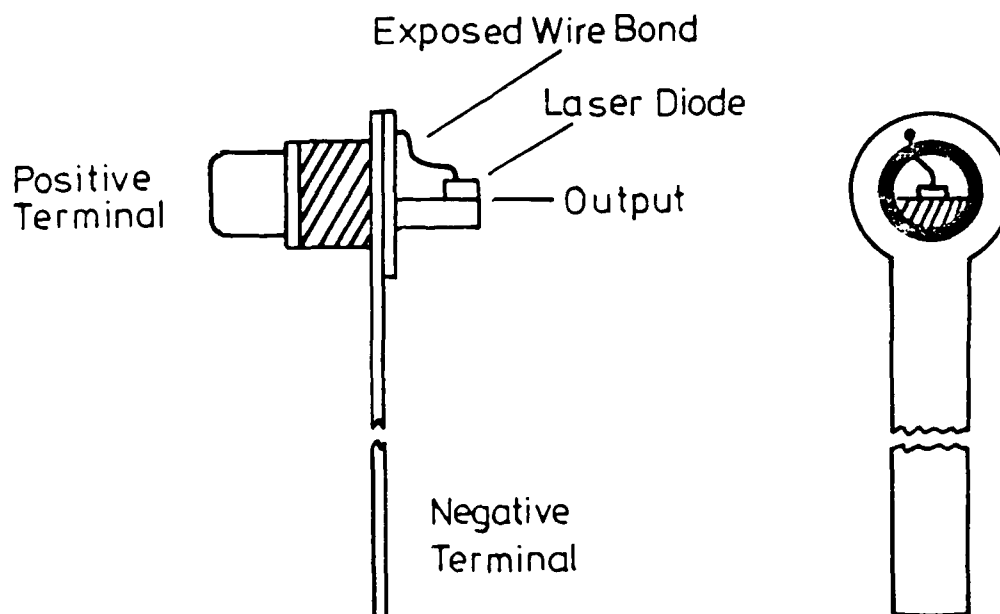




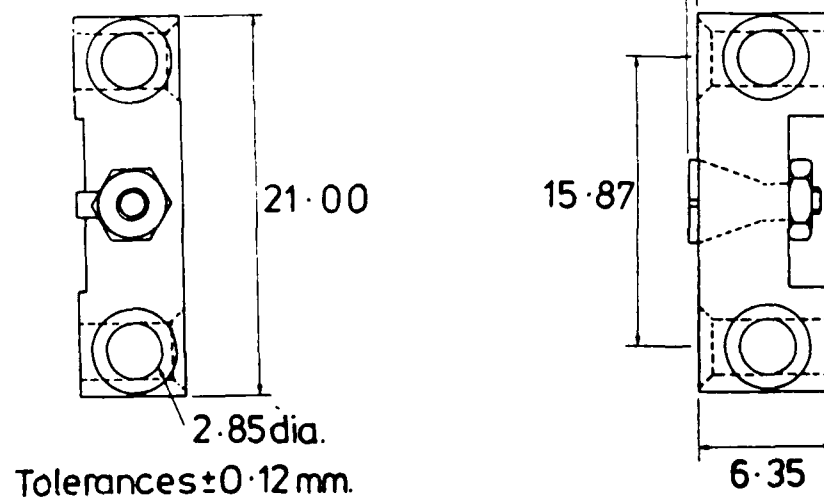
OE 280B#44



## Submount Details



### MOUNTING CLAMP All dimensions are in mm.



For device protection, please ensure that a load resistance (e.g.  $50\Omega$ ) is included in series with the laser and power supply before switch on.

Recommended pulse drive conditions for broad area GaAlInAs oxide isolated devices:

Pulse width 200 ns

Repetition Rate 1KHz



## *MISSION of Rome Air Development Center*

*RADC plans and executes research, development, test and selected acquisition programs in support of Command, Control, Communications and Intelligence (C<sup>3</sup>I) activities. Technical and engineering support within areas of competence is provided to ESD Program Offices (POs) and other ESD elements to perform effective acquisition of C<sup>3</sup>I systems. The areas of technical competence include communications, command and control, battle management information processing, surveillance sensors, intelligence data collection and handling, solid state sciences, electromagnetics, and propagation, and electronic reliability/maintainability and compatibility.*